Supplementary Information (SI) for Chemical Science.
This journal is © The Royal Society of Chemistry 2025

Supporting Information for:

Dinitrogen Reduction to Ammonia with a Pincer-Mo Complex: New Insights into the Mechanism of Nitride-to-Ammonia Conversion

Souvik Mandal,[a] Xiaoguang Zhou,[a] Quinton J. Bruch,[b,c] Rachel N. Allen,[a]
Laurence W. Giordano,[a] Nicholas J. I. Walker,[a] Thomas J. Emge,[a] Faraj Hasanayn,[d]
Alexander J. M. Miller,[b] Santanu Malakar,*[e] Alan S. Goldman*[a]

[a] Department of Chemistry and Chemical Biology, Rutgers, The State University of New Jersey, New Brunswick, New Jersey 08854, United States

[b] Department of Chemistry, University of North Carolina at Chapel Hill, Chapel Hill, North Carolina 27599-3290, United States

[c] Department of Chemistry, Stony Brook University, Stony Brook, NY 11794, United States

[d] Department of Chemistry, American University of Beirut, Beirut 1107 2020, Lebanon

[e] Department of Chemistry, Rutgers University–Camden, Camden, New Jersey 08102, United States

Table of Contents

I. General Considerations

Unless otherwise noted all reactions were performed in an argon- or nitrogen-filled glove box, or using standard Schlenk techniques. Solid chemicals were purchased from Sigma Aldrich, Fisher Scientific, or other commercial sources, and used without further purification. Anhydrous reagent-grade solvents were purchased from Sigma Aldrich and degassed before use. Deuterated solvents including $CDCl_3$, C_6D_6, toluene-d_8, and THF-d_8 were purchased from Cambridge Isotope Laboratories and deoxygenated by three freeze-pump-thaw cycles, dried over neutral alumina, and stored over molecular sieves prior to use. $^{15}N_2$ gas was obtained from Cambridge Isotope Laboratory and used without additional purification.

All NMR spectra (^{1}H (500 MHz), ^{31}P{^{1}H} (202 MHz), ^{11}B(160.4 MHz), ^{19}F (470 MHz), ^{15}N (50.6 MHz)) were acquired on a Bruker Avance 500-MHz or Varian VNMRS 500-MHz NMR spectrometer at ambient temperature (25 °C) unless noted otherwise. ^{1}H NMR chemical shifts are reported relative to TMS and were referenced via residual ^{1}H resonances of the corresponding deuterated solvent (C_6D_6: δ 7.16 ppm, THF-d_8: δ 3.58). ^{31}P{^{1}H} NMR signals are given relative to 85% H_3PO_4, ^{19}F NMR shifts are relative to $FCCl_3$, and ^{15}N NMR shifts relative to CH_3NO_2. Occasionally, ^{31}P{^{1}H} NMR spectra were referenced using a capillary with PMe_3 in C_6D_6 (-62.00 ppm) as external standard.

PSP,[S1] lutidinium chloride, lutidinium triflate,[S2] $[H(OEt_2)_2][BAr^F{}_4]$,[S3] and TEMPO-H,[S4] were prepared according to the reported literature process. $CoCp_2$ and $CoCp^*{}_2$ were purchased from Sigma-Aldrich and sublimed under vacuum (0.029 Torr) at 80 °C and 104 °C respectively prior to use. Commercial $[^nBu_4][PF_6]$ (Sigma-Aldrich) was triply recrystallized from hot ethanol before being crushed and dried for 3 days at 80 °C. All other chemicals were purchased from commercial sources and used without further purification.

Cyclic voltammetry was carried out using a Pine WaveDriver Bipotentiostat controlled by Aftermath software. Cyclic voltammograms were collected in an undivided three-electrode cell consisting of a glassy carbon (3 mm diameter) working electrode, a Pt wire counter electrode, and a Ag wire pseudo-reference electrode in a fritted sample holder separate compartment containing fresh electrolyte solution. CVs are referenced versus an internal standard to ferrocene ($[FeCp_2]^{+/0}$ at 0 V).

X-Ray crystallographic data were obtained using a Bruker Apex III instrument and a Rigaku Synergy instrument. MS data were obtained using a SYNAPT G2-SI qTOF instrument. FT-IR spectra of the carbonyl complexes were recorded on a Thermo Nicolet/Avatar 360 FTIR spectrometer.

II. Synthesis of molybdenum complexes

S2.1. Synthesis of (PSP)MoCl$_3$ (1-Cl$_3$)

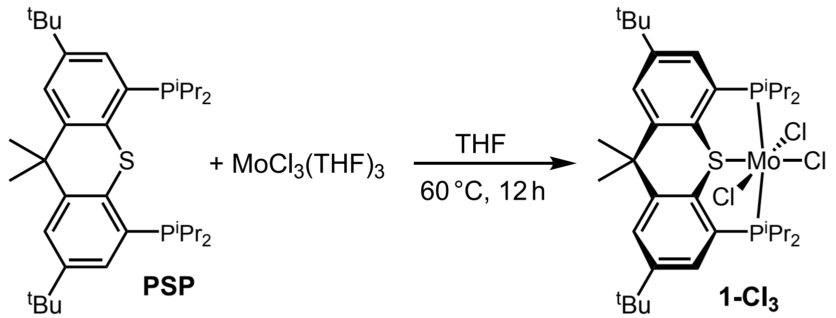

In an argon-filled glovebox, a 100-mL screw-cap Schlenk flask equipped with a magnetic stir bar was charged with PSP (300 mg, 0.530 mmol) and $MoCl_3(THF)_3$ (219 mg, 0.530 mmol) followed by addition of ca. 40 mL tetrahydrofuran (THF). The flask was then taken out of the glovebox and heated at 60 °C in an oil bath for 12 h and the reaction was then cooled to room temperature. The solvent was then concentrated to 5 mL, to which approximately 40 mL of pentane (or hexane) was added. An orange-colored precipitate formed which was then collected, washed with additional pentane (or hexane, 3 x 10 mL), and then dried under vacuum. The orange powder was stored at room temperature inside the glovebox. X-ray quality crystals were grown by slow diffusion of pentane into a saturated THF solution. Yield 81%

^{1}H NMR (THF-d$_8$, 500 MHz) Key paramagnetic signals, all broad: δ 22.71, δ 22.11, δ 12.92, δ 11.17.

MS m/z (ESI) for $C_{35}H_{56}P_2SClMo$, calc. 773.17, found 773.14

S2.2. Synthesis of [(PSP)Mo(N$_2$)$_2$](μ-N$_2$) (2) and (PSP)Mo(N$_2$)$_3$ (3)

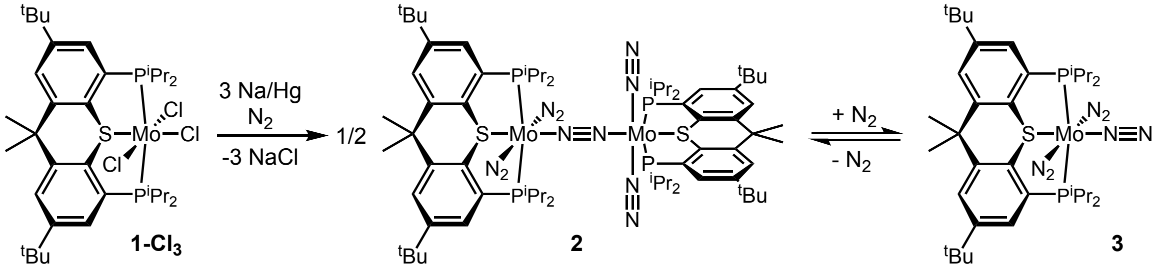

To a J. Young NMR tube, **1-Cl$_3$** (7.7 mg, 0.010 mmol, 1.0 equiv) was added and then dissolved in 0.45 mL of THF-d$_8$ (or C_6D_6) under N_2 atmosphere. Then 0.5 w/w% sodium amalgam (Na/Hg) (137 mg, 0.030 mmol Na, 3.0 equiv) was added and the mixture was shaken vigorously. The solution color changed to brown, and a white precipitate and metallic mercury settled at the bottom of the NMR tube. The reaction was continued for 2 hours. The $^{31}P\{^1H\}$ NMR spectrum was indicative of a complex mixture. Cooling the solution to -45 °C revealed an AB doublet at δ 80.1 and δ 78.3 ppm with a coupling constant $^2J_{PP}$ = 122.3 Hz.

When the reaction was performed in diethyl ether, X-ray quality crystals of **2** were formed at -35 °C in the reaction flask. The crystals were dissolved under N_2 atmosphere in THF-d_8. (Note that there were two diethyl ether molecules in the unit cell; hence there are signals corresponding to diethyl ether in the ^1H NMR spectrum).

^{1}H NMR (THF-d_8, 500 MHz) of crystals (at 298K): δ 7.58-7.55 (m, 2H), 7.49-7.48 (m, 2H), 3.24-3.26 (m, 2H), 2.47 (septet, 2H), 2.11 (s, 3 H), 1.61 (s, 3H), 1.39 (s, 9H), 1.32-1.28 (m, 3H), 1.24-1.16 (m, 6H), 1.18-0.85 (m, 3H)

^{31}P{^{1}H} NMR (THF-d_8, 202 MHz) of crystals (at 298 K): δ 80.8 (d, J = 120 Hz), 79.1 (d, J = 120 Hz)

IR of **2** (NaCl): 2024 cm^{-1},1998 cm^{-1},1895 cm^{-1}

IR of **3** (NaCl): 2078 cm^{-1}, 2008 cm^{-1}

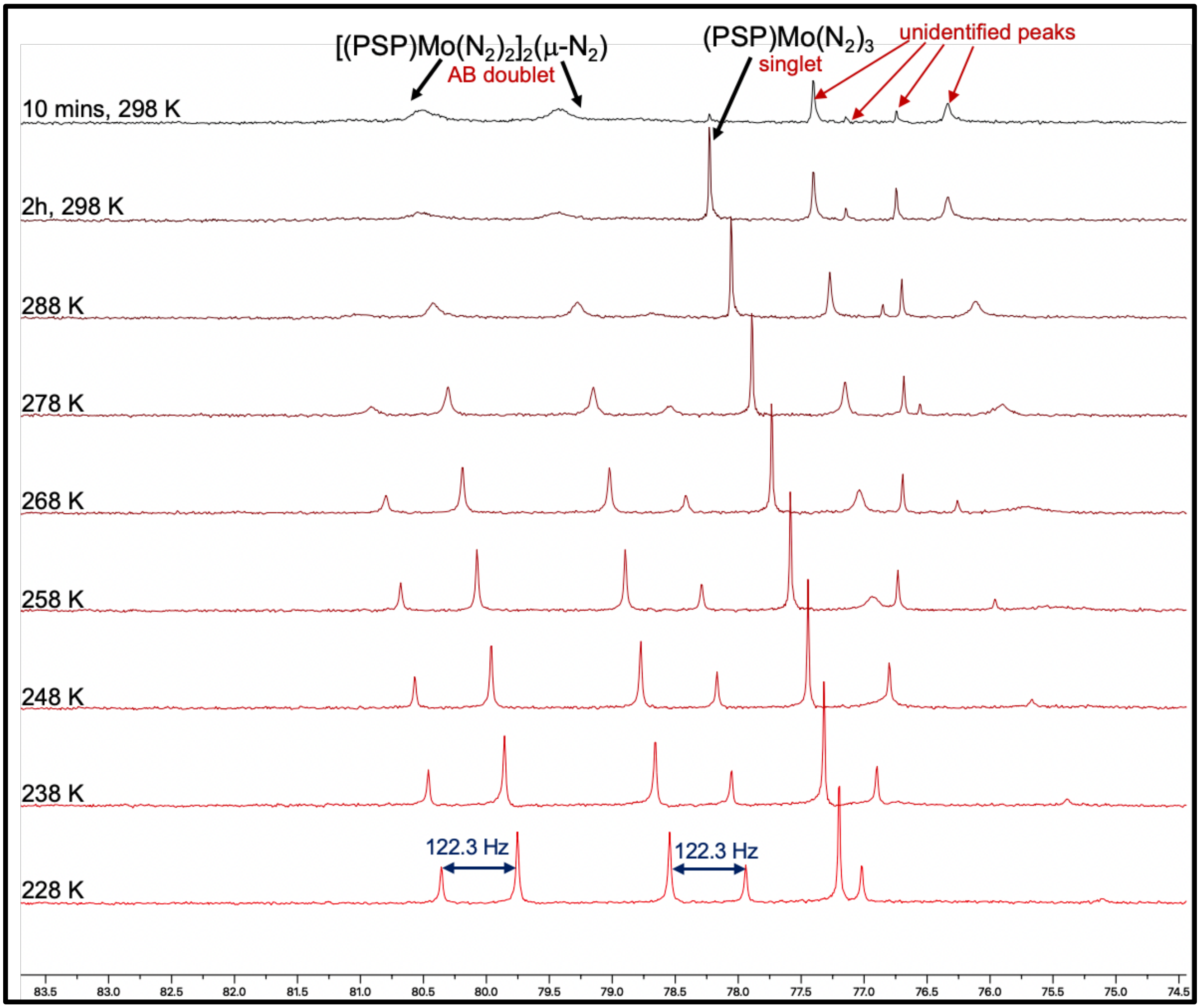

Figure S1. Variable temperature stacked plot of $^{31}P\{^1H\}$ NMR spectra of a mixture containing **2** (major product), **3** and other unidentified peaks.

The stacked $^{31}P\{^1H\}$ NMR spectra of crystals of **2** dissolved in THF-d_8 under N_2 (1 atm), taken at various temperatures, are shown in Figure S1. The peak at δ 78.2 corresponds to compound **3**. As seen in the stacked plot, (second from the top spectra), the peak at δ 78.2 had significantly increased after 2 hours at room temperature.

Determination of equilibrium between 2 and 3

$$\underset{\mathbf{2}}{[(\mathrm{PSP})\mathrm{Mo}(\mathrm{N_2})_2]_2(\mu\text{-}\mathrm{N_2})} + \mathrm{N_2} \overset{\mathrm{K_{eq}}}{\rightleftharpoons} \underset{\mathbf{3}}{2\ (\mathrm{PSP})\mathrm{Mo}(\mathrm{N_2})_3}$$

Based on the above equation, $\mathrm{K_{eq}} = \frac{[\mathbf{3}]^2}{[\mathbf{2}]\times \mathrm{p_{N_2}}}$

To a high-pressure J. Young NMR tube, a 50 mM (in Mo) mixture of predominantly **2** and **3** (formed by reduction of **1-Cl$_3$** under N_2 atmosphere) was dissolved in 0.2 mL of THF-d_8 under argon atmosphere. The $^{31}P\{^1H\}$ NMR spectrum was recorded, and the atmosphere was then exchanged with N_2 inside a N_2-filled glove box. Periodically, $^{31}P\{^1H\}$ NMR spectra were recorded at 25 °C, -25 °C and -45 °C (the lower temperatures for the ease of NMR integration, as seen in Figure S1). It was found out that the equilibrium between **2** and **3** is reached very slowly at room temperature. After concentrations of **2** and **3** eventually reached a steady state, the N_2 pressure was increased to 7.12 atm. The concentrations of **2** and **3** were again monitored by $^{31}P\{^1H\}$ NMR spectroscopy. The concentration of **3** was observed to slowly increase over the course of 6 days, plateauing at 10.8 mM while the concentration of **2** leveled off at 4.7 mM. The N_2 pressure above the solution was then decreased to 1.0 atm and, again, the concentration of **2** was observed to increase over 6 days, reaching 8.2 mM while [**3**] reached 5.2 mM. The values corresponding to K_{eq} for the interconversion of **2** and **3** as shown in Scheme 2, were in very good agreement (Table S1): 3.5×10^{-3} M•atm^{-1} and 3.3×10^{-3} M•atm^{-1}, respectively. The N_2 pressure above the solution was then again increased to 7.12 atm, the concentrations of **2** and **3** returned to approximately the same values as observed initially under 7.12 atm.

Table S1: Calculating K_{eq}

p_{N_2} (atm)	[**2**] (mM)	[**3**] (mM)	K_{eq} (M•atm^{-1})
7.12	4.7	10.8	3.5×10^{-3}
1	8.2	5.2	3.3×10^{-3}

S2.3. Synthesis of [(PSP)Mo(CO)$_2$](μ-N$_2$) (4) and (PSP)Mo(CO)$_3$ (5)

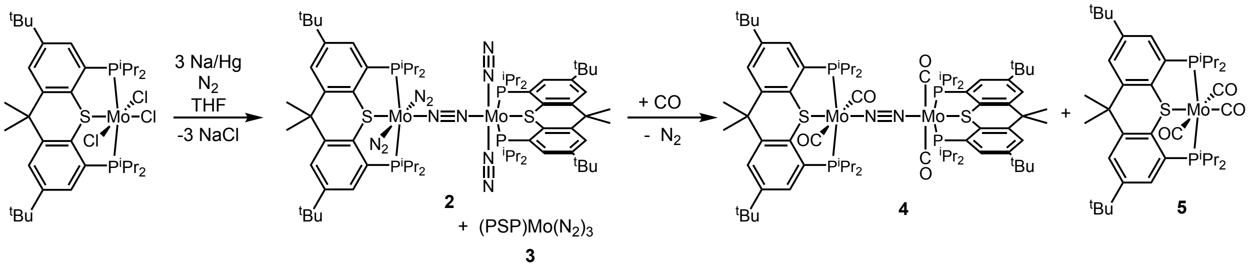

In a J-Young NMR tube, **1-Cl$_3$** (7.7 mg, 0.010 mmol, 1.0 equiv) was weighed, and dissolved in 0.5 mL of THF under N$_2$ atmosphere. 0.5 w/w% sodium amalgam (Na/Hg) (134 mg, 0.030 mmol, 3.0 equiv) was then added, the reaction was shaken vigorously, and the NMR tube was rotated at room temperature for 2 hours. To this reaction mixture, after removing the N$_2$ atmosphere by freeze-pump-thaw cycle, CO (1 atm) was charged, and the sample was shaken vigorously. The NMR tube was then left rotating at room temperature for two days. Solvent was then removed under vacuum and solid was extracted with benzene. The benzene solution was then subjected to recrystallization by slow diffusion with pentane. This process yielded two products, one being yellow crystals of (PSP)Mo(CO)$_3$ (**5**) (as determined by scXRD), while the other product was an orange-red solid. The crystals were manually separated from the orange-red solid, and the solid was then dissolved in C$_6$D$_6$ to obtain ^{1}H and ^{31}P{^{1}H} NMR spectra. Based on the NMR spectra the orange-red solid was determined to be compound **4**. Finally, the NMR sample was transferred to a 4-mL vial and subjected to slow diffusion of pentane which yielded the X-ray quality crystals of **4**.

^{1}H NMR (C$_6$D$_6$, 500 MHz) of **4**: δ 7.62 (s, 4H), 7.43 (s, 4H), 2.91-3.20 (m, 4H), 2.53-2.66 (m, 4H), 1.94-2.08 (m, 12H), 1.90 (s, 6H), 1.58 (s, 6H), 1.37-1.55 (m, 24H), 1.29 (s, 36H), 1.16-1.24 (m, 18H).

^{31}P{^{1}H} NMR (C$_6$D$_6$, 500 MHz) of **4**: δ 88.4(br doublet, *J* = 187 Hz)

IR (THF) 1852 cm^{-1}, 1827 cm^{-1} (IR sample was made from a mixture of **4** and **5**, with 70% **4** based on ^{31}P{^{1}H} NMR spectroscopy)

^{1}H NMR (C$_6$D$_6$, 500 MHz) of dissolved crystals of **5** (at 298 K): δ 7.55 (s, 2H), 7.47 (s, 2H), 2.80-3.03 (m, 4H), 1.94 (s, 3H), 1.67 (s, 3H), 1.60-1.67 (m, 6H), 1.49-1.57 (m, 6H), 1.26-1.37 (m, 12H), 1.24 (s, 18H)

^{31}P{^{1}H} NMR (C$_6$D$_6$, 500 MHz) of crystals of **5** (at 298 K): δ 85.9 (s)

S2.4. Synthesis of (PSP)Mo(N)I (1-(N)I)

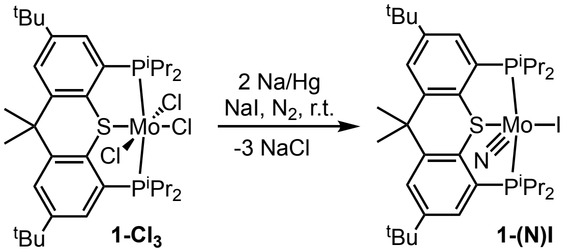

In a 20-mL vial equipped with a magnetic stir bar, **1-Cl$_3$** (154 mg, 0.20 mmol, 1.0 equiv) and NaI (60 mg, 0.40 mmol, 2.0 equiv) were dissolved in 0.5 mL of THF under N_2 atmosphere. The mixture was stirred for at least an hour. Then 0.5 w/w% sodium amalgam (Na/Hg) (1.8 g, 0.40 mmol Na, 2.0 equiv) was added and the mixture was stirred vigorously (1200 rpm) for 30 min. The reaction was then left stirring at lower stirring speed (750 rpm) for the next 16 h. After the reaction was completed, the solution was filtered twice with a 22-μm PTFE syringe filter to remove mercury metal and some NaCl. The solution was then dried under vacuum. From this solid, the product was extracted with toluene (10 mL x 5). All the extracted fractions were combined, and toluene was evaporated, which yielded the product as a brown solid. Isolated yield: 63%.

^{1}H NMR (THF-d_8, 500 MHz): δ 7.77 (s, 2H), 7.22-7.07 (m, 2H), 3.32-3.25 (m, 2H), 2.70-2.65 (m, 2H), 2.15 (s, 3H), 1.69 (s, 3H), 1.53-1.48 (m, 6H), 1.39 (s, 18H), 1.27-1.21 (m, 6H), 1.21-1.17 (m, 6H), 0.97-0.85 (m, 6H)

^{31}P{^{1}H} NMR (THF-d_8, 202 MHz): δ 79.8 (s)

^{13}C{^{1}H} NMR (THF-d_8, 126 MHz): δ 152.9 (t, *J* = 2.0 Hz), 145.2 (t, *J* = 4.0 Hz), 142.8 (t, *J* = 10.4 Hz), 132.6 (t, *J* = 13.8 Hz), 129.8, 129.1, 128.7, 126.2, 125.2, 42.5, 36.0, 31.8, 28.6 (t, *J* = 8.6 Hz), 26.6, 21.7, 20.4 (t, *J* = 3.0 Hz), 19.0, 18.4

IR (NaCl) 1039 cm^{-1}

MS m/z (ESI) for $C_{35}H_{56}NP_2SIMo$, calc. 809.171, found 809.155

For the synthesis of **1-(^{15}N)I**, the reaction was set up in an argon-filled glovebox. After addition of Na/Hg the reaction was quickly removed from the glove box and frozen immediately with liquid N_2. Argon was then removed by vacuum and $^{15}N_2$ was added. The reaction was then allowed to thaw and stirred well for 16 h. The work-up process was the same as that for unlabeled **1-(N)I**, and the compound was isolated as 87% pure (based on $^{31}P\{^1H\}$ NMR spectroscopy)

^{15}N NMR (THF-d_8, 50.6 Hz): δ 445.7 (s)

MS m/z (ESI) for $C_{35}H_{56}(^{15}N)P_2SIMo$: calc. 810.168, found 810.162

S2.5. Synthesis of (PSP)Mo(NH)(I)Cl (1-(NH)ICl)

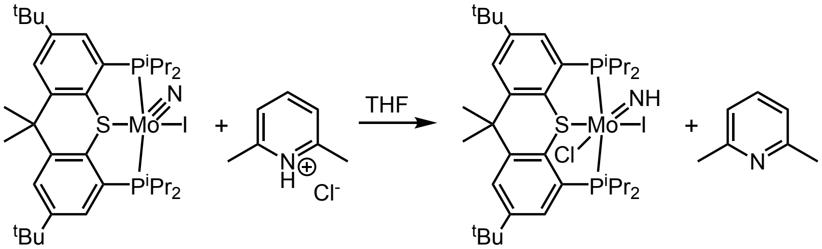

For NMR scale reactions: In a J-Young NMR tube (PSP)Mo(N)I (7.7 mg, 0.010 mmol, 1.0 equiv) and [LutH]Cl (4.3 mg, 0.030 mmol, 3.0 equiv) were weighed and 0.5 mL of THF-d_8 (or C_6D_6) was added. The reaction was shaken and after 2 h the $^{31}P\{^1H\}$ and ^1H NMR spectra were obtained, which indicated the formation of the desired compound (two species in a 4:1 ratio) in addition to residual lutidine and unreacted [LutH]Cl.

X-ray quality crystals were obtained by diffusion of pentane into a C_6D_6 solution of a reaction mixture such as that described above.

Larger scale: In a 20-mL glass vial (PSP)Mo(N)I (50 mg, 0.062 mmol, 1.0 equiv) and [LutH]Cl (27 mg, 0.19 mmol, 3.0 equiv) were weighed, and 3 mL THF was added. The reaction was stirred at room temperature for 4 h. Excess lutidinium chloride was then filtered off using a 22-μm PTFE syringe filter (2 x). The filtrate was collected and dried under vacuum to yield a yellow powder. Yield: 84%.

^{1}H NMR (THF-d_8, 500 MHz) Major species: δ 7.72-7.61 (m, 4H), 6.40 (br s, 1H), 3.22-3.14 (m, 2H), 2.87 (s, 6H), 2.48-2.36 (m, 2H), 1.86-1.73 (m, 6H), 1.39 (s, 18H), 1.37-1.32 (m, 6H), 1.31-1.26 (m, 6H), 1.26-1.21 (m, 6H)

$^{31}P\{^1H\}$ NMR (THF-d_8, 202 MHz): δ 64.0 (s, major species); 64.9 (s, minor species)

$^{13}C\{^1H\}$ NMR (THF-d_8, 126 MHz): δ 151.9 (t, *J* = 2.2 Hz), 144.2 (t, *J* = 3.8 Hz), 143.1 (t, *J* = 8.5 Hz), 135.3, 135.2, 129.2, 124.0, 42.8, 35.9, 35.2, 29.6 (t, *J* = 8.1 Hz), 28.2, 27.5 (t, *J* = 7.1 Hz), 23.4, 21.0, 20.8, 19.6 (t, *J* = 3.4 Hz), 18.5, 14.5

MS m/z (ESI) for $C_{35}H_{57}NP_2SClIMo$ (major species): calc. 845.1475, found 845.1573. $C_{35}H_{57}NP_2SCl_2Mo$ (minor species): calc. 753.2113, found 753.2188

For ^{15}N labelled isotopologue: NMR scale reaction was performed with (PSP)Mo(^{15}N)I (4.2 mg, 0.005 mmol, 1 equiv) with 1.2 equiv of lutidinium chloride (1.0 mg, 0.006 mmol, 1.2 equiv). NMR conversion, 99%; yield >98%.

^{1}H NMR (THF-d_8, 500 MHz) (N-H peak): δ 6.42 (dt, $^1J_{N\text{-}H}$ = 73 Hz, $^3J_{P\text{-}H}$ = 3.6 Hz; major species); 6.55 (d, $^1J_{N\text{-}H}$ = 75 Hz; minor species; upfield branch of this doublet overlaps with the downfield branch of the major species).

^{31}P{^{1}H} NMR (THF-d_8, 202 MHz): δ 64.0 (d, $^2J_{P\text{-}N}$ = 6 Hz, major species); 64.9 (d, $^2J_{P\text{-}N}$ = 6 Hz, minor species)

^{15}N NMR (THF-d_8, 50.6 MHz): δ -3.2 (d, $^1J_{N\text{-}H}$ = 73 Hz, $^2J_{P\text{-}N}$ = 6 Hz)

^{1}H-^{15}N HSQC: Strong correlation at {6.42, -2.9}

S2.6. Synthesis of [(PSP)Mo(NH)(I)][BAr$^F{}_4$] (1-(NH)(I)BAr$^F{}_4$)

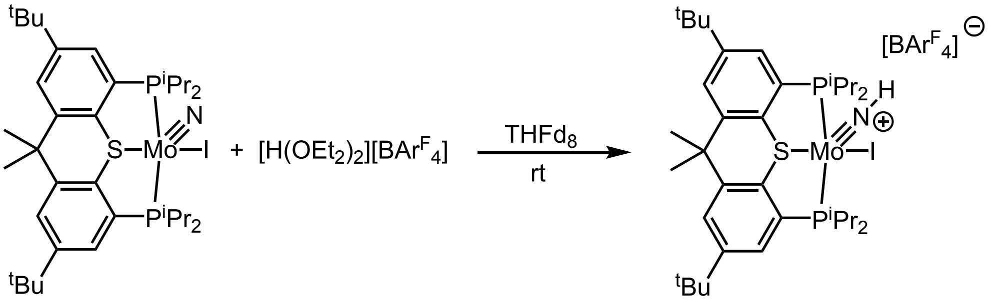

In a J-Young NMR tube (PSP)Mo(N)I (2.3 mg, 0.0028 mmol, 1.0 equiv) and [H(OEt$_2$)$_2$]BAr$^F{}_4$ (2.6 mg, 0.003 mmol, 1 equiv) were weighed and 0.5 mL of THF-d$_8$ (or C$_6$D$_6$) was added. The reaction was shaken, ^{1}H and ^{31}P{^{1}H} NMR spectra were recorded after 10 min, and the desired compound was observed. The proton bound to the nitride ligand was not unambiguously detected by ^{1}H NMR. However, when the reaction was performed with **1-(^{15}N)I**, and 2D correlations were recorded, it was found that N-H proton signal is overlapped with the para C-H signals of BAr$^F{}_4$ anion. NMR conversion > 98%.

^{1}H NMR (THF-d$_8$, 500 MHz): δ 7.78 (s, 8H), 7.57 (s, 5H), 7.20-7.07 (m, 4H), 2.54-2.51 (m, 2H), 2.31 (s, 3H), 2.21-2.18 (m, 2H), 1.87-1.80 (m, 6H), 1.68 (s, 3H), 1.41 (s, 18H), 1.39-1.35 (m, 12 H), 1.28-1.20 (m-6H)

^{31}P{^{1}H} NMR (THF-d$_8$, 202 MHz): δ 67.3 (s)

^{11}B NMR (THF-d$_8$, 160.4 MHz): δ -6.47 (quintet, *J* = 3 Hz)

^{19}F NMR (THF-d$_8$, 470 MHz): δ -63.42 (s)

^{15}N NMR (THF-d$_8$, 50.6 MHz): δ 50.7 (d, $^1J_{N\text{-}H}$ = 73 Hz)

^{1}H-^{15}N HSQC: Strong correlation at {7.56, 50.9}

S2.7. Reaction of (PSP)Mo(N)I with [LutH]OTf

In a J-Young NMR tube (PSP)Mo(N)I (6.6 mg, 0.0082 mmol, 1.0 equiv) was weighed and dissolved in 0.5 mL of THF-d_8. To the above solution [LutH]OTf was weighed and added sequentially until a total of 12 equiv was added. To this mixture, lutidine was then sequentially added (2 equiv x 2). After each addition the mixture was thoroughly shaken and $^{31}P\{^1H\}$ and ^1H NMR spectra were recorded.

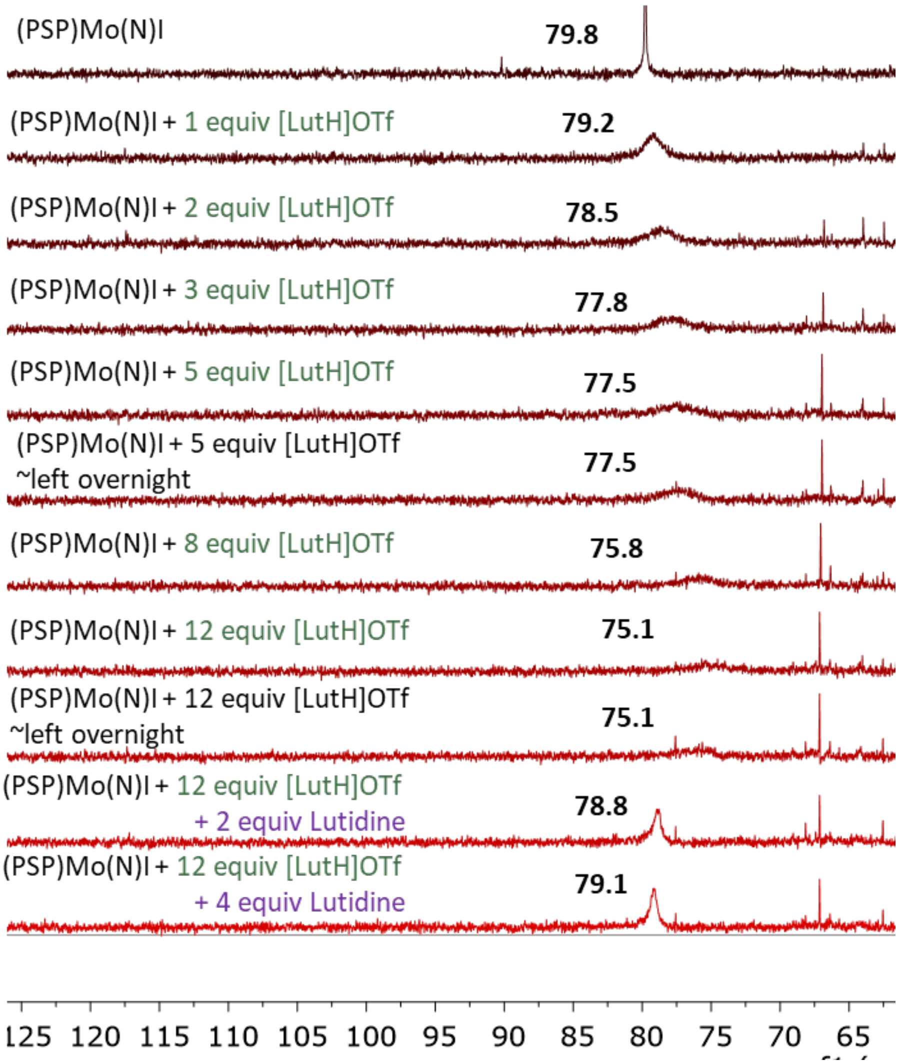

Figure S2. Stacked $^{31}P\{^1H\}$ NMR spectra of a THF-d_8 solution of **1-(N)I** (14 mM) with addition of [LutH]OTf followed by addition of lutidine.

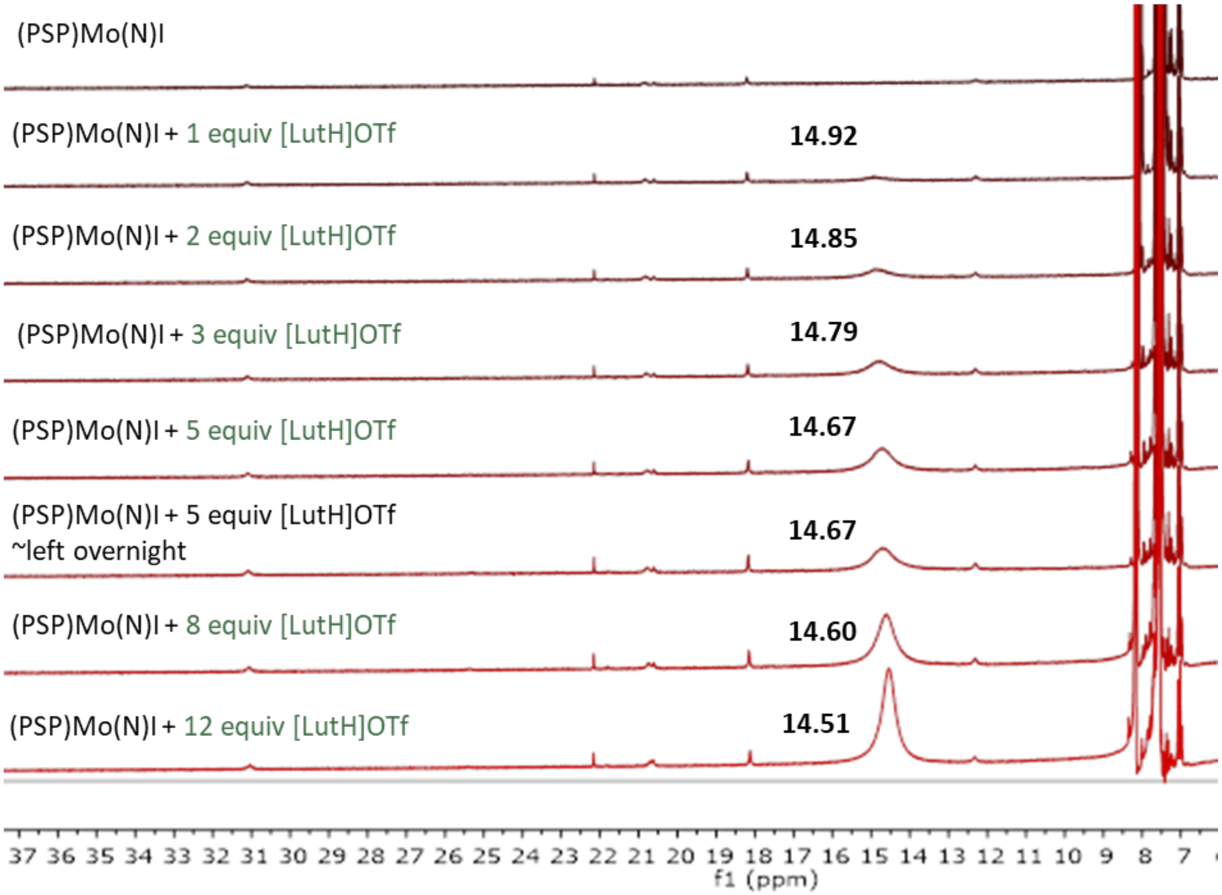

Figure S3. Stacked ^{1}H NMR spectra of a THF-d_8 solution of **1-(N)I** (14 mM) with addition of [LutH]OTf (up to 12 equiv)

^1H-^{15}N HSQC NMR spectroscopy of the reaction products

[LutH]OTf (4.8 mg, 0.019 mmol, 3.0 equiv) was added to a solution of (PSP)Mo(^{15}N)I (4.2 mg, 0.0050 mmol, 1.0 equiv) in THF-d_8 and the ^1H-^{15}N HSQC spectrum was recorded (Figure S4). Two correlations were observed (Figure S4) with ^{15}N chemical shifts at δ -2.8 and δ -2.1. Both are consistent with assignment as (PSP)Mo(NH)(I)(OTf) with coordinated triflate (cf. (PSP)Mo(NH)(I)Cl which has a ^{15}N NMR chemical shift of δ -2.9); the two individual species are possibly isomers.

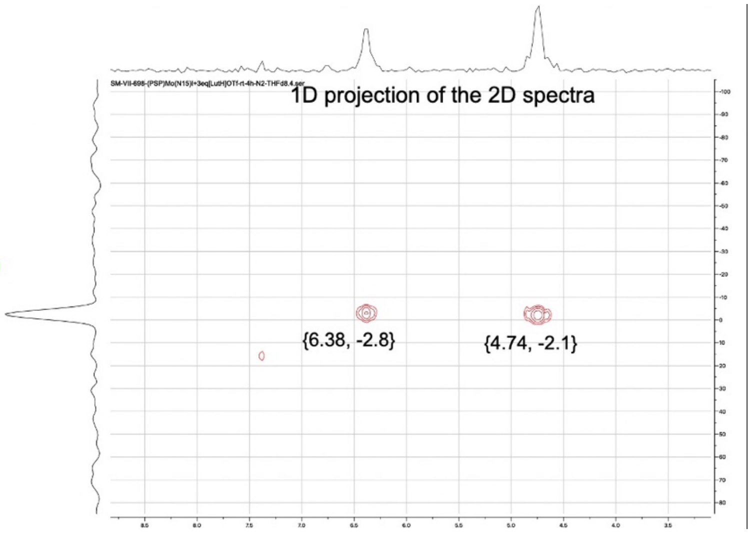

Figure S4: ^1H-^{15}N HSQC plot of addition of [LutH]OTf (3 equiv) to **1-(N)I**

S2.8. Reaction of (1-(NH)(I)Cl) with H atom donors; quantifying formation of ammonium chloride

S2.8.1. Reaction of 1-(NH)(I)Cl with TEMPO-H

S2.8.1.1. Reaction of 1-(NH)(I)Cl (in-situ generated) with TEMPO-H in presence of excess lutidinium chloride

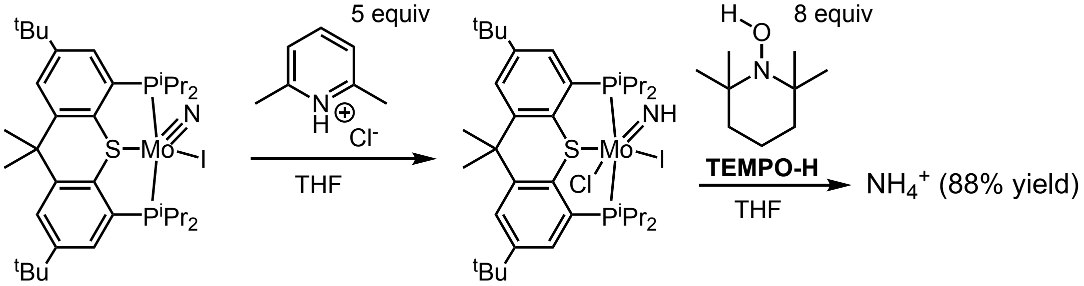

In a Strauss flask equipped with a magnetic stir bar, (PSP)Mo(N)I (12.5 mg, 0.015 mmol, 1.0 equiv) and lutidinium chloride (11.1 mg, 0.077 mmol, 5.0 equiv) were weighed and then 2 mL THF was added. The reaction was stirred for 2 hours before TEMPO-H (19.7 mg, 0.12 mmol, 8.0 equiv) was added and allowed to react for 24 h. Volatiles were then transferred under vacuum, using a T-shaped adapter, to another Strauss flask filled with HCl in diethyl ether. The solids in both receiving and parent flasks were then analyzed by ^{1}H NMR spectroscopy in DMSO-d$_6$. Ammonium chloride was only found in the parent flask (where excess [LutH]Cl trapped the formed ammonia), in 88% yield. In the receiving flask [LutH]Cl was found to be the sole product (formed from the transfer of lutidine from the parent flask to the receiving flask).

S2.8.1.2. Reaction of 1-(NH)(I)Cl with TEMPO-H

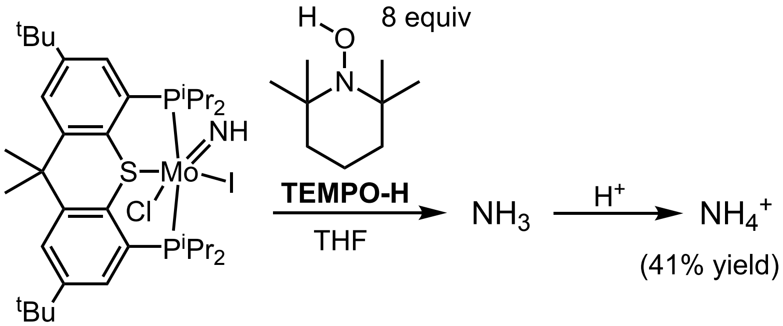

In a Strauss flask equipped with a magnetic stir bar, (PSP)Mo(NH)(I)Cl (10.0 mg, 0.012 mmol, 1.0 equiv) and TEMPO-H (15.3 mg, 0.096 mmol, 8.0 equiv) were weighed and then 2 mL THF was added. The reaction was stirred for 24 hours. Volatiles were then transferred under vacuum, using a T-shaped adapter, to another Strauss flask filled with HCl in diethyl ether. The solids in both receiving and parent flasks were then analyzed by ^{1}H NMR spectroscopy in

DMSO-d_6. Ammonium chloride was only found in the receiving flask, in 41% yield. (Figure S29) [This apparent low yield of NH_4^+ is attributed to some loss of NH_3 during vacuum transfer].

S2.8.2 Reaction of (1-(NH)(I)Cl) with $CpCr(CO)_3H$

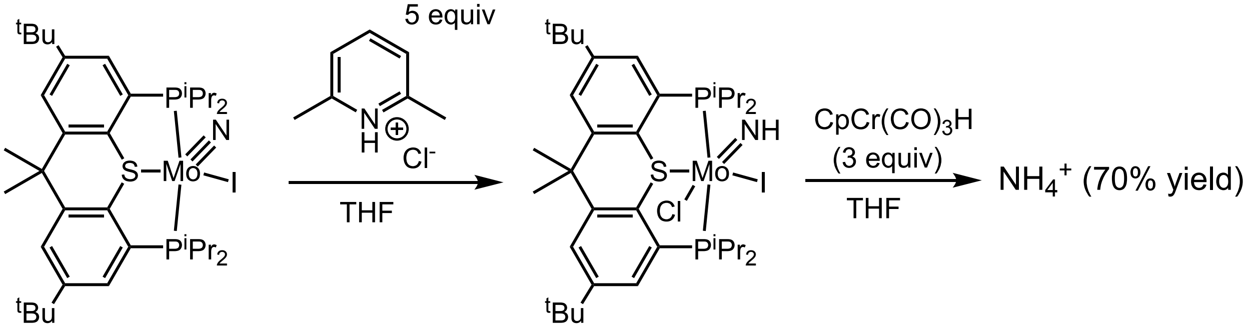

NMR scale: In a J-Young NMR tube (PSP)Mo(N)I (4.0 mg, 0.0050 mmol, 1.0 equiv) and lutidinium chloride (2.8 mg, 0.020 mmol, 4.0 equiv) were weighed and 0.5 mL of THF-d_8 was added to generate (PSP)Mo(NH)(I)Cl. To the above mixture, $CpCr(CO)_3H$ (5.0 mg, 0.025 mmol, 5.0 equiv) was added and ^1H and $^{31}P\{^1H\}$ NMR spectra were recorded periodically. In the $^{31}P\{^1H\}$ NMR spectrum the ^{31}P resonances corresponding to (PSP)Mo(NH)(I)Cl and (PSP)Mo(NH)Cl_2 disappeared within 3 hours. Additionally, the ^1H NMR spectra revealed the disappearance of the Cr-H resonance and the appearance of the (PSP)MoX_3 (X = Cl, I) characteristic paramagnetic resonances. The volatiles were then trapped using HCl in a second NMR tube and then both the samples were dried. Solids in both NMR tubes were further analyzed by ^1H NMR in DMSO-d_6. However, no NH_4^+ resonances were detected (likely due to overlap with the several aromatic resonances).

Bulk scale: In a Strauss flask equipped with a magnetic stir bar, (PSP)Mo(N)I (8.5 mg, 0.011 mmol, 1.0 equiv) and lutidinium chloride (7.5 mg, 0.052 mmol, 5.0 equiv) were weighed and then 2 mL of THF was added. The reaction was stirred for 1 hour before $CpCr(CO)_3H$ (6.4 mg, 0.032 mmol, 3.0 equiv) was added and allowed to react for 12 h. Volatiles were then transferred under vacuum to another Strauss flask filled with HCl in diethyl ether, using a T-shaped adapter. The solids in both the receiving and parent flasks were then analyzed by ^1H NMR spectroscopy in DMSO-d_6. Ammonium chloride was found only in the parent flask (where excess [LutH]Cl had trapped the formed ammonia), in 70% yield. In the receiving flask [LutH]Cl was found to be the sole product.

S2.8.2 Reaction of (1-(NH)(I)Cl) with 1,4-cyclohexadiene

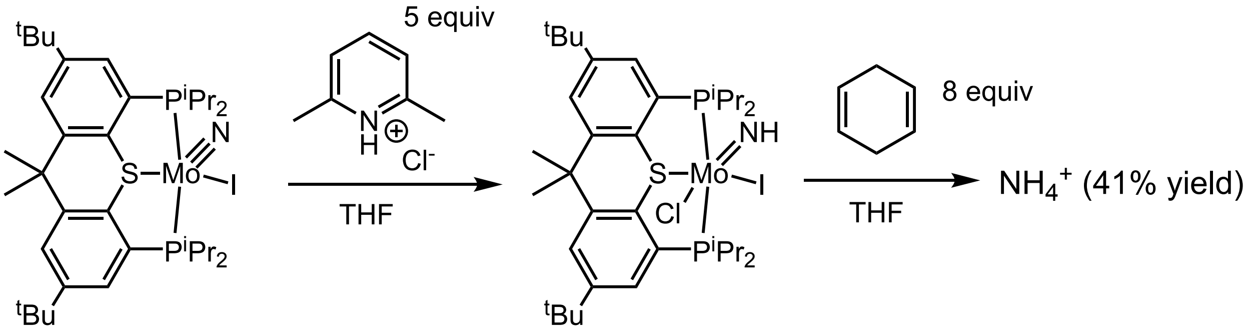

In a Strauss flask equipped with a magnetic stir bar, (PSP)Mo(N)I (10.6 mg, 0.013 mmol, 1.0 equiv) and lutidinium chloride (9.4 mg, 0.066 mmol, 5.0 equiv) were weighed and then 2 mL of THF was added. The reaction was stirred for 1 hour before 1,4-cyclohexadiene (19 μL, 0.11 mmol, 8.0 equiv) was added and allowed to react for 12 h. The volatiles were then transferred under vacuum to another Strauss flask filled with HCl in diethyl ether, using a T-shaped adapter. The solids in both the receiving and parent flasks were then analyzed by ^{1}H NMR spectroscopy in DMSO-d_6. Ammonium chloride was found only in the parent flask (where excess [LutH]Cl trapped the formed ammonia), in 41% yield.

S2.9. Stoichiometric NH_3 formation and regeneration of (PSP)$MoCl_3$

S2.9.1 Regeneration of (PSP)$MoCl_3$

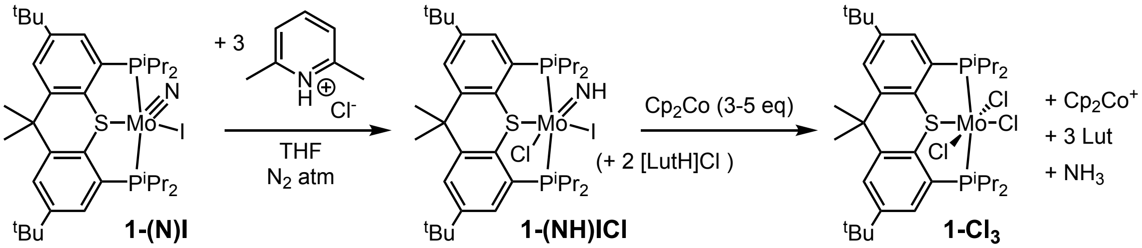

In a J-Young NMR tube (PSP)Mo(N)I (8.1 mg, 0.010 mmol, 1.0 equiv) and lutidinium chloride (4.3 mg, 0.030 mmol, 3.0 equiv) was weighed and 0.5 mL of THF-d_8 was added to generate (PSP)Mo(NH)(I)Cl. To the above mixture cobaltocene (1.9 mg, 0.010 mmol, 1.0 equiv) was added until total of 5 equiv of cobaltocene was added. After each addition, ^{1}H and ^{31}P{^{1}H} NMR spectra were recorded. Based on ^{1}H NMR spectrum (Figure S30) the peak at -0.02 ppm, which could be assigned to NH_3. Also, the characteristic paramagnetic NMR signals attributed for (PSP)$MoCl_3$ had also been assigned.

S2.9.2 Quantification of NH_3

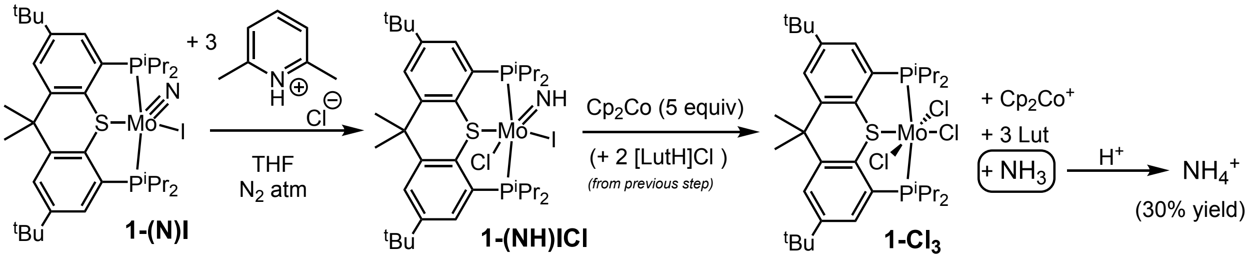

In a Strauss flask equipped with a magnetic stir bar, (PSP)Mo(N)I (10.0 mg, 0.012 mmol, 1.0 equiv) and lutidinium chloride (5.3 mg, 0.036 mmol, 3.0 equiv) were weighed and 1.0 mL of THF was added and stirred for 2 hours to generate (PSP)Mo(NH)(I)Cl. To this mixture, cobaltocene (11.7 mg, 0.060 mmol, 5.0 equiv) solution in 1.0 mL of THF was added dropwise, 1 drop every 2 seconds. (The slow addition of cobaltocene is extremely important to avoid H_2 formation, the predominant side reaction.) After the addition was completed, the reaction was left stirring for 12 hours at room temperature. The volatiles were then transferred under vacuum to another Strauss flask, containing HCl in diethyl ether, using a T-shaped adapter. The solids in both receiving and parent flasks were then analyzed by ^{1}H NMR spectroscopy in DMSO-d_6. Ammonium chloride was only found in the receiving flask, in 30% yield, along with lutidinium chloride (formed from the transfer of lutidine from the parent flask to the receiving flask). (Figure S31). Products of decomposition of (PSP)Mo complexes, and cobaltocenium salts, were found in the parent flask.

S2.10. Reaction of 1-Cl_3 with Oxidant and NH_3 to yield (PSP)Mo(N)X

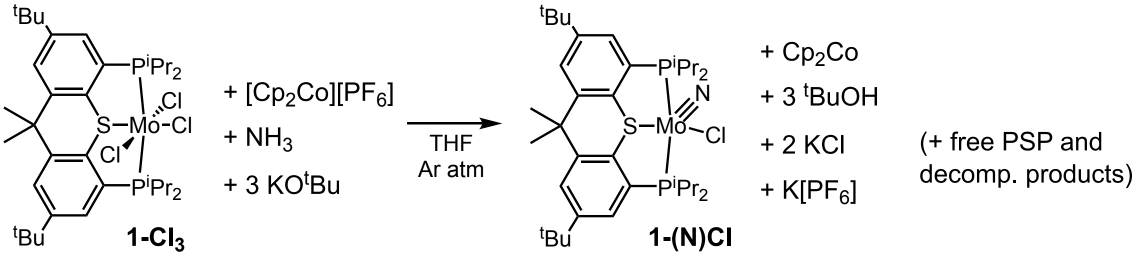

In a J-Young NMR tube (PSP)MoCl_3 (8.6 mg, 0.011 mmol, 1.0 equiv), $[Cp_2Co]PF_6$ (11.1 mg, 0.033 mmol, 3.0 equiv), and KO^{t}Bu (3.7 mg, 0.033 mmol, 3.0 equiv) were weighed, and 0.5 mL THF-d_8 was added. To this mixture, 50 μL of 0.4 M NH_3 solution in THF (0.022 mmol, 2.0 equiv of NH_3) was added. The reaction was shaken, and ^{1}H and ^{31}P{^{1}H} NMR spectra were recorded. Based on ^{31}P chemical shift values, formation of (PSP)Mo(N)X (X= Cl or O^{t}Bu) was observed in 25% yield, along with free PSP ligand and decomposition products (Figure S33 and Figure S34).

S2.11 Independent synthesis of (PSP)Mo(N)Cl/(PSP)Mo(N)I.

In a Strauss flask equipped with a magnetic stir bar, (PSP)Mo(N)I (50 mg, 0.06 mmol, 1.0 equiv) and [LutH]Cl (26.7 mg, 0.19 mmol, 3.0 equiv) were added to THF. The expected product (**1-(NH)ICl**) was filtered through silica gel for purification. However, a 4:1 mixture of (PSP)Mo(N)Cl (^{31}P chemical shift: 77.2 ppm) and (PSP)Mo(N)I (^{31}P NMR chemical shift 79.8 ppm) was isolated (Figure S34).

III. Catalytic ammonia formation reactions

In a 4-mL Kontes-valve-adapted flask equipped with a magnetic stir bar, (PSP)Mo(N)(I) (2.0 mg, 0.0025 mmol, 1.0 equiv) and [LutH]Cl or [LutH]OTf (19.7 mg or 35.4 mg respectively, 0.14 mmol, 55 equiv) were weighed. To the vial, 1-2 mL of THF was then added and stirred. In another vial, Cp_2Co (19 mg, 0.10 mmol, 40 equiv) or $Cp^*{}_2Co$ (34 mg, 0.10 mmol, 40 equiv) was weighed and dissolved in 2 mL THF. Using a 1-mL syringe the solution of Cp_2Co or $Cp^*{}_2Co$ was added dropwise to the flask containing the complex and the acid over the course of one hour. The vial was then capped and stirred for an additional 2 hours. KO^tBu (31 mg, 0.28 mmol, 110 equiv) was weighed and dissolved in 0.1 mL THF and kept aside in a 1 mL syringe. The flask was taken out of the glovebox and the solution was frozen. Under a continuous flow of inert gas (N_2 or Ar) the flask was then opened and the KO^tBu solution was quickly added, and frozen immediately. The valve plug was replaced to the vessel and closed, and the headspace atmosphere was removed under vacuum. The solution was allowed to thaw, and was stirred for 30 min at room temperature. The sealed tube was connected by one side of a T-joint adapter while the other side was connected to another flask containing 2 M HCl in Et_2O (27.5 μL, 0.55 mmol, 220 equiv) solution (head space is removed). Under static vacuum, the volatiles from the parent flask were transferred to the HCl/Et_2O solution which is frozen with liquid nitrogen. The receiving flask was then thawed, and solvent was removed under vacuum. The solid was then dissolved in DMSO-d_6, and the ^1H NMR spectrum was recorded. The yield of NH_4Cl was calculated based on ^1H NMR integrals using 1,3,5-trimethoxybenzene as external standard.

IV. NMR spectra

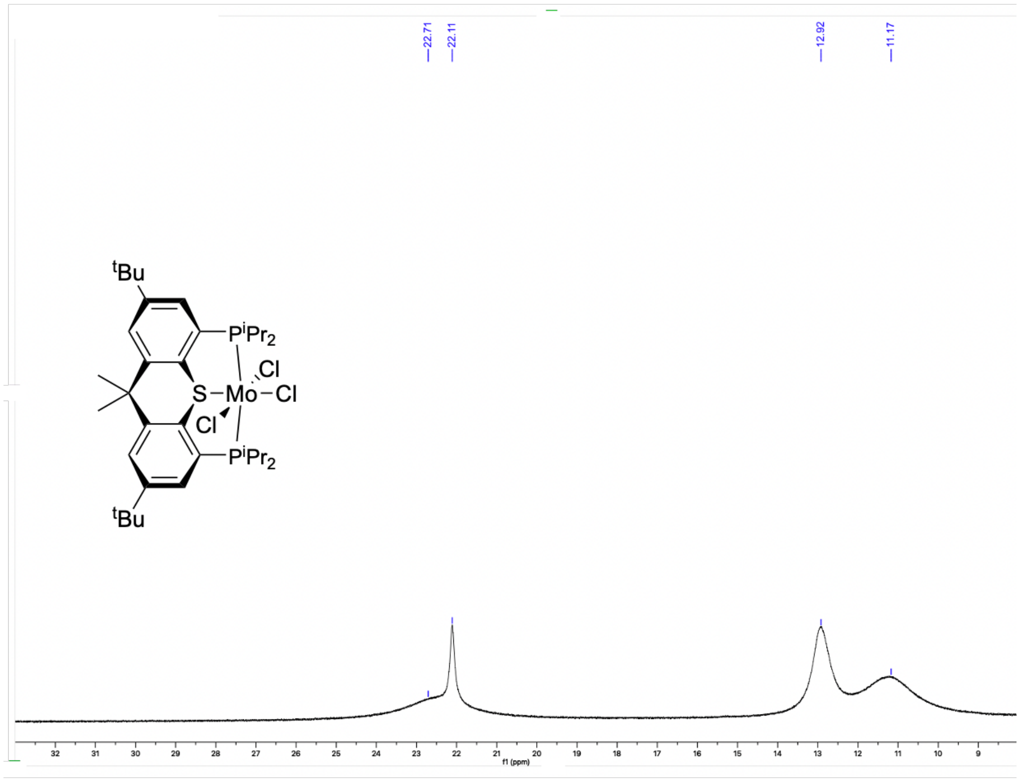

Figure S5. ^{1}H NMR spectrum (paramagnetic resonances) of **1-Cl$_3$**

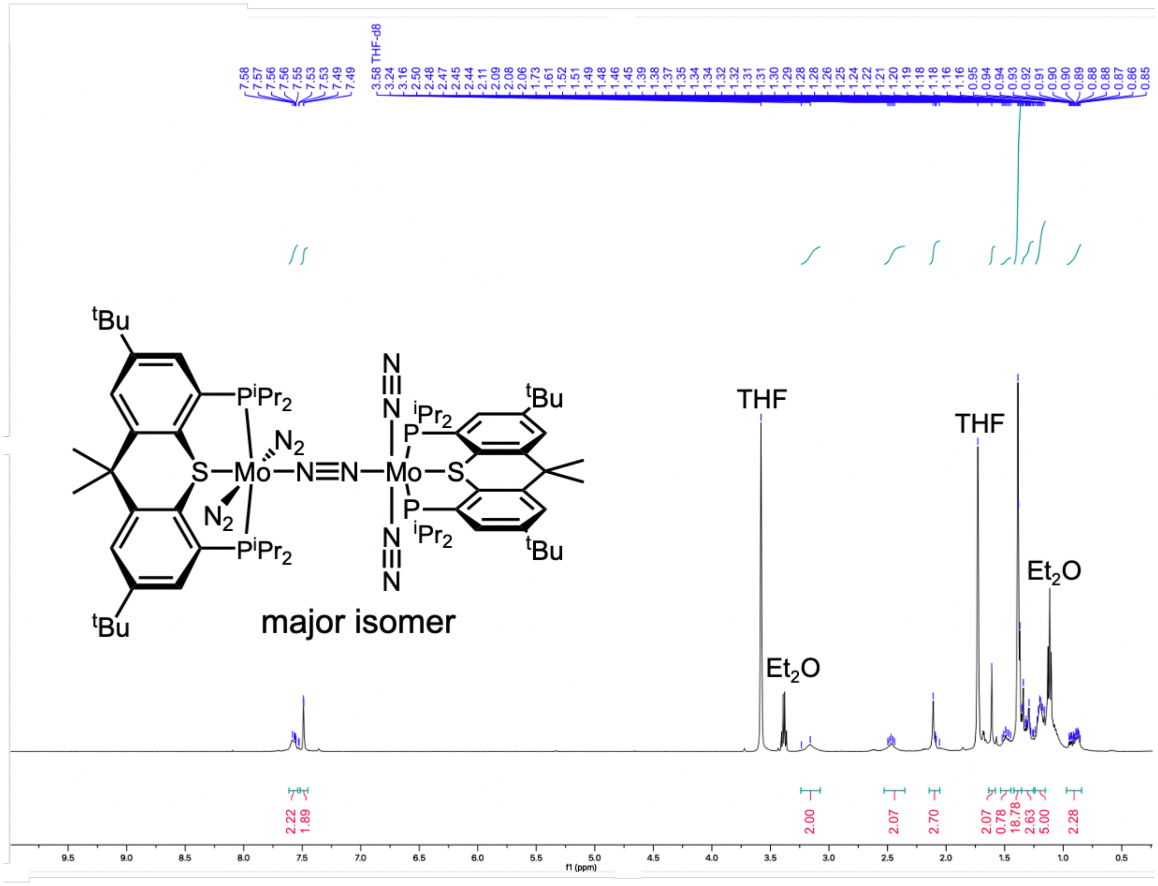

Figure S6. ^{1}H NMR spectrum of **2** (major isomer) along with **3** and other unidentified products

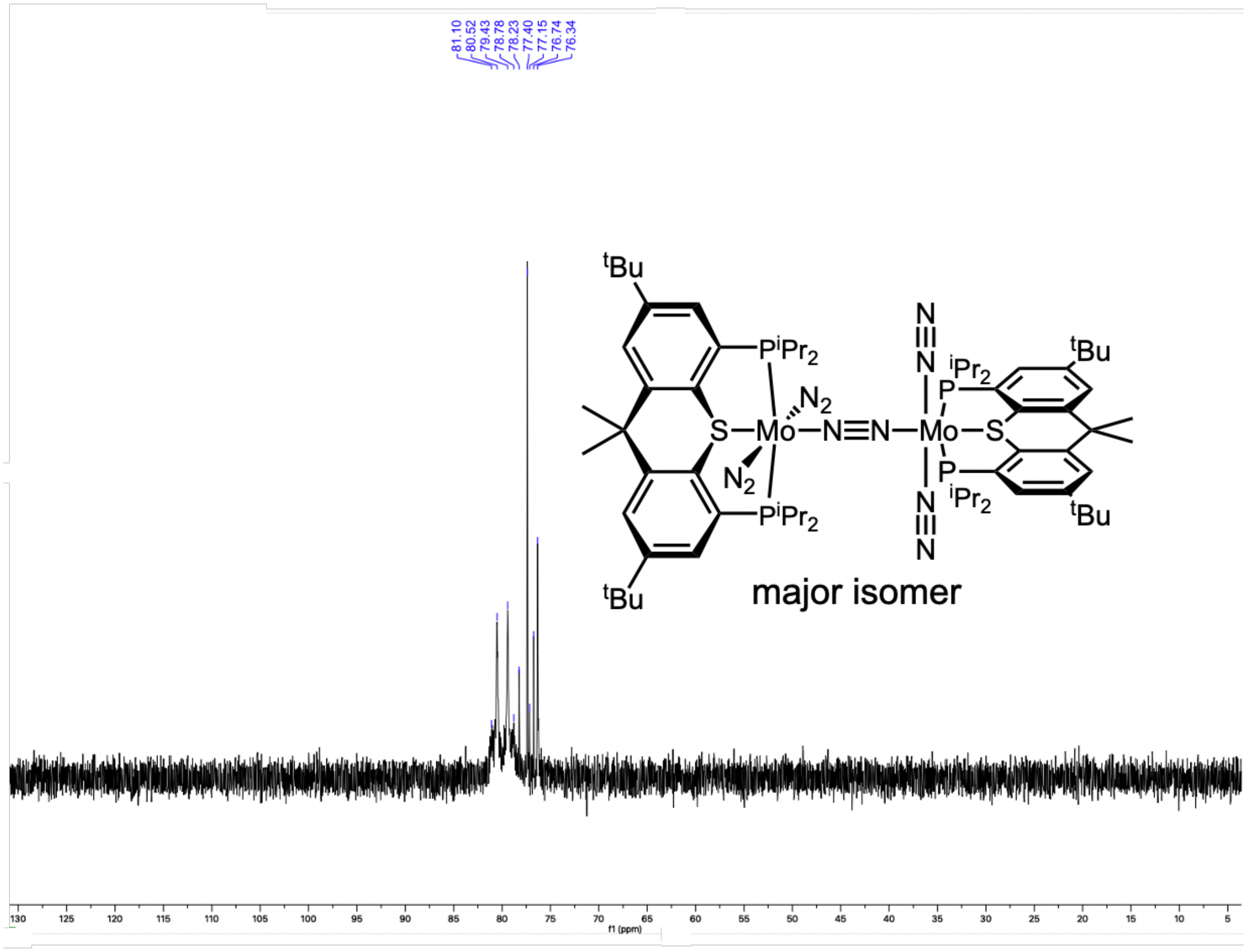

Figure S7. $^{31}P\{^1H\}$ NMR spectrum of **2** (major isomer) along with **3** and other unidentified products

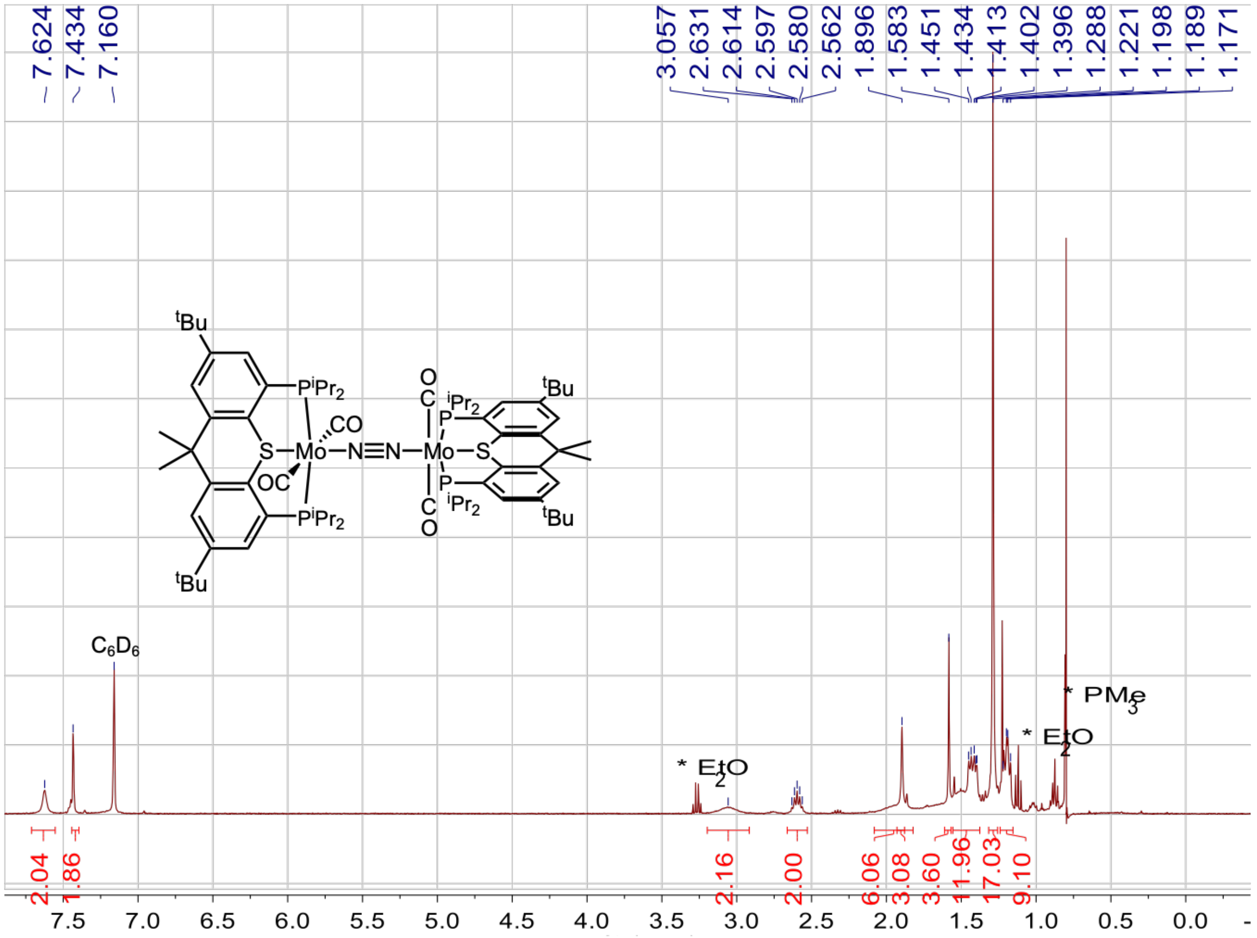

Figure S8. ^{1}H NMR spectrum of **4** along with **5** and other unidentified products

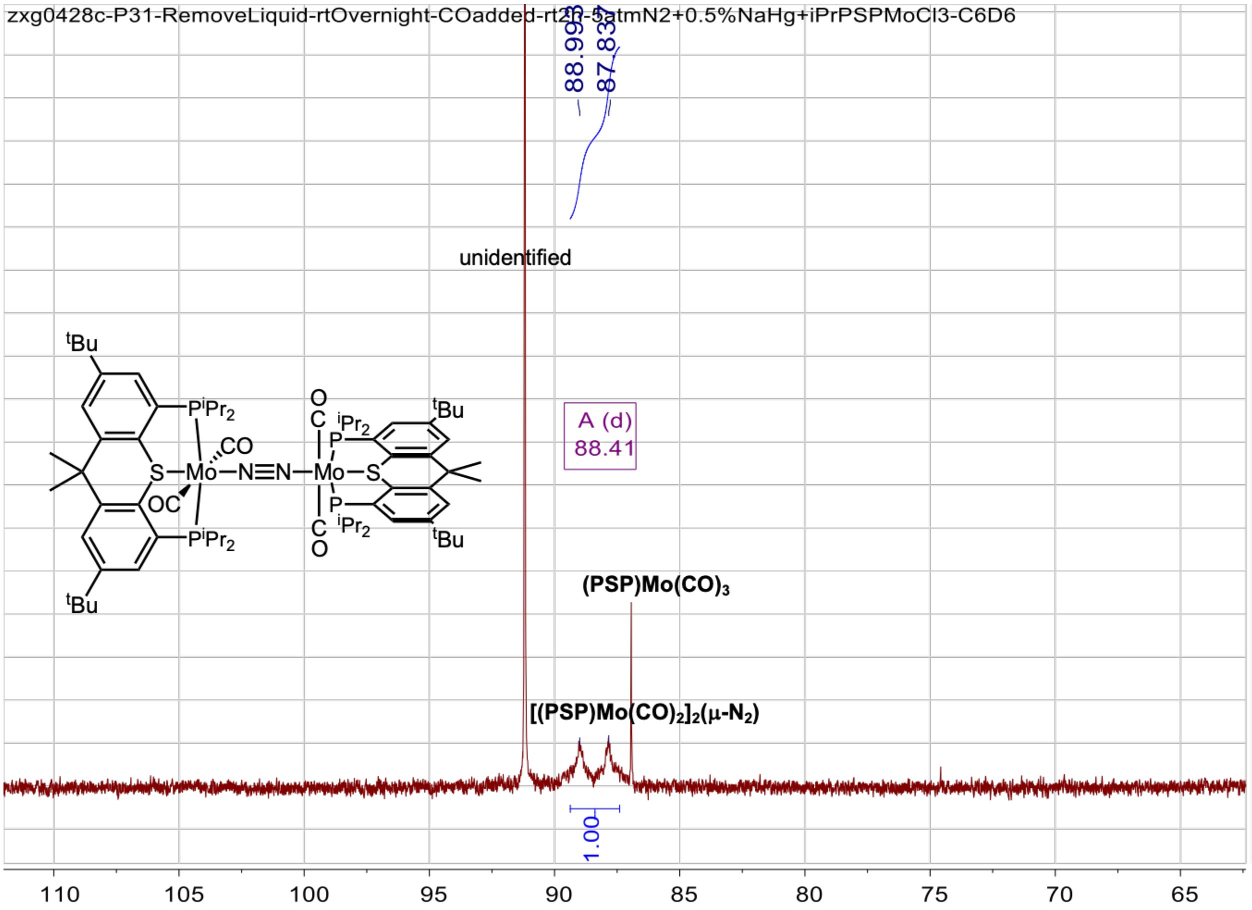

Figure S9. ^{31}P{^{1}H} NMR spectrum of **4**, with **5** and other unidentified products

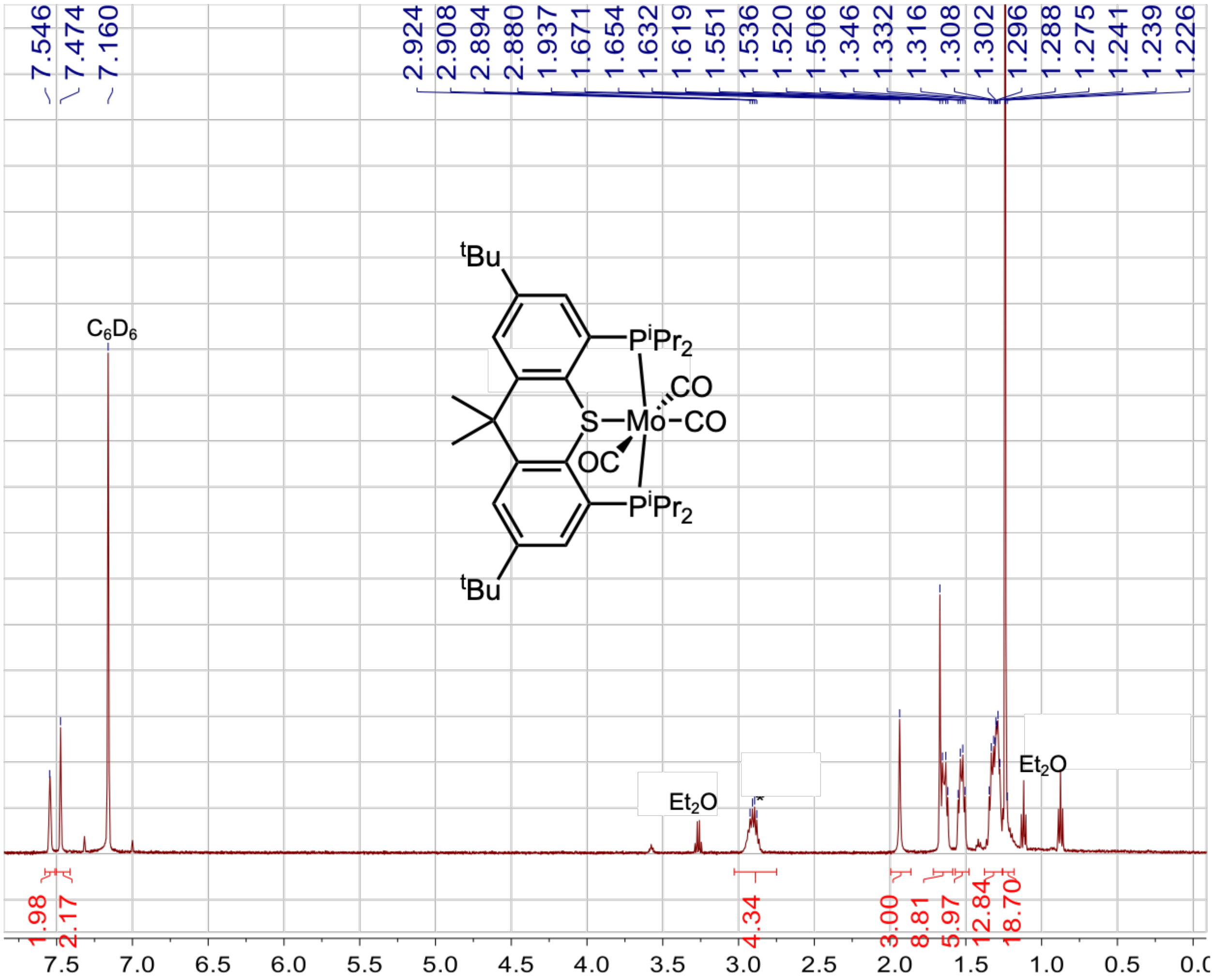

Figure S10. ^{1}H NMR spectrum of (PSP)Mo(CO)$_3$ (**5**)

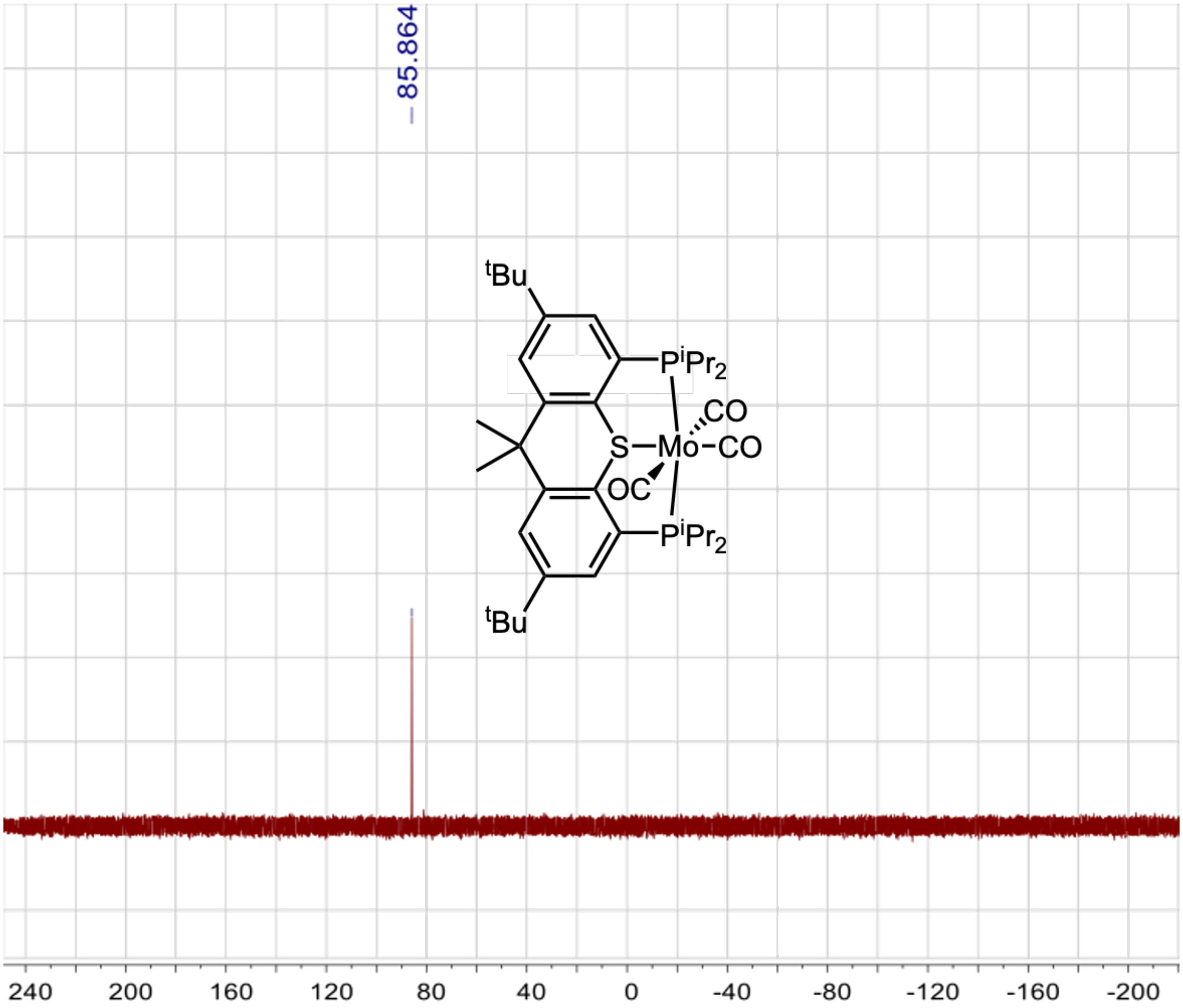

Figure S11. $^{31}P\{^1H\}$ NMR spectrum of (PSP)Mo(CO)$_3$ (**5**)

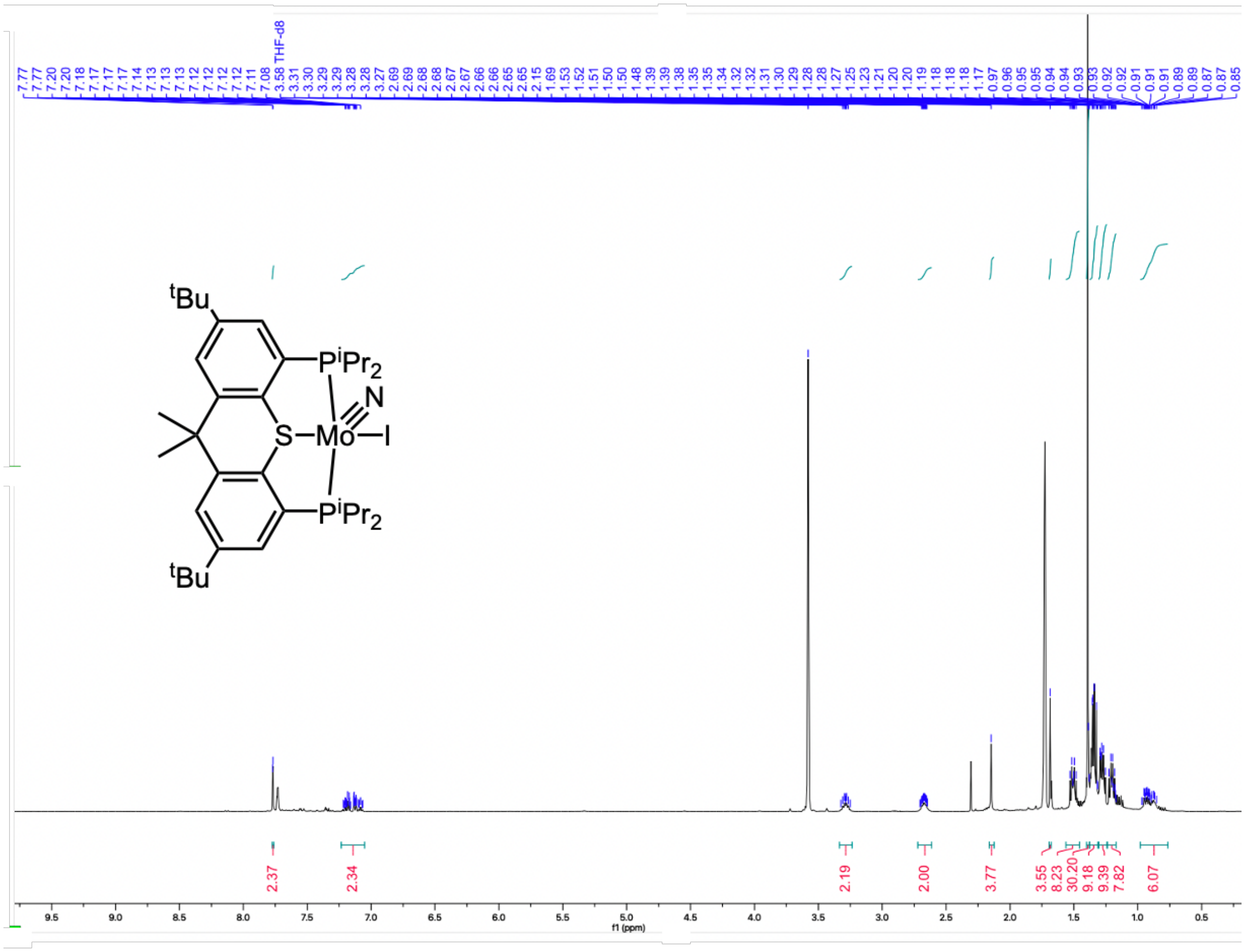

Figure S12. ^{1}H NMR spectrum of **1-(N)I**

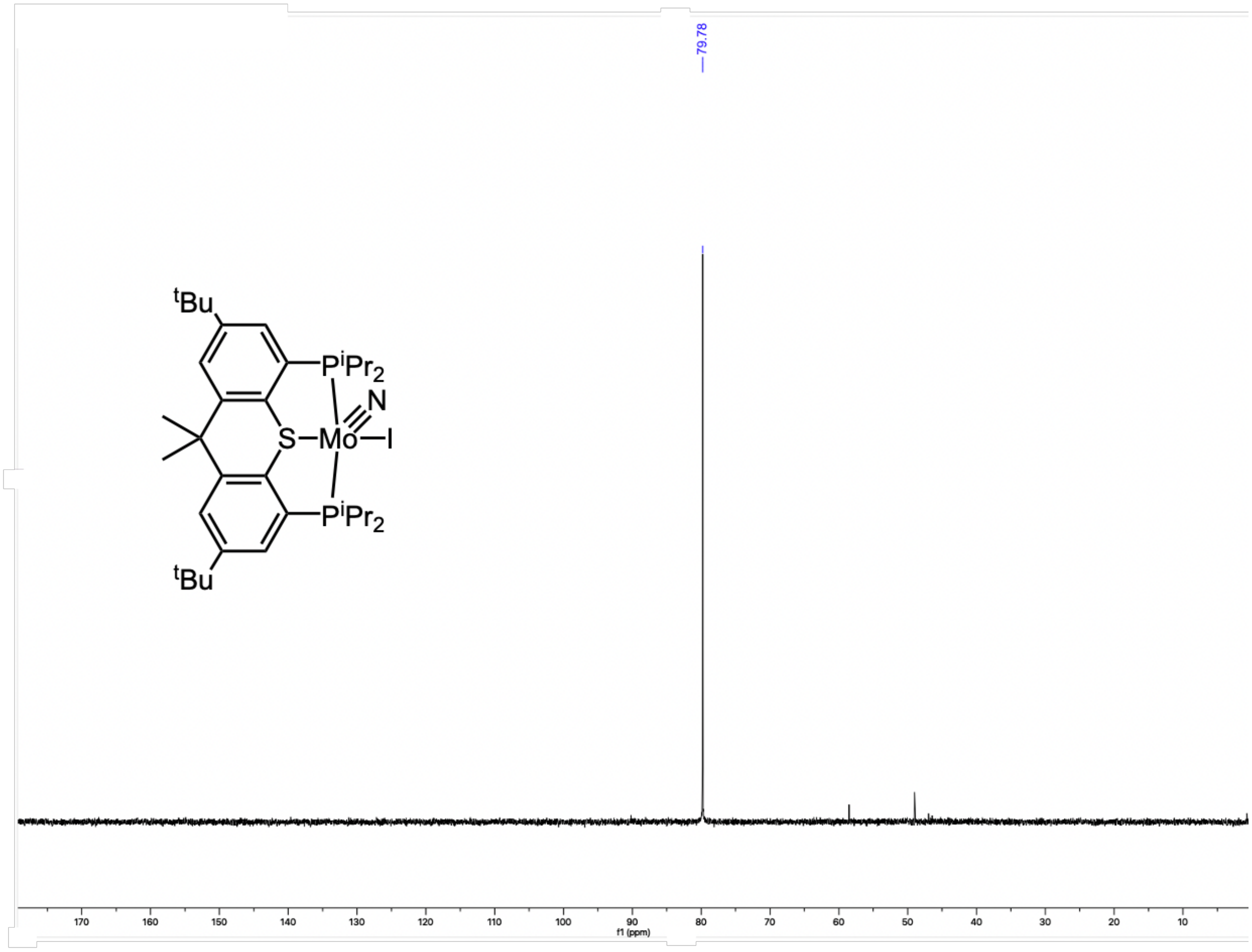

Figure S13. $^{31}P\{^1H\}$ NMR spectrum of **1-(N)I**

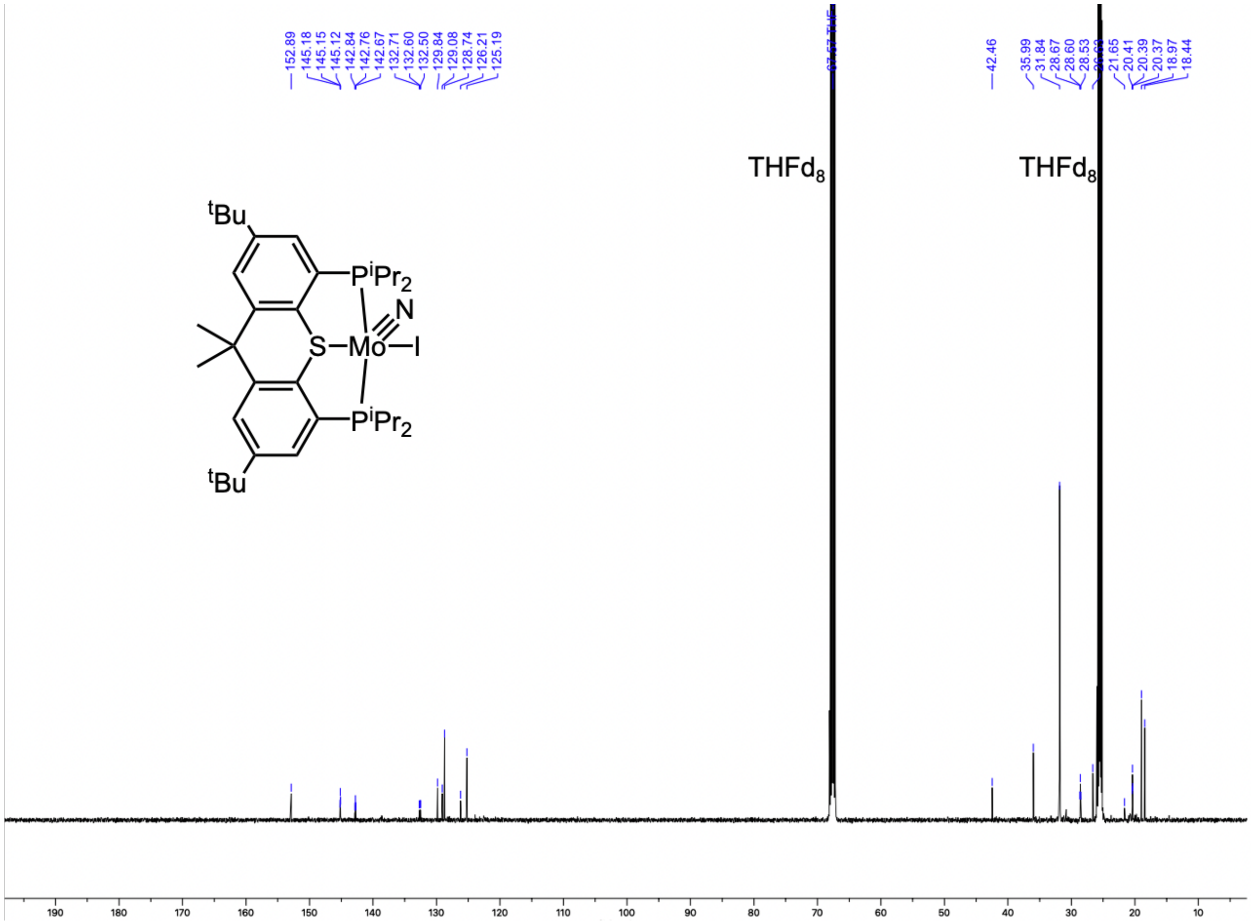

Figure S14. $^{13}C\{^{1}H\}$ NMR spectrum of **1-(N)I**

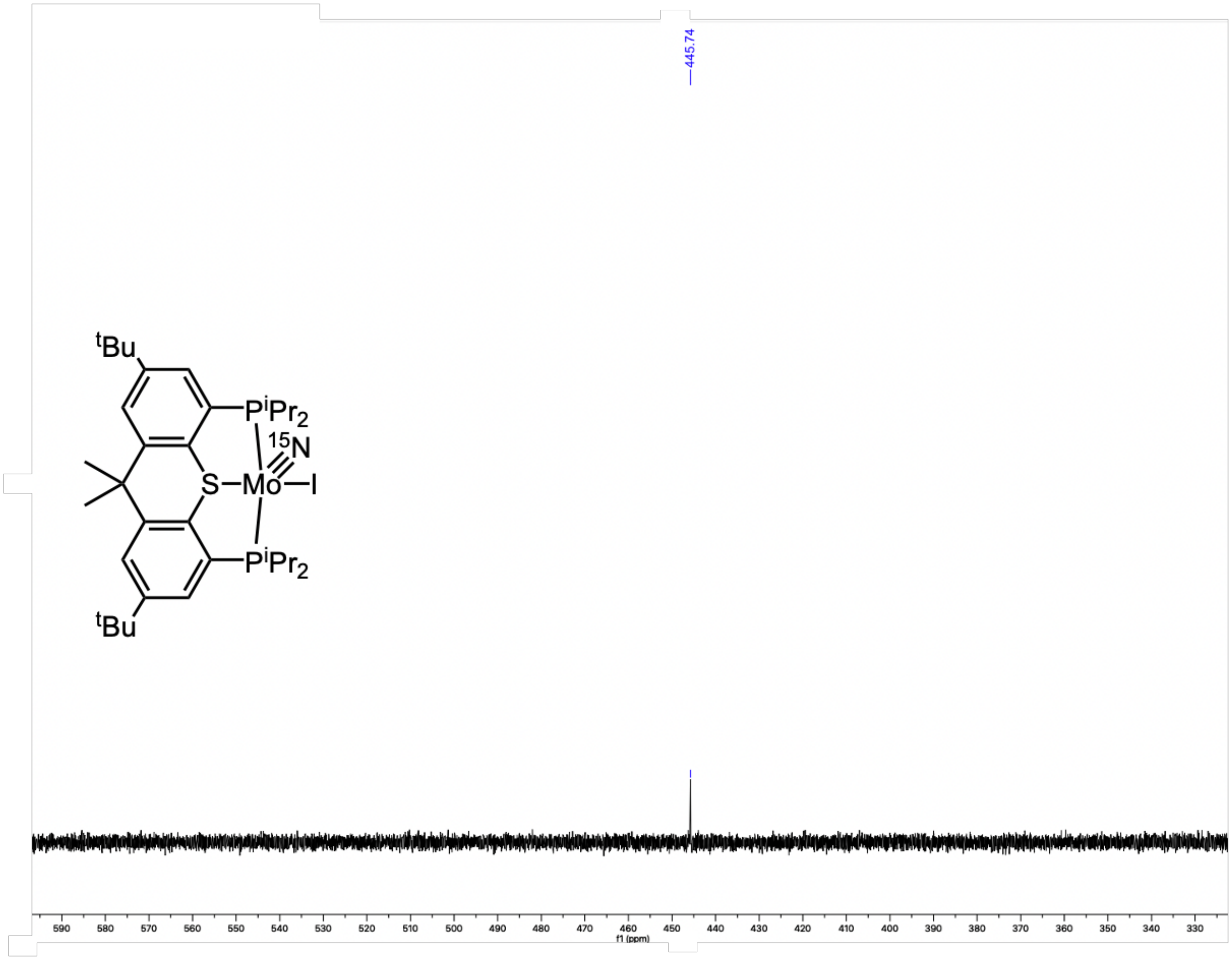

Figure S15. ^{15}N NMR spectrum of **1-(N)I**

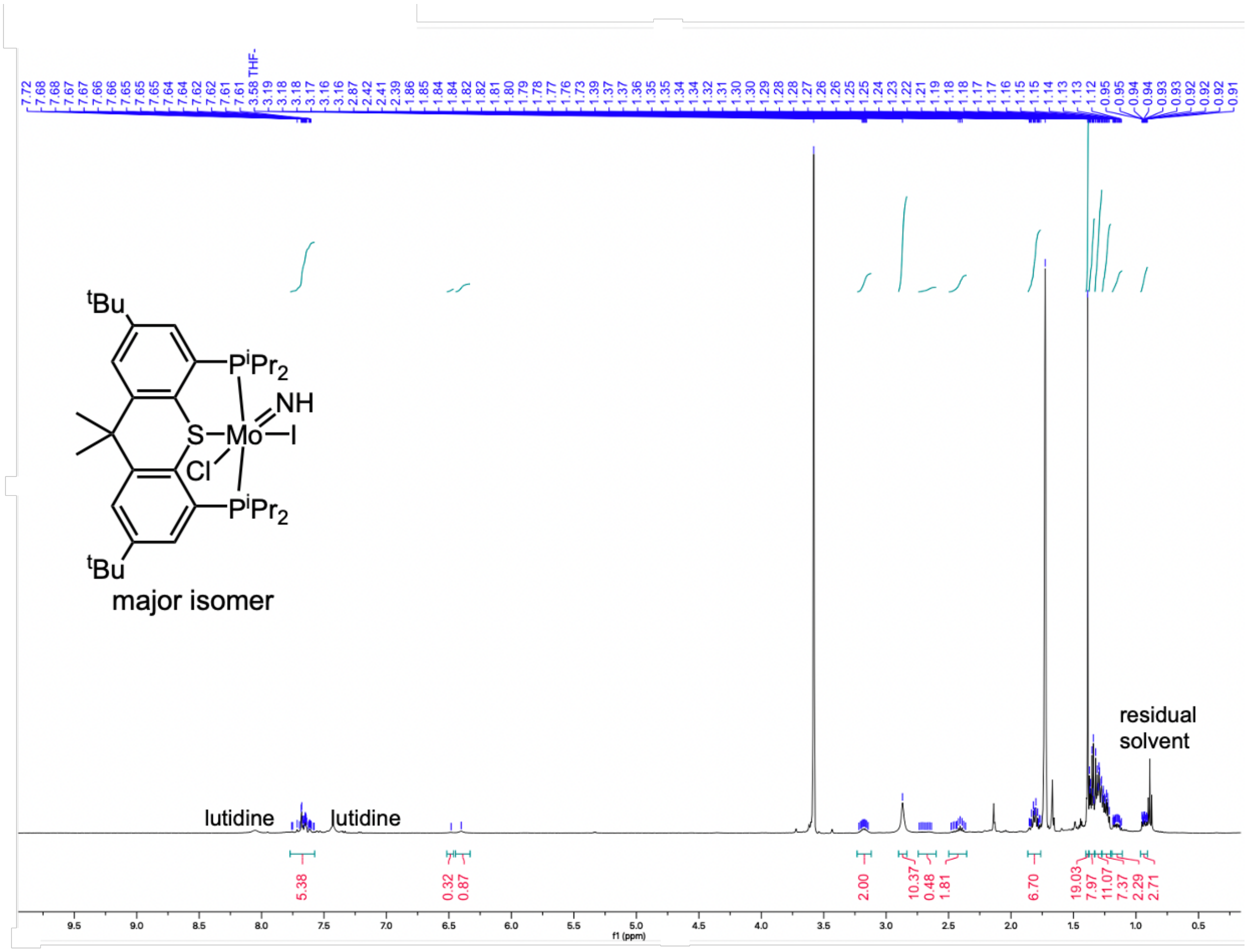

Figure S16. ^{1}H NMR spectrum of **1-(NH)(I)Cl** (major species along with minor species presumed to be **1-(NH)Cl$_2$**)

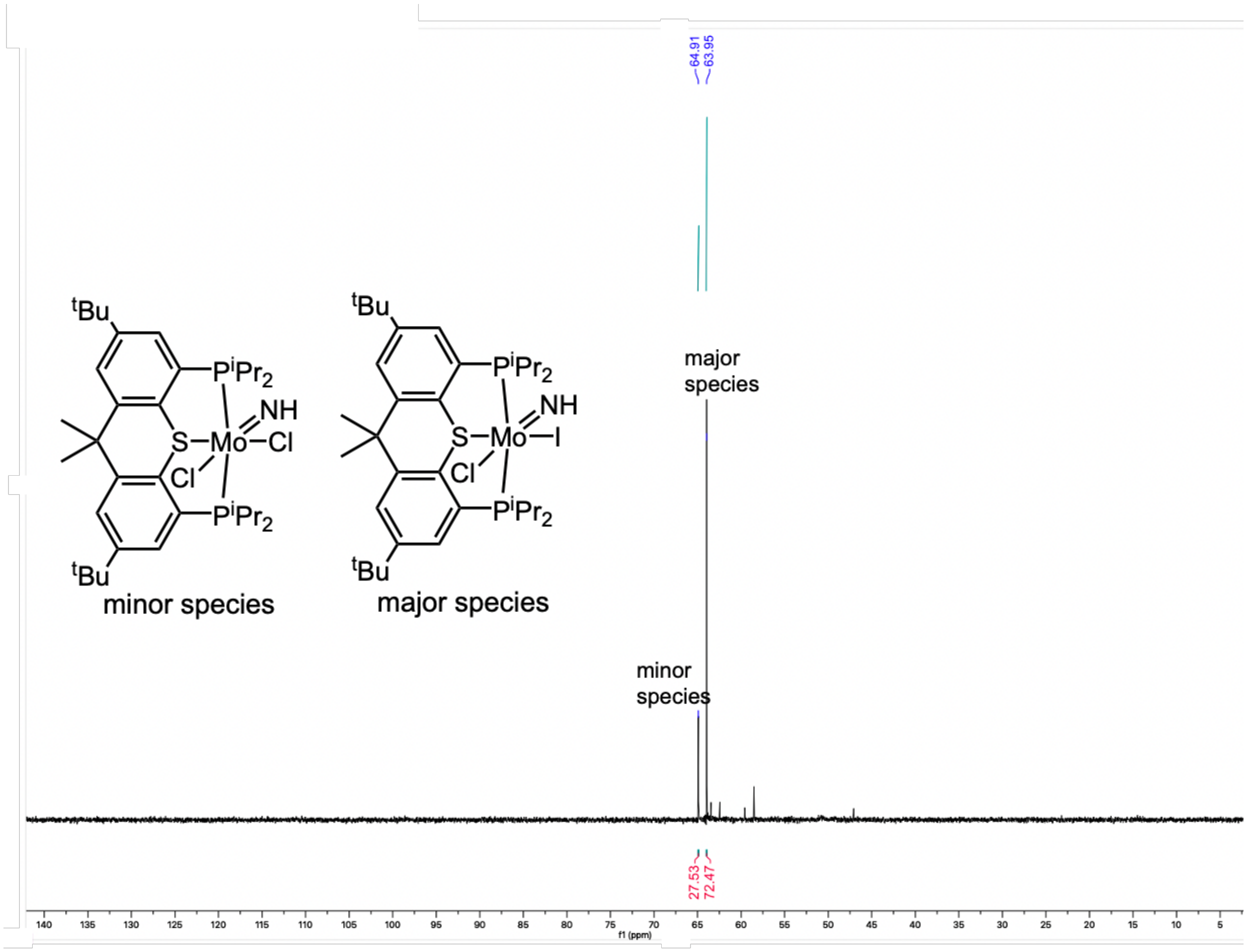

Figure S17. ^{31}P{^{1}H} NMR spectrum of **1-(NH)(I)Cl** (major isomer along with minor species presumed to be **1-(NH)Cl$_2$**)

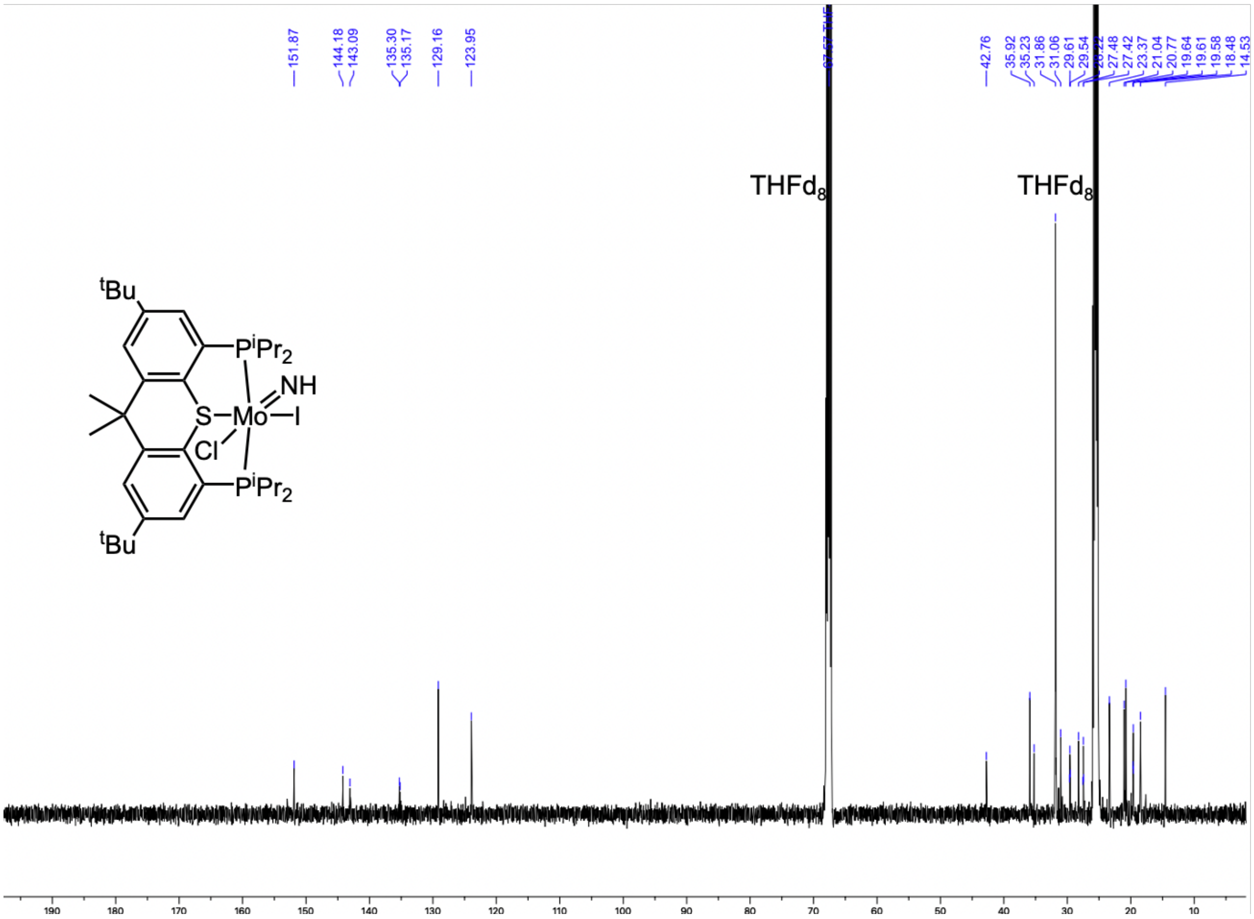

Figure S18. $^{13}C\{^1H\}$ NMR spectrum of **1-(NH)(I)Cl** (major isomer along with minor species presumed to be **1-(NH)Cl₂**)

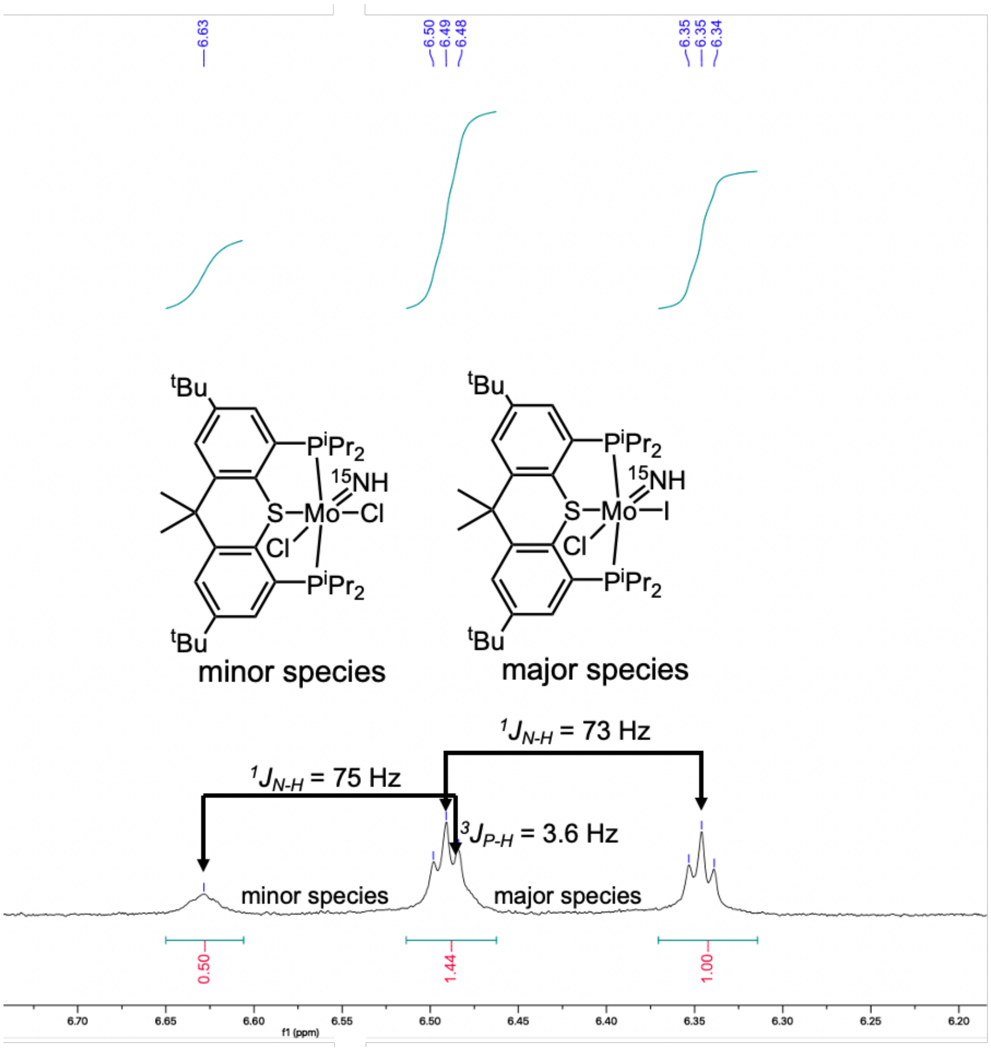

Figure S19. Partial ^{1}H NMR spectrum (N-H region) of **1-(^{15}NH)(I)Cl** and minor species presumed to be **1-(^{15}NH)Cl$_2$**)

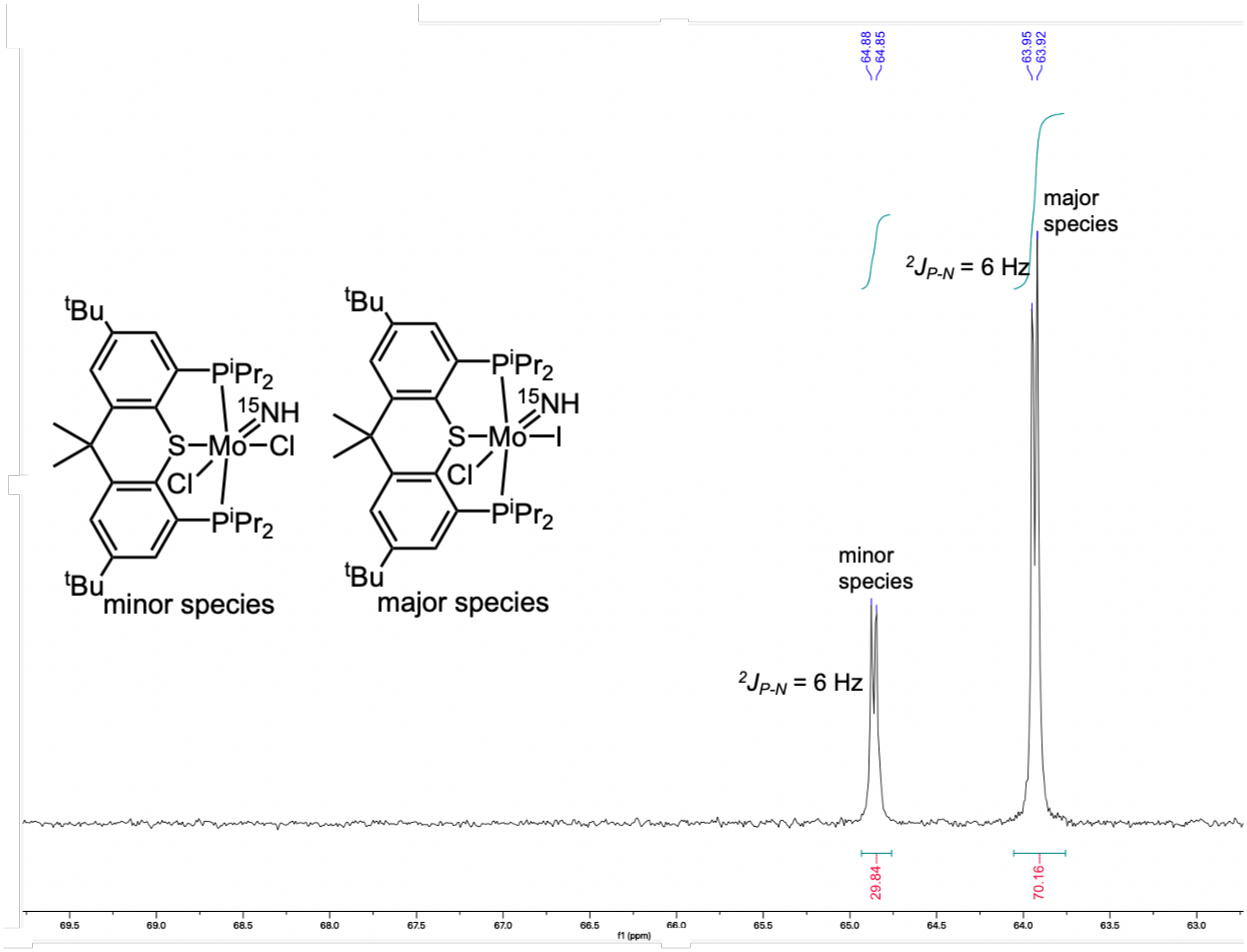

Figure S20. $^{31}P\{^1H\}$ NMR spectrum of **1-(^{15}NH)(I)Cl** (major isomer along with minor species presumed to be **1-(^{15}NH)Cl$_2$**)

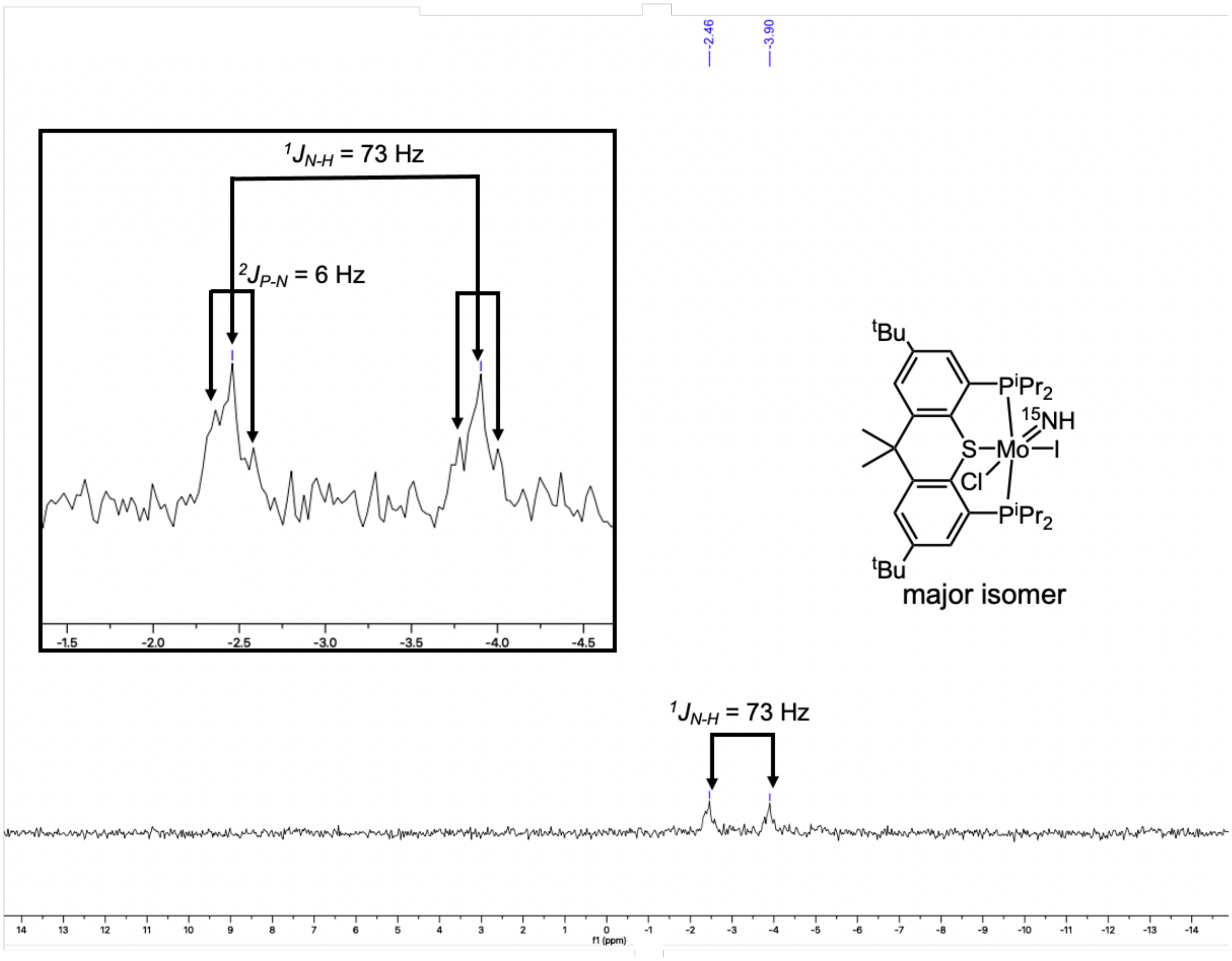

Figure S21. ^{15}N NMR spectrum of **1-(^{15}NH)(I)Cl** (major species)

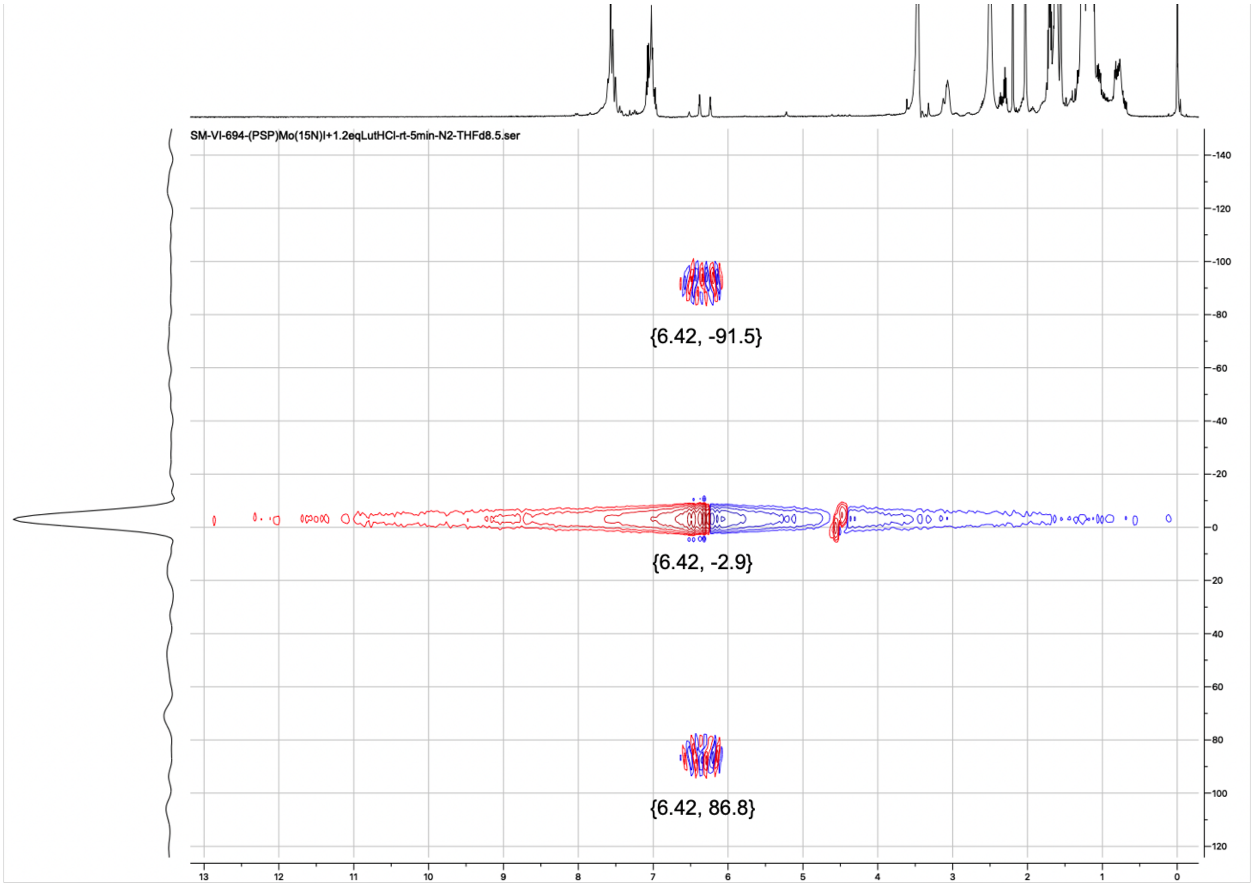

Figure S22. ^{1}H-^{15}N HSQC of **1-(^{15}NH)(I)Cl**

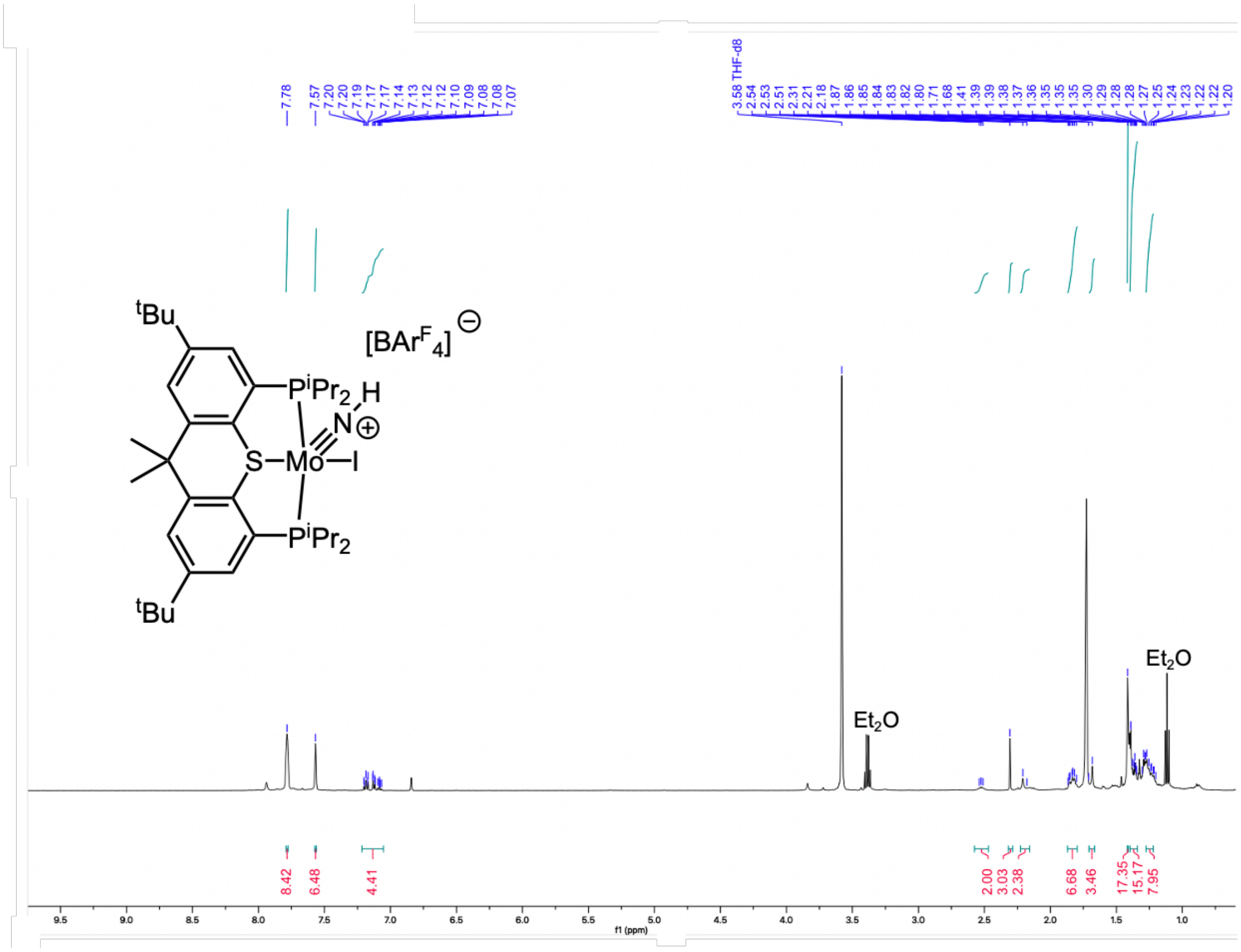

Figure S23. ^{1}H NMR spectrum of **[1-(NH)I][BAr^F$_4$]**

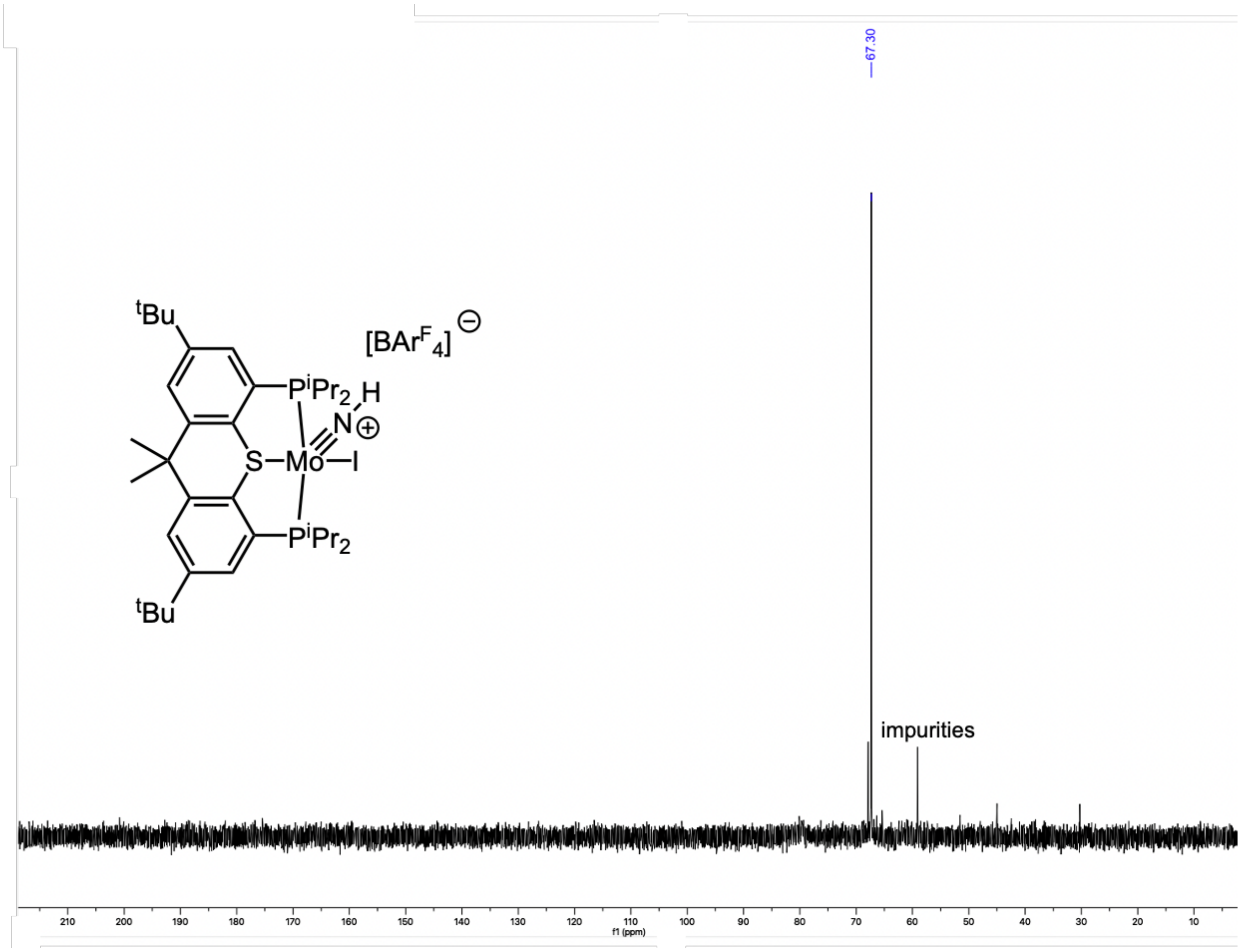

Figure S24. ${}^{31}P\{{}^{1}H\}$ NMR spectrum of **[1-(NH)I][BAr$^{F}_{4}$]**

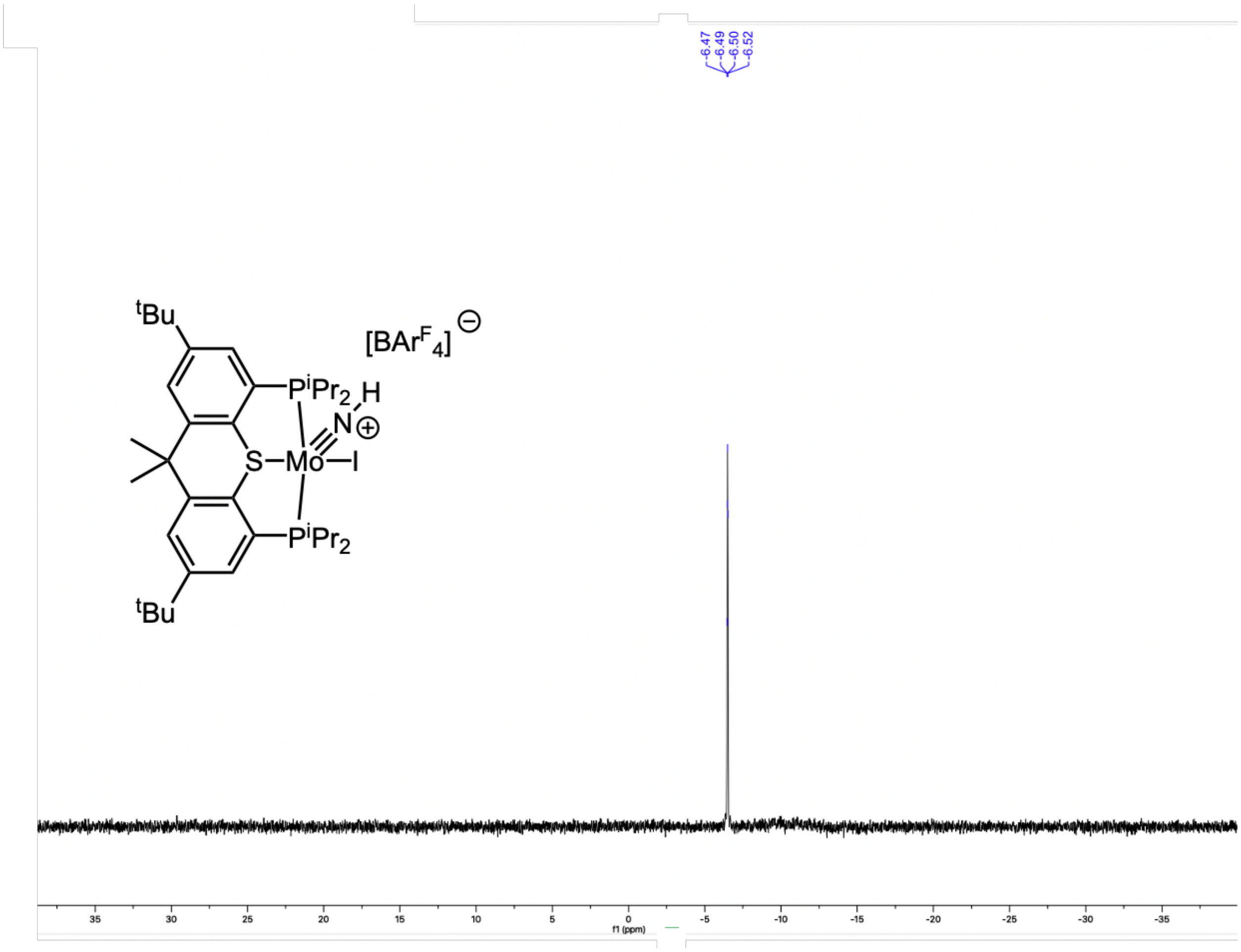

Figure S25. ^{11}B NMR spectrum of **[1-(NH)I][BAr^F$_4$]**

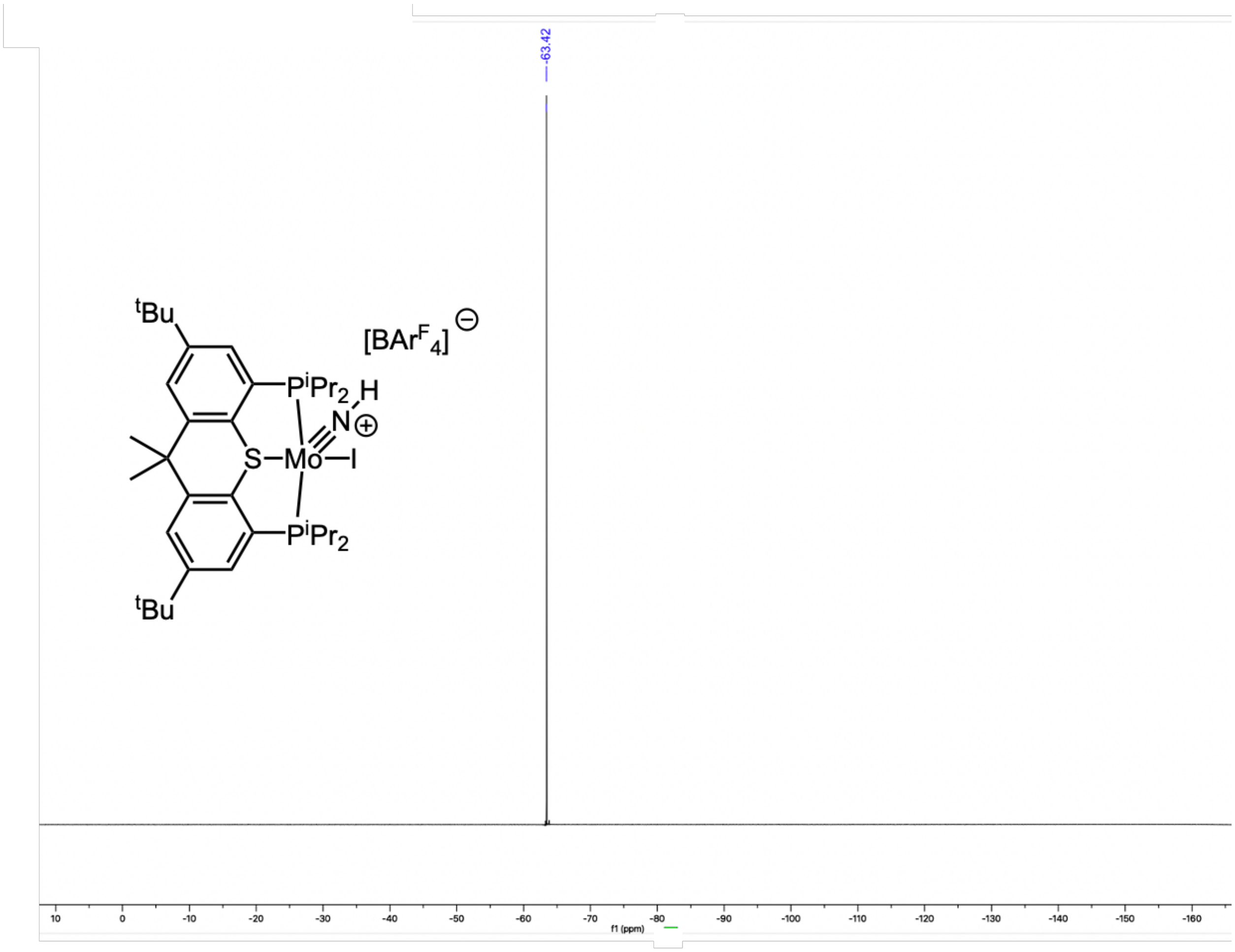

Figure S26. ^{19}F NMR spectrum of **[1-(NH)I][BAr^F$_4$]**

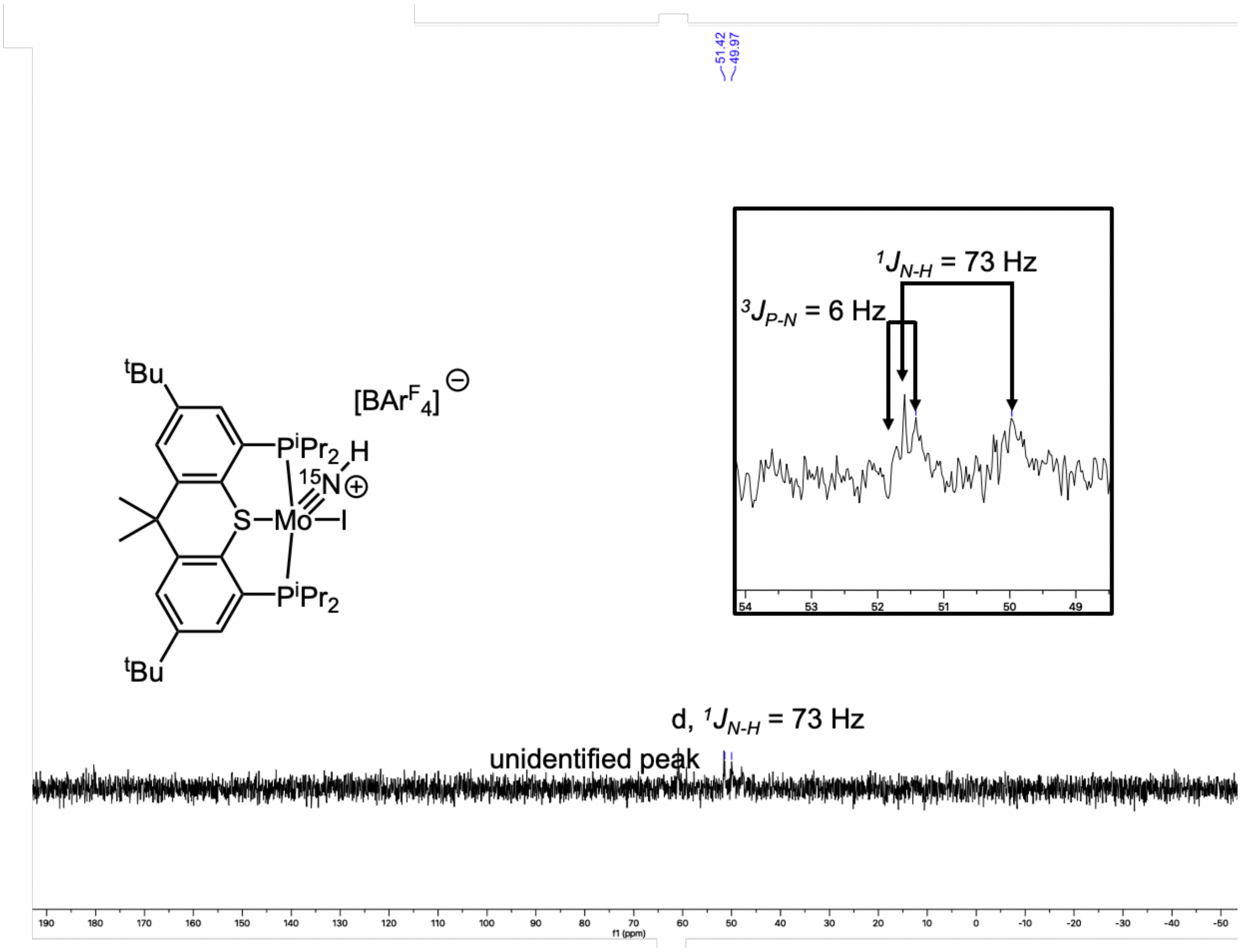

Figure S27. ^{15}N NMR spectrum of **[1-(^{15}NH)I][BAr$^F{}_4$]**

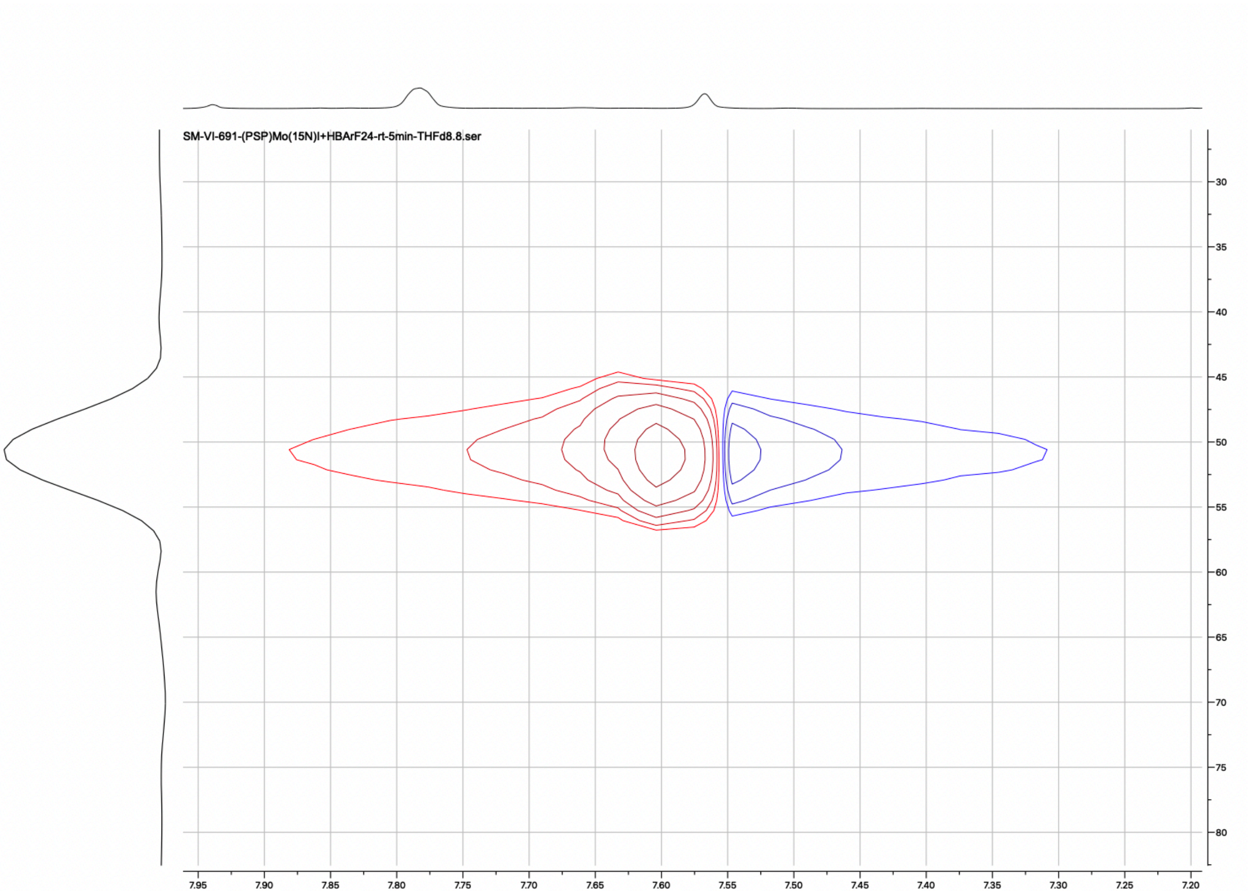

Figure S28. ^{1}H-^{15}N HSQC of **[1-(^{15}NH)I][BAr$^{F}{}_{4}$]**

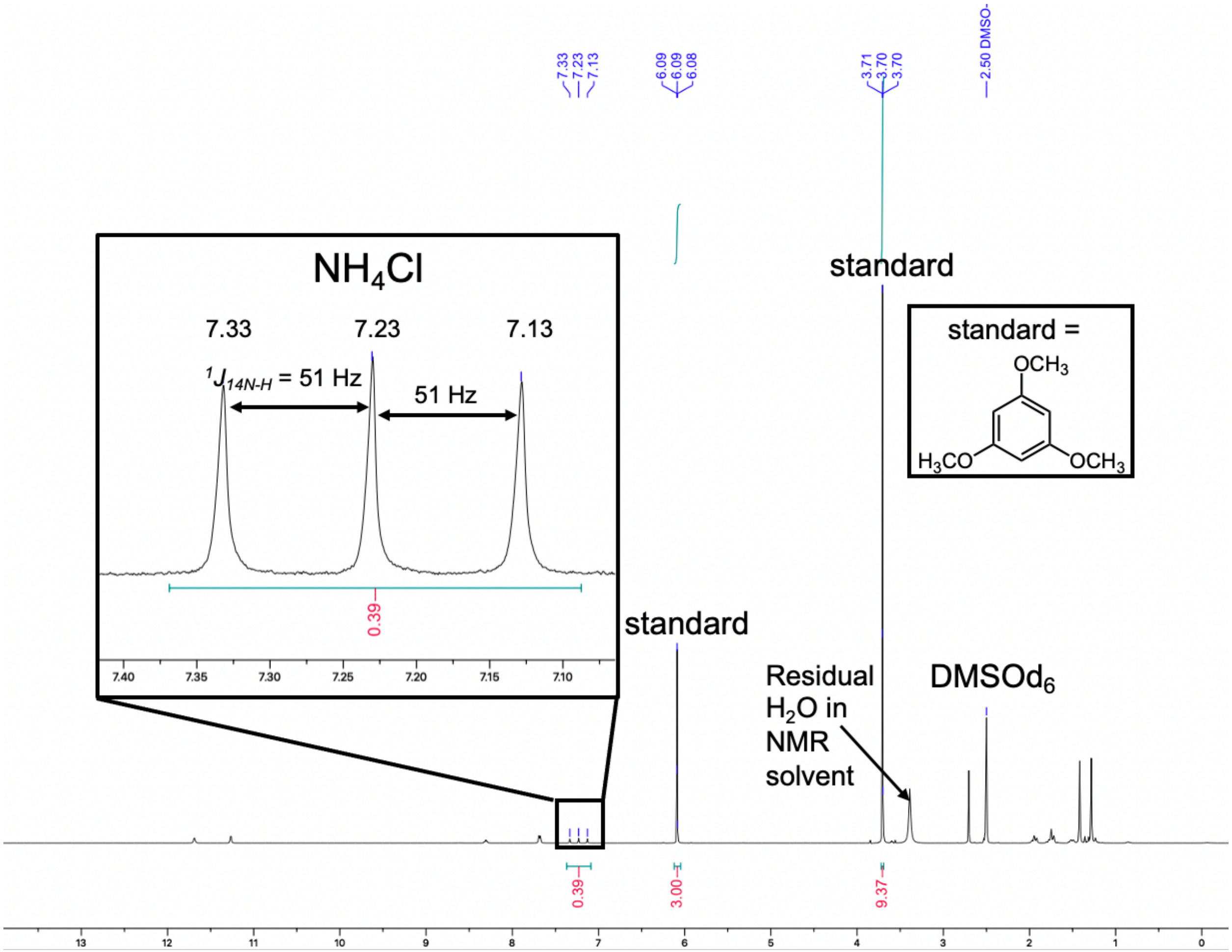

Figure S29. ^{1}H NMR spectrum of trapped NH_4^+ from the reaction of 1-(NH)(I)Cl with TEMPO-H (reaction scheme S2.8.1.2)

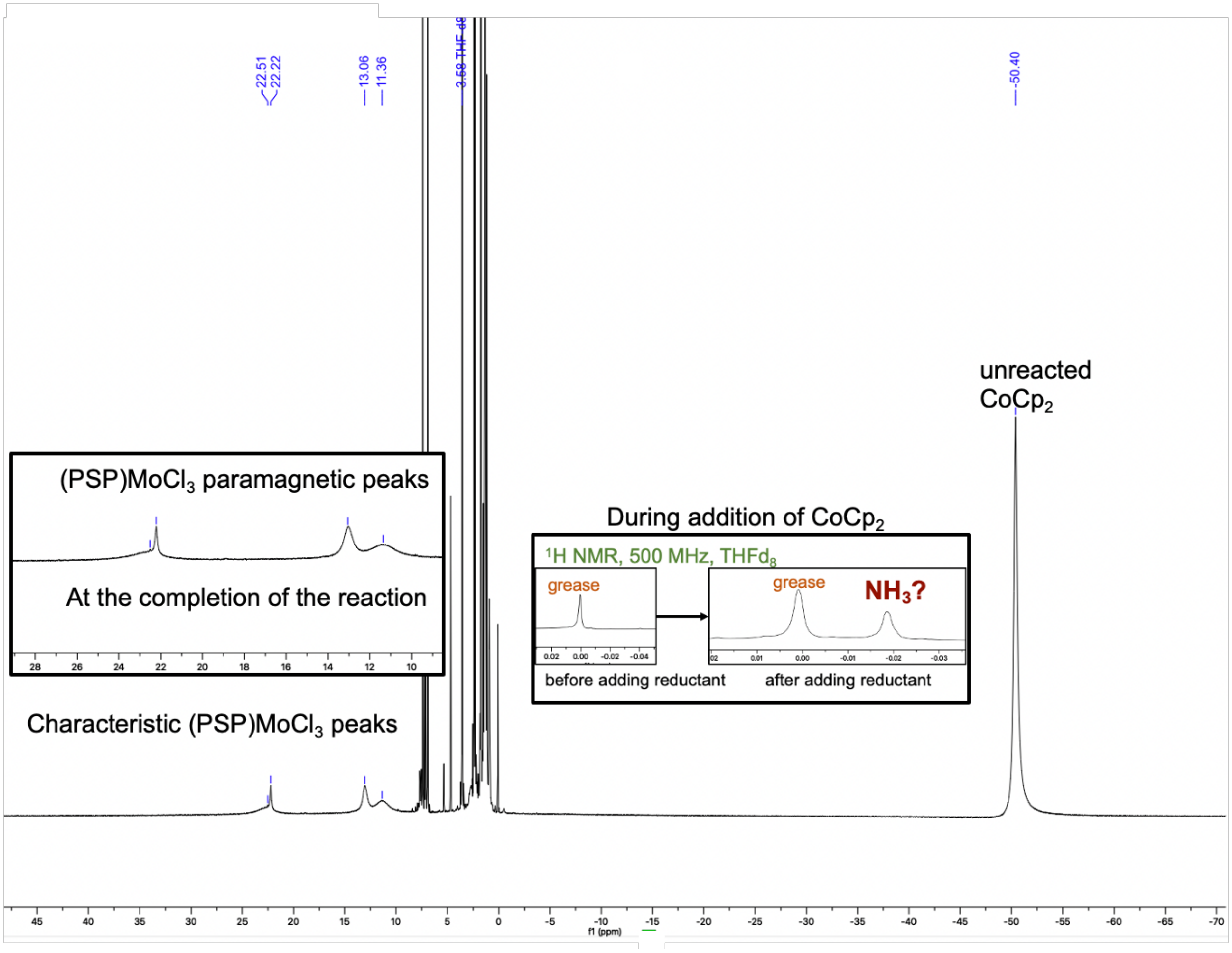

Figure S30. ^{1}H NMR spectrum of addition of $CoCp_2$ to (PSP)Mo(NH)(I)Cl: Stoichiometric generation of NH_3 and (PSP)$MoCl_3$

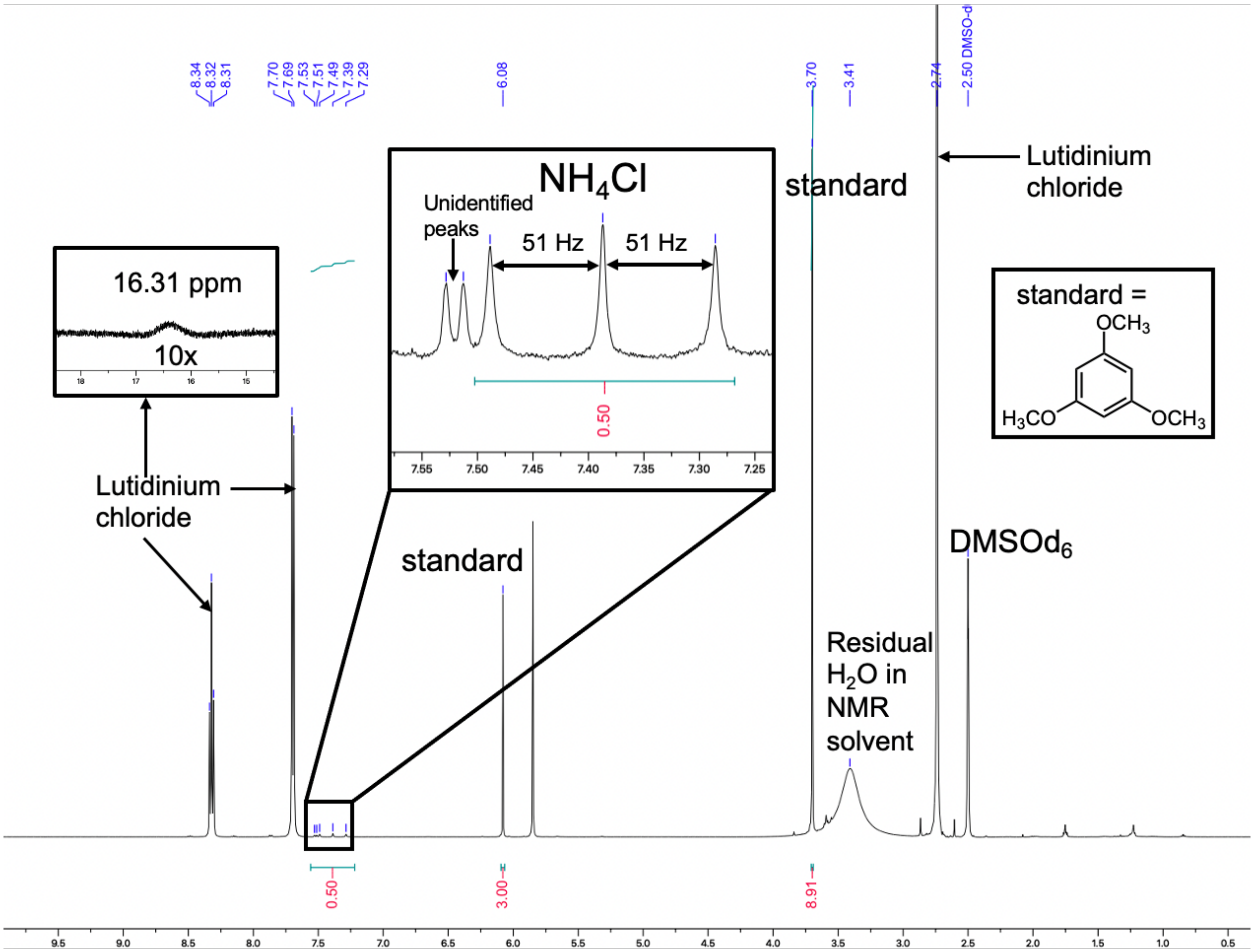

Figure S31. ^{1}H NMR spectrum of the trapped NH_4^+ along with lutidinium chloride (reaction scheme: S2.9.2): addition of $CoCp_2$ to (PSP)Mo(NH)(I)Cl (in presence of lutidinium chloride)

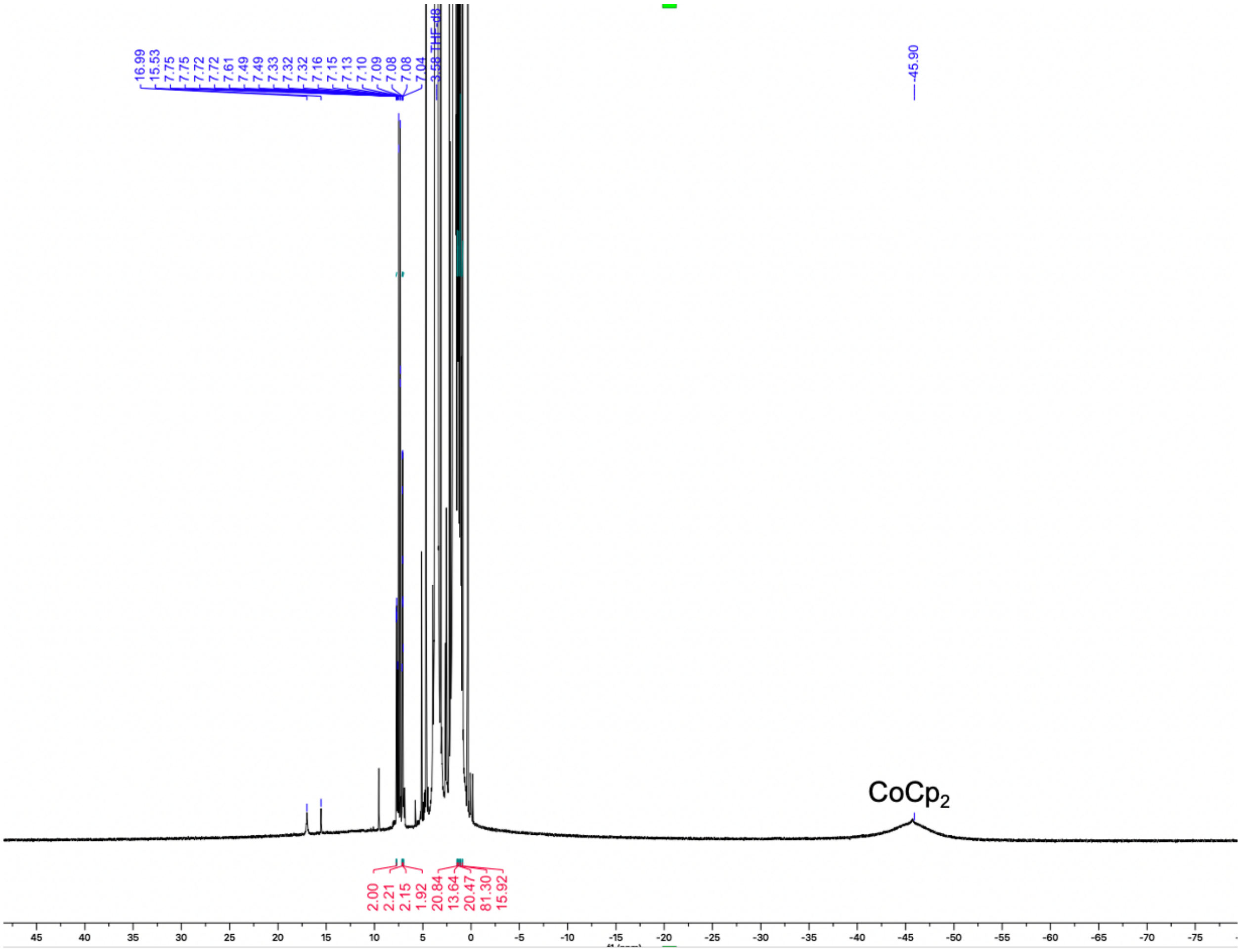

Figure S32. ^{1}H NMR spectrum of a reaction mixture of (PSP)MoCl$_3$, NH$_3$, KO^{t}Bu and [CoCp$_2$]PF$_6$, showing formation of cobaltocene

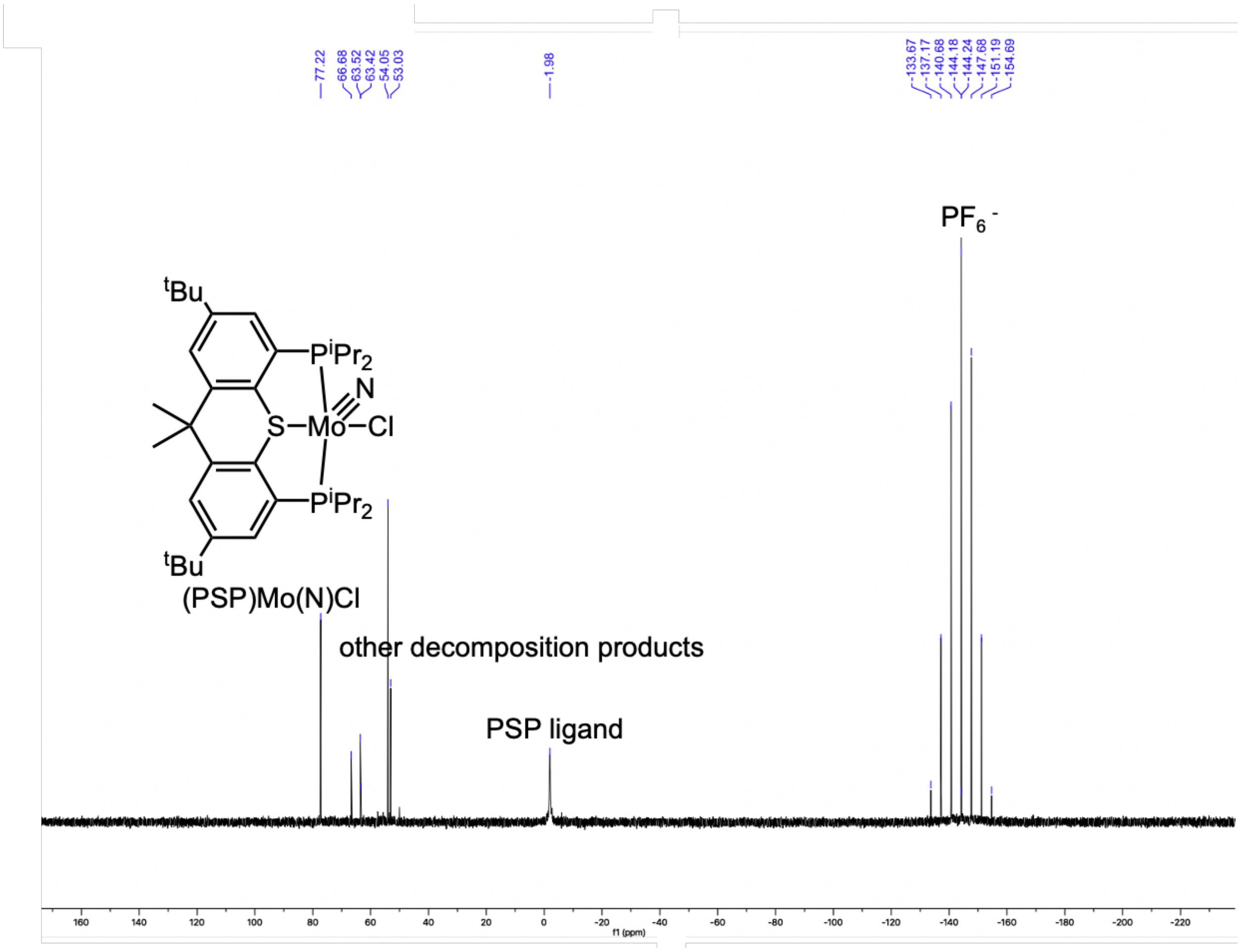

Figure S33. $^{31}P\{^{1}H\}$ NMR spectrum of a reaction of (PSP)MoCl$_3$, NH$_3$, KO^{t}Bu and [CoCp$_2$]PF$_6$

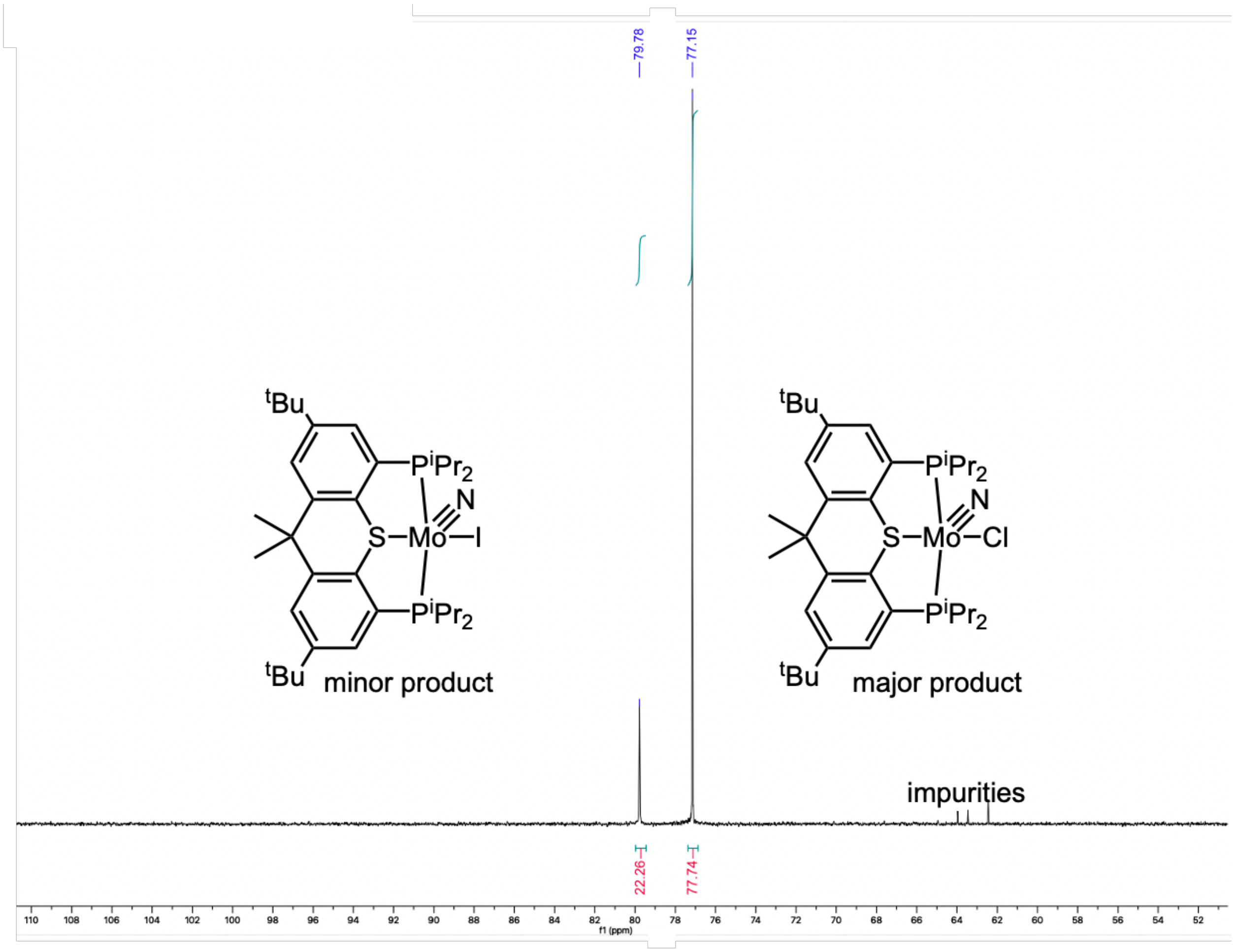

Figure S34. $^{31}P\{^1H\}$ NMR spectrum of a mixture of **1-(N)I** and **1(N)Cl** (major product)

V. Cyclic voltammetry

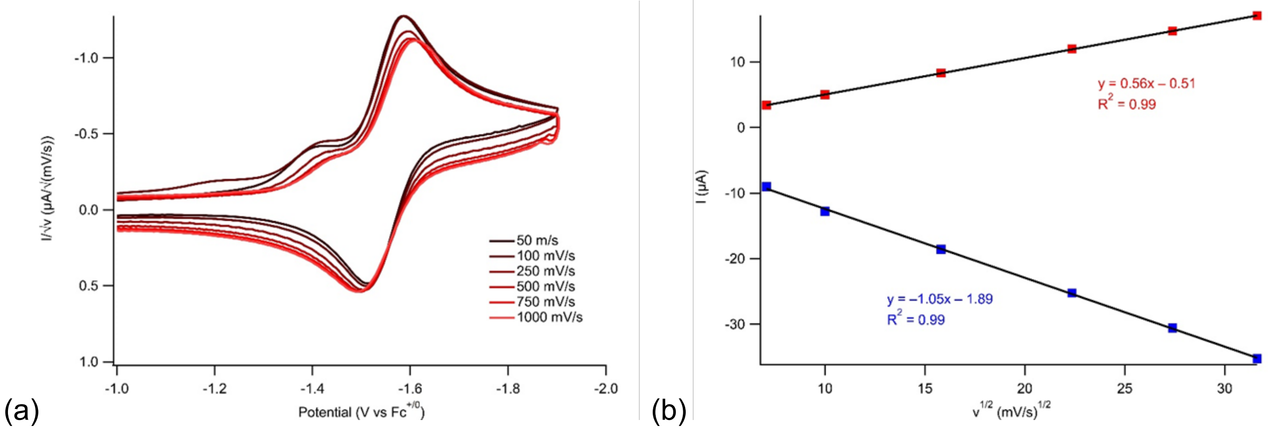

Figure S35. (a) CV of the first reduction of 1 mM (PSP)MoCl$_3$ in THF (0.2 M [^{n}Bu$_4$N][PF$_6$]) under N$_2$ at varying scan rates. Measured ΔE_p of Fc$^{+/0}$ at 100 mV/s is 95 mV and the ΔE_p of the Mo$^{III/II}$ couple at 100 mV/s is 88 mV. The current is divided by the square root of the scan rate such that the good overlay of voltammograms indicates well-behaved diffusion-controlled electron transfer. The pre-wave feature observed is attributed to a small impurity. B) Randles-Sevcik plot comparing the cathodic and anodic peak potentials as a function of the square root of scan rate. Linearity indicates that the redox couple is reversible.

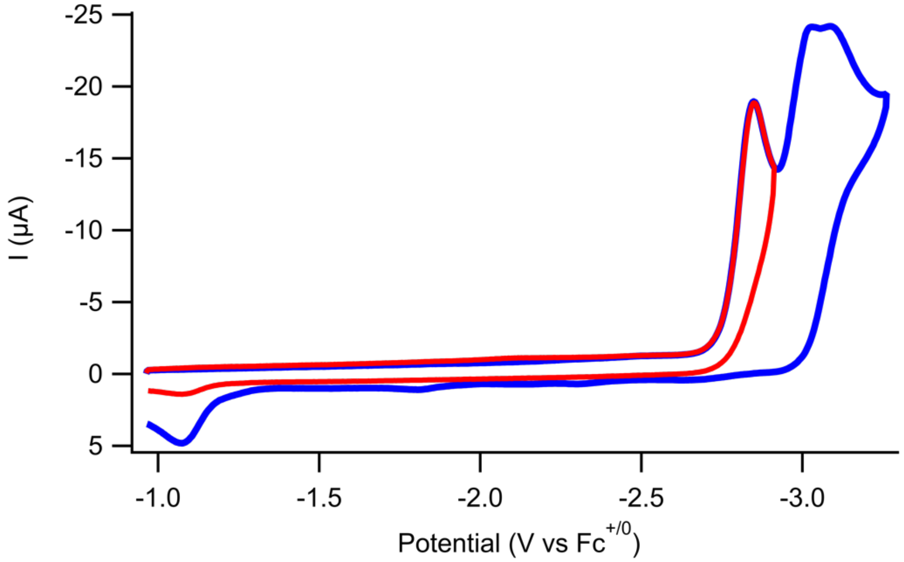

Figure S36. CV of 1 mM (PSP)Mo(N)(I) in 0.2 M [^{n}Bu$_4$N][PF$_6$] in THF under N$_2$ at 100 mV/s sweeping cathodically showing the first (red) and subsequent (blue) irreversible reductions.

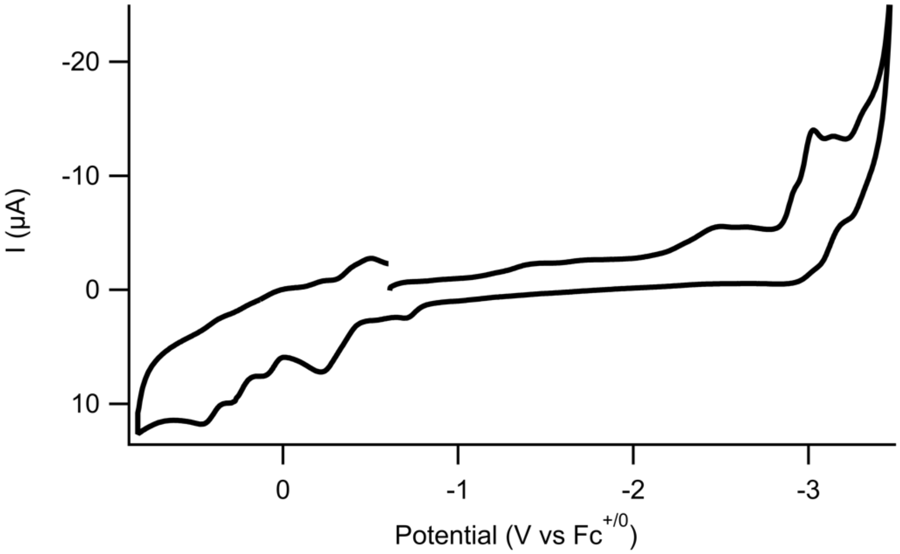

Figure S37. CV of 1 mM (PSP)Mo(NH)(I)(Cl) in 0.2 M [^{n}Bu$_4$N][PF$_6$] in THF under N$_2$ at 100 mV/s sweeping cathodically.

VI. Crystallographic Data

S6. a. Crystallographic data for (PSP)$MoCl_3$ (**1-Cl_3**)

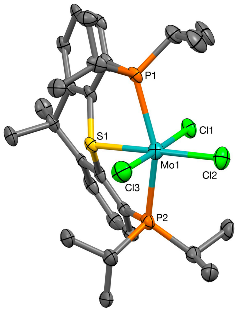

Figure S38. ORTEP representation (50% probability ellipsoids) of the structure of **1-Cl_3** determined by X-ray diffraction; hydrogen atoms and PSP *t*-butyl groups omitted for clarity.

Crystal data and structure refinement for mopspcl3_C2c.

Identification code	mopspcl3_C2c	
Empirical formula	C37 H60 Cl3 Mo O0.50 P2 S	
Formula weight	809.14	
Temperature	120(2) K	
Wavelength	0.71073 Å	
Crystal system	Monoclinic	
Space group	C2/c	
Unit cell dimensions	a = 37.379(3) Å	α = 90°.
	b = 11.6548(11) Å	β = 90.266(3)°.
	c = 37.069(3) Å	γ = 90°.
Volume	16149(3) $Å^3$	
Z	16	
Density (calculated)	1.331 Mg/m^3	
Absorption coefficient	0.680 mm^{-1}	
F(000)	6800	
Crystal size	0.190 x 0.070 x 0.020 mm^3	
Theta range for data collection	1.090 to 26.022°.	
Index ranges	-45<=h<=46, -14<=k<=14, -45<=l<=45	
Reflections collected	77899	
Independent reflections	15917 [R(int) = 0.1292]	
Completeness to theta = 25.242°	100.0 %	
Absorption correction	Semi-empirical from equivalents	
Max. and min. transmission	0.4920 and 0.4088	
Refinement method	Full-matrix least-squares on F^2	
Data / restraints / parameters	15917 / 1504 / 865	
Goodness-of-fit on F^2	1.052	
Final R indices [I>2sigma(I)]	R1 = 0.0846, wR2 = 0.1713	
R indices (all data)	R1 = 0.1393, wR2 = 0.1951	
Extinction coefficient	n/a	
Largest diff. peak and hole	1.530 and -0.945 e.$Å^{-3}$	

S6. b. Crystallographic data for $[(\mathrm{PSP})\mathrm{Mo}(\mathrm{N}_2)_2]_2(\mu\text{-}\mathrm{N}_2)$ (**2**)

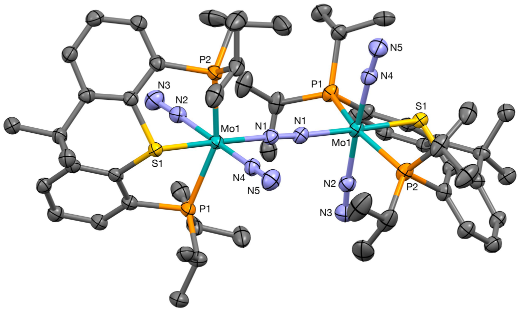

Figure S39. ORTEP representation (50% probability ellipsoids) of the structure of **2** determined by X-ray diffraction; hydrogen atoms and PSP *t*-butyl groups omitted for clarity.

Crystal data and structure refinement for SM-647a_Pcca_faces.

Identification code	SM-647a_Pcca_faces	
Empirical formula	C38 H63.50 Mo N5 O0.75 P2 S	
Formula weight	792.37	
Temperature	100(2) K	
Wavelength	1.54184 Å	
Crystal system	Orthorhombic	
Space group	Pcca	
Unit cell dimensions	a = 31.9495(3) Å	α = 90°.
	b = 14.14073(19) Å	β = 90°.
	c = 18.9898(2) Å	γ = 90°.
Volume	8579.39(17) Å^3	
Z	8	
Density (calculated)	1.227 Mg/m^3	
Absorption coefficient	3.905 mm^{-1}	
F(000)	3364	
Crystal size	0.240 x 0.040 x 0.020 mm^3	
Theta range for data collection	3.125 to 79.364°.	
Index ranges	-40<=h<=40, -17<=k<=17, -23<=l<=13	
Reflections collected	65614	
Independent reflections	8599 [R(int) = 0.0674]	
Completeness to theta = 67.684°	99.5 %	
Absorption correction	Gaussian	
Max. and min. transmission	1.000 and 0.374	
Refinement method	Full-matrix least-squares on F^2	
Data / restraints / parameters	8599 / 1077 / 548	
Goodness-of-fit on F^2	1.109	
Final R indices [I>2sigma(I)]	R1 = 0.0546, wR2 = 0.1249	
R indices (all data)	R1 = 0.0667, wR2 = 0.1318	
Extinction coefficient	n/a	
Largest diff. peak and hole	0.971 and -0.582 e.Å^{-3}	

S6. c. Crystallographic data for (PSP)Mo(N)(I) (**1-(N)I**)

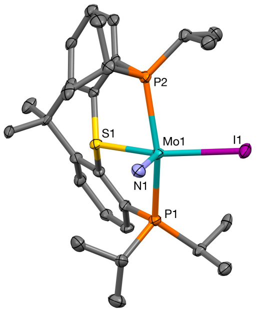

Figure S40. ORTEP representation (50% probability ellipsoids) of the structure of **1-(N)I** determined by X-ray diffraction; hydrogen atoms and PSP *t*-butyl groups omitted for clarity.

Crystal data and structure refinement for PSP-Mo-N-I_P-1.

Identification code	PSP-Mo-N-I_P-1	
Empirical formula	C35 H55 I Mo N P2 S	
Formula weight	806.64	
Temperature	100(2) K	
Wavelength	0.71073 Å	
Crystal system	Triclinic	
Space group	P-1	
Unit cell dimensions	a = 10.0985(17) Å	α = 76.957(3)°.
	b = 12.043(2) Å	β = 82.444(3)°.
	c = 16.428(3) Å	γ = 73.782(3)°.
Volume	1863.9(5) Å^3	
Z	2	
Density (calculated)	1.437 Mg/m^3	
Absorption coefficient	1.345 mm^{-1}	
F(000)	826	
Crystal size	0.220 x 0.040 x 0.020 mm^3	
Theta range for data collection	1.276 to 28.670°.	
Index ranges	-13<=h<=13, -16<=k<=16, -22<=l<=22	
Reflections collected	19263	
Independent reflections	9502 [R(int) = 0.0548]	
Completeness to theta = 25.242°	99.8 %	
Absorption correction	Semi-empirical from equivalents	
Max. and min. transmission	.9999 and .9240	
Refinement method	Full-matrix least-squares on F^2	
Data / restraints / parameters	9502 / 0 / 385	
Goodness-of-fit on F^2	1.066	
Final R indices [I>2sigma(I)]	R1 = 0.0705, wR2 = 0.1396	
R indices (all data)	R1 = 0.1065, wR2 = 0.1546	
Extinction coefficient	n/a	
Largest diff. peak and hole	2.315 and -1.209 e.Å^{-3}	

S6. d. Crystallographic data for (PSP)Mo(NH)(I)(Cl) (**1-(NH)ICl**)

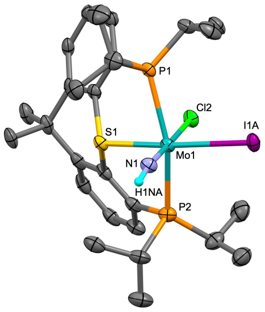

Figure S41. ORTEP representations (50% probability ellipsoids) of the structure of **1-(NH)ICl** determined by X-ray diffraction; hydrogen atoms (other than the imido H), PSP *t*-butyl groups, and minor components of iodide site omitted for clarity. Fixed position of the imido proton determined from electron density map.

Crystal data and structure refinement for MoPSPIClNH2_P21c_b.

Identification code	MoPSPIClNH2_P21c_b	
Empirical formula	C41 H63 Cl1.18 I0.82 Mo N P2 S	
Formula weight	905.41	
Temperature	120(2) K	
Wavelength	0.71073 Å	
Crystal system	Monoclinic	
Space group	$P2_1/c$	
Unit cell dimensions	a = 18.017(3) Å	α = 90°.
	b = 13.531(3) Å	β = 97.035(3)°.
	c = 18.041(3) Å	γ = 90°.
Volume	4364.9(14) Å^3	
Z	4	
Density (calculated)	1.378 Mg/m^3	
Absorption coefficient	1.099 mm^{-1}	
F(000)	1870	
Crystal size	0.150 x 0.100 x 0.050 mm^3	
Theta range for data collection	1.886 to 26.484°.	
Index ranges	-22<=h<=22, -16<=k<=16, -22<=l<=22	
Reflections collected	31610	
Independent reflections	8984 [R(int) = 0.0694]	
Completeness to theta = 25.242°	100.0 %	
Absorption correction	Semi-empirical from equivalents	
Max. and min. transmission	.9999 and 0.8339	
Refinement method	Full-matrix least-squares on F^2	
Data / restraints / parameters	8984 / 1012 / 492	
Goodness-of-fit on F^2	1.093	
Final R indices [I>2sigma(I)]	R1 = 0.0458, wR2 = 0.1024	
R indices (all data)	R1 = 0.0587, wR2 = 0.1088	
Extinction coefficient	n/a	
Largest diff. peak and hole	1.149 and -0.918 e.Å^{-3}	

S6. e. Crystallographic data for $[(PSP)Mo(CO)_2]_2(\mu\text{-}N_2)$

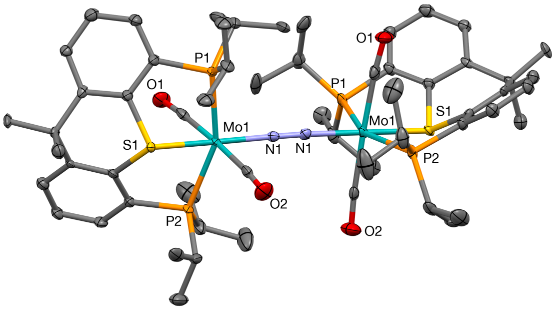

Figure S42. ORTEP representation (50% probability ellipsoids) of the structure of $[(PSP)Mo(CO)_2]_2(\mu\text{-}N_2)$ determined by X-ray diffraction; hydrogen atoms and PSP *t*-butyl groups omitted for clarity.

Crystal data and structure refinement for dinitrogen_Pcca_final.

Identification code	dinitrogen_Pcca_final	
Empirical formula	C41 H65.50 Mo N O2 P2 S	
Formula weight	794.38	
Temperature	426(2) K	
Wavelength	0.71073 Å	
Crystal system	Orthorhombic	
Space group	Pcca	
Unit cell dimensions	a = 31.877(8) Å	α = 90°.
	b = 14.204(4) Å	β = 90°.
	c = 18.861(5) Å	γ = 90°.
Volume	8540(4) $Å^3$	
Z	8	
Density (calculated)	1.236 Mg/m^3	
Absorption coefficient	0.464 mm^{-1}	
F(000)	3380	
Crystal size	0.40 x 0.08 x 0.01 mm^3	
Theta range for data collection	1.905 to 24.194°.	
Index ranges	-36<=h<=32, -16<=k<=16, -21<=l<=21	
Reflections collected	35946	
Independent reflections	6868 [R(int) = 0.1336]	
Completeness to theta = 24.194°	100.0 %	
Absorption correction	Semi-empirical from equivalents	
Max. and min. transmission	0.7452 and 0.4992	
Refinement method	Full-matrix least-squares on F^2	
Data / restraints / parameters	6868 / 841 / 483	
Goodness-of-fit on F^2	1.166	
Final R indices [I>2sigma(I)]	R1 = 0.0913, wR2 = 0.1875	
R indices (all data)	R1 = 0.1222, wR2 = 0.2014	
Extinction coefficient	n/a	
Largest diff. peak and hole	1.007 and -1.462 e.$Å^{-3}$	

S6. f. Crystallographic data for (PSP)Mo(CO)$_3$

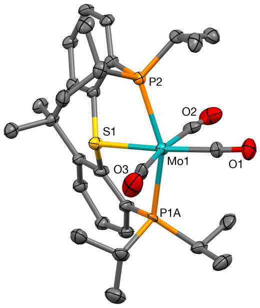

Figure S43. ORTEP representation (50% probability ellipsoids) of the structure of (PSP)Mo(CO)$_3$ determined by X-ray diffraction; hydrogen atoms and PSP *t*-butyl groups omitted for clarity.

Crystal data and structure refinement for mopspco_P-1_FINAL.

Identification code	mopspco_P-1_FINAL	
Empirical formula	C40.50 H61 Mo O3 P2 S	
Formula weight	785.83	
Temperature	120(2) K	
Wavelength	0.71073 Å	
Crystal system	Triclinic	
Space group	P-1	
Unit cell dimensions	a = 11.6654(9) Å	α = 93.254(2)°.
	b = 19.2138(15) Å	β = 103.495(2)°.
	c = 19.8632(16) Å	γ = 105.235(2)°.
Volume	4143.8(6) Å^3	
Z	4	
Density (calculated)	1.260 Mg/m^3	
Absorption coefficient	0.478 mm^{-1}	
F(000)	1664	
Crystal size	0.100 x 0.001 x 0.001 mm^3	
Theta range for data collection	1.435 to 29.574°.	
Index ranges	-16<=h<=16, -26<=k<=26, -27<=l<=27	
Reflections collected	47937	
Independent reflections	22826 [R(int) = 0.0567]	
Completeness to theta = 25.242°	99.6 %	
Absorption correction	Semi-empirical from equivalents	
Max. and min. transmission	0.7462 and 0.6295	
Refinement method	Full-matrix least-squares on F^2	
Data / restraints / parameters	22826 / 2071 / 1042	
Goodness-of-fit on F^2	1.099	
Final R indices [I>2sigma(I)]	R1 = 0.0639, wR2 = 0.1372	
R indices (all data)	R1 = 0.0856, wR2 = 0.1464	
Extinction coefficient	n/a	
Largest diff. peak and hole	1.539 and -0.918 e.Å^{-3}	

VII. Computational Details and Energies

Electronic structure calculations, based on Density Functional Theory (DFT), were performed using the Gaussian16 (revision A.03)[S5] program. Stationary points on the potential energy surfaces were located by geometry optimization using the parametrized M06 exchange correlation density functional[S6] with Pople-type 6-31G(d,p)[S7] basis sets for all atoms, except Mo, Co, Br and I. For Mo, Co Br and I, the Stuttgart-Dresden effective core potential, SDD[S8] was used for the core electrons for the heavy atoms; the associated triple-ζ quality basis set was used for the valence electrons respectively. The structures were optimized with a 'guess=mix' keyword for systems with non-singlet spin state. Spin state stabilities were further checked using single point calculations with 'stable=opt' keyword following optimization of geometries. The PSP ligand was generally modeled with an asymmetric derivative bearing t-butylmethylphosphine groups instead of bis(isopropyl)phosphine groups to avoid multiple conformational possibilities, while maintaining the same ligand steric profile.[S9] Unless explicitly mentioned, this model has been used for all calculations pertinent to (PSP)Mo halide complexes. Bis(isopropyl)phosphino groups, however, were used for calculations involving the triflate anion to more precisely model the greater steric demands of the triflate ion and the absence of symmetry for triflate-coordinated and especially ion-paired triflate complexes.

Geometries were calculated for stationary points along the reaction paths using standard optimization procedure. Intrinsic Reaction Coordinate (IRC) calculations were conducted on important transition states to properly locate matching reactants/products. Normal mode analysis was performed to further verify the nature of a particular stationary point (minimum, transition state). The resulting set of vibrational frequencies was employed (without scaling) to determine zero-point energy corrections. Some of the geometry optimizations required the use of an enhanced integration grid size ('superfine' grid) for integral evaluation and tighter optimization criteria (relative to the Gaussian16 default values) to achieve satisfactory convergence to a stationary point.

Vibrational frequencies (from the normal mode analysis) were employed (without scaling) to determine zero-point energy corrections. Thermal corrections were evaluated at standard conditions of pressure (P = 1.0 atm) and temperature (T = 298.15 K = 25.00 °C) using standard statistical mechanical expressions based on ideal gas law behavior. These corrections allow us to convert from a set of computed potential energies (E) to enthalpies (H) and Gibbs free energies (G). [S10]

Activation energies for electron transfer steps were calculated based on Marcus theory[S11]. The energy of contact ion-pairs initially resulting from electron-transfer from Cp^*_2Co to a neutral

(PYP)Mo complex could generally not be optimized in a straightforward fashion since ΔE was invariably positive before relaxation, and in some cases after relaxation. The energy of ion-pairing was therefore modeled with the optimization of a contact ion-pair of the respective (PYP)Mo anion and 1-*tert*-butyl-1-azaadamantan-1-ium (NR_4^+) cation, in order to obtain the full thermodynamics (including ΔG^0) of the electron transfer step. This cation was chosen to model the shape and size of the $[CoCp^*_2]^+$ cation, through use of the Multiwfn 3.8 program (see results tabulated in Table S6.2.[S12]), and thereby correctly capture electrostatic interaction energies.

For the calculation of the reorganization energies of the reactants using the four-point method, the reduced anion and $[CoCp^*_2]^+$ geometries were optimized separately followed by a single point calculation of these geometries as well as without the electron transfers to calculate reorganization energies (λ_1-λ_4).[S13] The difference between the total electronic energies for the ground state optimized structure and the "reorganized" single point calculation structure provides the value for the overall reorganization energy (λ) calculated as a geometric mean.[S14] The solvent reorganization for benzene was calculated according to eq S1 and was found to be negligible largely stemming from the $\left(\frac{1}{\varepsilon_{op}} - \frac{1}{\varepsilon}\right)$ factor in the equation (for benzene the factor is ca. 3.92 x 10^{-3}).[S15] Hence, it was not considered in the calculation of $\Delta G^{\ddagger}$ for the electron transfers. An illustration has been shown in Table S6.1.

$$\lambda_0 = \left(332\frac{kcal}{mol}\right)\left(\frac{1}{2a_1} + \frac{1}{2a_2} - \frac{1}{R}\right)\left(\frac{1}{\varepsilon_{op}} - \frac{1}{\varepsilon}\right) \qquad \text{(eq S1)}$$

$\lambda_0 = Reorganization\ Energy\ of\ Solvent$ (benzene)

$a_1 and\ a_2 = Radii\ of\ molecules\ involved\ in\ ET$

$R = a_1 + a_2$

$\varepsilon_{op} = Optical\ dielectric\ constant\ (square\ of\ RI\ of\ benzene\ (1.50)) = 2.25$

$\varepsilon = Static\ dielectric\ constant = 2.27$

Improved potential energies, which also include some of the effects of bulk solvation, were obtained from single point calculations at the optimized gas phase geometries employing the M06 functional, the all-electron Karlsruhe basis set def2-QZVP for all atoms,[S8, S16] and the SMD dielectric continuum solvation model (benzene was the model solvent) [S17]. For all the pathways examined in this study, these potential energies are collected in Tables S6.2-S6.16 (below) in columns labelled ΔE. We then combined these potential energies with the thermal corrections determined from the optimized (gas phase) structures (as described above) to form Gibbs free energies, G, which approximate the results of free energy calculations carried out at the higher basis set level with (some) inclusion of bulk solvent effects.

All Gibbs free energies cited in the manuscript are derived from these procedures and are reported in kcal/mol. For all the pathways examined in this study, Gibbs free energies are collected in Tables S6.2-S6.16 (below) in columns labelled ΔG.

Table S7.1. Calculation of $\Delta G^{\ddagger}$ for reduction of $(PNP)Mo^{IV}(NH)Cl_2$ to $[(PNP)Mo(NH)Cl_2]^-[CoCp^*_2]^+$ (as described in the computational methodology section)

$(PNP)Mo(NH)Cl_2$	-2683.704808 Hartree	A
$[(PNP)Mo(NH)Cl_2]^-$	-2683.757636 Hartree	B
$[(PNP)Mo(NH)Cl_2]$ single point energy in the optimized geometry of $[(PNP)Mo(NH)Cl_2]^-$ by removal of 1e-	-2683.678312 Hartree	A’
$[(PNP)Mo(NH)Cl_2]^-$ single point energy in the optimized geometry of $[(PNP)Mo(NH)Cl_2]$ by addition of 1e-	-2683.747765 Hartree	B’
	Reorganization Energy from A and A’ (λ_1)	16.6 kcal/mol
	Reorganization Energy from B and B’ (λ_2)	6.2 kcal/mol
$CoCp^*_2$	-2162.776317 Hartree	C
$[CoCp^*_2]^+$	-2162.655984 Hartree	D
$CoCp^*_2$ single point energy in the optimized geometry of $[CoCp^*_2]^+$ by addition of 1e-	-2162.765575 Hartree	C’
$[CoCp^*_2]^+$ single point energy in the optimized geometry of $CoCp^*_2$ by removal of 1e-	-2162.646409 Hartree	D’
	Reorganization Energy from C and C’ (λ_3)	6.7 kcal/mol
	Reorganization Energy from D and D’ (λ_4)	6.0 kcal/mol
Total Reorganization Energy (λ): Geometric Mean[S10]	$\sqrt[2]{(\lambda_1 + \lambda_3)(\lambda_2 + \lambda_4)}$	16.9 kcal/mol
$[(PNP)Mo(NH)Cl_2]^-[CoCp^*_2]^+$ energy calculated from optimized geometry of $[(PNP)Mo(NH)Cl_2]^-[NR_4]^+$	Energy calculated as $[(PNP)Mo(NH)Cl_2]^-[CoCp^*_2]^+ = [(PNP)Mo(NH)Cl_2]^-[NR_4]^+ + [CoCp^*_2]^+ - [NR4]^+$	
ΔG^0		25.4 kcal/mol
Calculated $\Delta G^{\ddagger}$	$\Delta G^{\ddagger} = (\Delta G^0 + \lambda)^2/4\lambda$	**26.5** kcal/mol

Table S7.2. Comparison of NR_4^+ and $CoCp^*{}_2^+$ cation dimensions analyzed by Multiwfn3.8 from optimized geometries

NR_4^+

Farthest distance:
10 (H)- - -28 (H): 7.325 Angstrom
vdw radius of 10(H): 1.200 Angstrom
vdW radius of 28(H): 1.200 Angstrom
Diameter of the system: **9.725** Angstrom
Radius of the system: **4.863** Angstrom
Length of the three sides: 9.270 7.330 7.009 Angstrom

$CoCp^*{}_2^+$

Farthest distance:
22 (H)- - -41 (H): 8.175 Angstrom
vdw radius of 22(H): 1.200 Angstrom
vdW radius of 41(H): 1.200 Angstrom
Diameter of the system: **10.575** Angstrom
Radius of the system: **5.287** Angstrom
Length of the three sides: 7.832 8.824 8.897 Angstrom

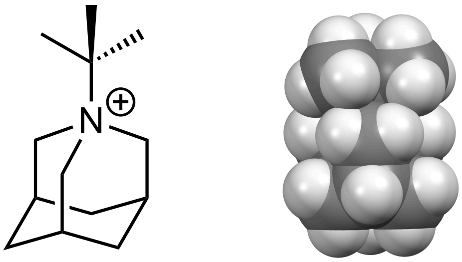

1-*tert*-butyl-1-azaadamantan-1-ium cation

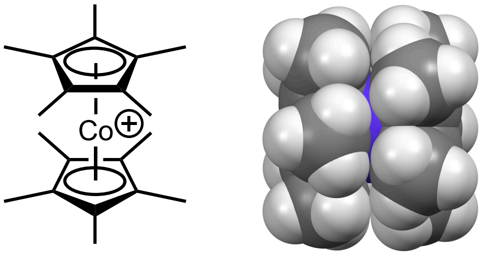

$CoCp^*{}_2^+$

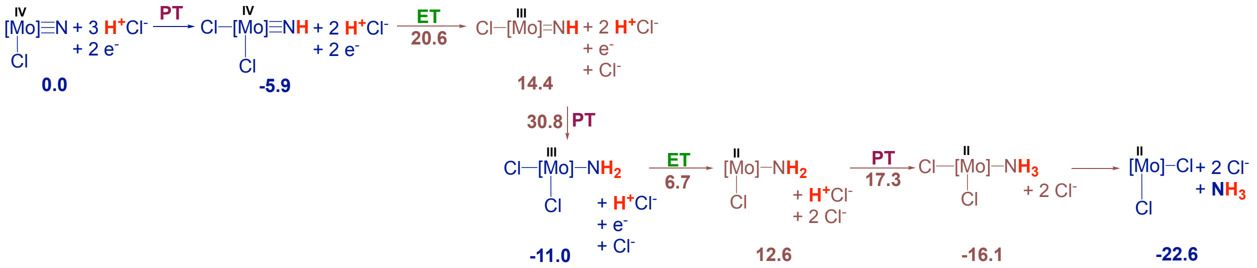

Scheme S7.1. Gibbs free energies for the overall reduction of (PNP)Mo^{IV}(≡N)Cl to (PNP)Mo^{II}Cl$_2$ and NH$_3$ via consecutive additions of H$^+$ (LutH$^+$Cl$^-$) and electrons from e$^-$ (CoCp*$_2$) (alternating).

Table S7.3. Energies for the "alternating" pathway for conversion of (PNP)Mo(N)Cl to (PNP)MoCl$_2$ by addition of protons from H$^+$Cl$^-$(LutH$^+$Cl$^-$) and electrons from e$^-$ (CoCp*$_2$). Cl$^-$ represents [CoCp*$_2$]$^+$Cl$^-$. Energies (kcal/mol) are referenced to T = 298.15 K and P = 1 atm.

Name	Spin State	ΔE	ΔG
(PNP)Mo(N)Cl + 3 H$^+$Cl$^-$ + 2 e$^-$	Singlet	0.0	**0.0**
TS-PT-1 (Proton Transfer) + 2 H$^+$Cl$^-$ + 2 e$^-$	Singlet	X.X[a]	**X.X[a]**
(PNP)Mo(NH)Cl$_2$ + 2 H$^+$Cl$^-$ + 2 e$^-$	Singlet	-9.9	**-5.9**
TS-ET-1 (Electron Transfer) + 2 H$^+$Cl$^-$ + e$^-$	Doublet	-	**20.6**
[(PNP)Mo(NH)Cl$_2$]$^-$[CoCp*$_2$]$^+$ + 2 H$^+$Cl$^-$ + e$^-$	Doublet	-3.2	**19.5**
(PNP)Mo(NH)Cl + 2 H$^+$Cl$^-$ + e$^-$ + Cl$^-$	Doublet	10.5	**14.4**
TS-PT-2 (Proton Transfer) + H$^+$Cl$^-$ + e$^-$ + Cl$^-$	Doublet	9.3	**30.8**
(PNP)Mo(NH$_2$)Cl$_2$ + H$^+$Cl$^-$ + e$^-$ + Cl$^-$	Quartet	-19.6	**-11.0**
TS-ET-2 (Electron Transfer) + H$^+$Cl$^-$+ 2 Cl$^-$	Triplet	-	**6.7**
[(PNP)Mo(NH$_2$)Cl$_2$]$^-$[CoCp*$_2$]$^+$ + H$^+$Cl$^-$+ 2 Cl$^-$	Triplet	-22.3	**6.0**
(PNP)Mo(NH$_2$)Cl + H$^+$Cl$^-$+ 2 Cl$^-$	Triplet	3.4	**12.6**
TS-PT-3 (Proton Transfer) + 2 Cl$^-$	Triplet	-9.3	**17.3**
(PNP)Mo(NH$_3$)Cl$_2$ + 2 Cl$^-$	Triplet	-31.3	**-16.1**
(PNP)MoCl$_2$ + 2 Cl$^-$ + **NH$_3$**	Quintet	-22.3	**-22.6**

[a] TS could not be located even after multiple attempts

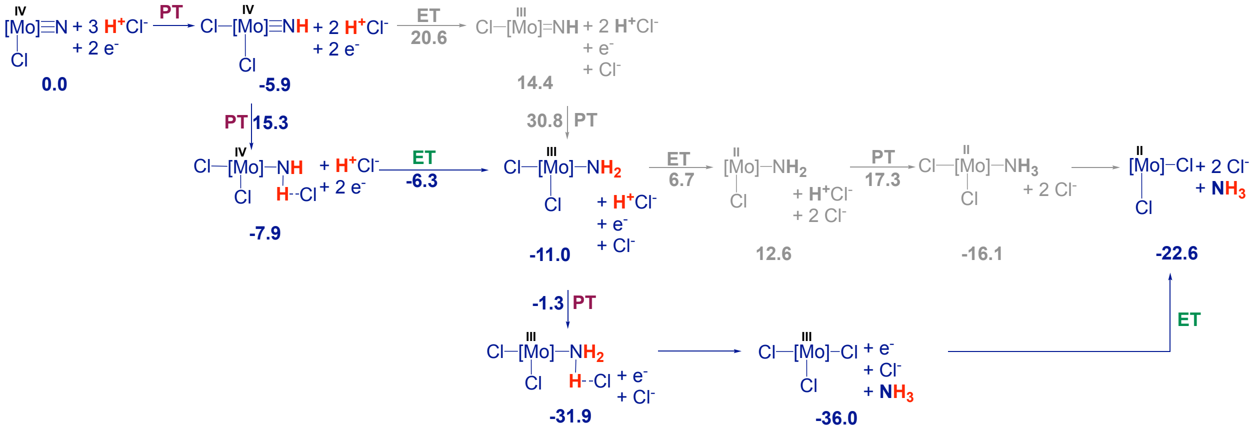

Scheme S7.2. Gibbs free energies for the overall reduction of (PNP)Mo^{IV}(≡N)Cl to (PNP)$Mo^{II}Cl_2$ and NH_3 via non-consecutive additions of H^+ and e^- (protons first, in color). The "alternating" mechanism has been shown here (in gray). Energies in kcal/mol.

Table S7.4. Energies for the "protons first" pathway for conversion of (PNP)Mo(N)Cl to (PNP)$MoCl_2$ by addition of protons from H^+Cl^-(LutH^+Cl^-) and electrons from e^- ($CoCp^*_2$). Cl^- represents $[CoCp^*_2]^+Cl^-$. Energies (kcal/mol) are referenced to T = 298.15 K and P = 1 atm.

Name	Spin State	ΔE	ΔG
(PNP)Mo(N)Cl + 3 H^+Cl^- + 2 e^-	Singlet	0.0	**0.0**
TS-PT-1 (Proton Transfer)	Singlet	X.X[a]	**X.X[a]**
(PNP)Mo(NH)Cl_2 + 2 H^+Cl^- + 2 e^-	Singlet	-9.9	**-5.9**
TS-PT-2' (Proton Transfer) + H^+Cl^- + 2 e^-	Singlet	-4.0	**15.3**
[(PNP)Mo(NH_2)Cl_2]$^+$$Cl^-$ + H^+Cl^- + 2 e^-	Triplet	-13.0	**-7.9**
TS-ET-1' (Electron Transfer) + H^+Cl^- + e^-	Quartet	-	**-6.3**
[(PNP)Mo(NH_2)Cl_3]$^-$[$CoCp^*_2$]$^+$ + H^+Cl^- + e^-	Quartet	-37.7	**-12.4**
(PNP)Mo(NH_2)Cl_2 + H^+Cl^- + e^- + Cl^-	Quartet	-19.6	**-11.0**
TS-PT-3' (Proton Transfer) + e^- + Cl^-	Quartet	-28.4	**-1.3**
[(PNP)Mo(NH_3)Cl_2]$^+$$Cl^-$ + e^- + Cl^-	Quartet	-43.9	**-31.9**
(PNP)MoCl_3 + Cl^- + **NH_3**	Quartet	-35.7	**-36.0**
(PNP)MoCl_2 + 2 Cl^- + **NH_3**	Quintet	-22.3	**-22.6**

[a] TS could not be located even after multiple attempts

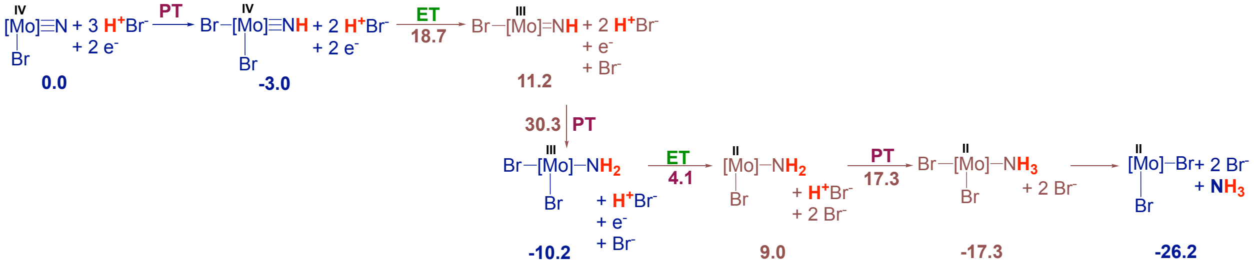

Scheme S7.3. Gibbs free energies for the overall reduction of (PNP)Mo^{IV}(≡N)Br to (PNP)$Mo^{II}Br_2$ and NH_3 via consecutive additions of H^+ and e^- (alternating).

Table S7.5. Energies for the "alternating" pathway for conversion of (PNP)Mo(N)Br to (PNP)$MoBr_2$ by addition of protons from H^+Br^-(LutH^+Br^-) and electrons from e^- ($CoCp^*_2$). Br^- represents $[CoCp^*_2]^+Br^-$. Energies (kcal/mol) are referenced to T = 298.15 K and P = 1 atm.

Name	Spin State	ΔE	ΔG

(PNP)Mo(N)Br + 3 H^+Br^- + 2 e^-	Singlet	0.0	**0.0**
TS-PT-1 (Proton Transfer) + 2 H^+Br^- + 2 e^-	Singlet	X.X[b]	**X.X[b]**
(PNP)Mo(NH)Br_2 + 2 H^+Br^- + 2 e^-	Singlet	-4.6	**-3.0**
TS-ET-1 (Electron Transfer) + 2 H^+Br^- + e^-	Doublet	-	**18.7**
[(PNP)Mo(NH)Br_2]$^-$[CoCp*$_2$]$^+$ + 2 H^+Br^- + e^-	Doublet	-0.7	**18.7**
(PNP)Mo(NH)Br + 2 H^+Br^- + e^- + Br^-	Doublet	11.2	**11.2**
TS-PT-2 (Proton Transfer) + H^+Br^- + e^- + Br^-	Doublet	14.4	**30.3**
(PNP)Mo(NH_2)Br_2 + H^+Br^- + e^- + Br^-	Quartet	-14.0	**-10.2**
TS-ET-2 (Electron Transfer) + H^+Br^-+ 2 Br^-	Triplet	-	**4.1**
[(PNP)Mo(NH_2)Br_2]$^-$[CoCp*$_2$]$^+$ + H^+Br^-+ 2 Br^-	Triplet	-18.7	**3.9**
(PNP)Mo(NH_2)Br + H^+Br^-+ 2 Br^-	Triplet	5.5	**9.0**
TS-PT-3 (Proton Transfer) + 2 Br^-	Triplet	-2.8	**17.3**
(PNP)Mo(NH_3)Br_2 + 2 Br^-	Triplet	-25.0	**-17.3**
(PNP)MoBr_2 + 2 Br^- + **NH_3**	Quintet	-18.4	**-26.2**

[b] TS could not be located even after multiple attempts

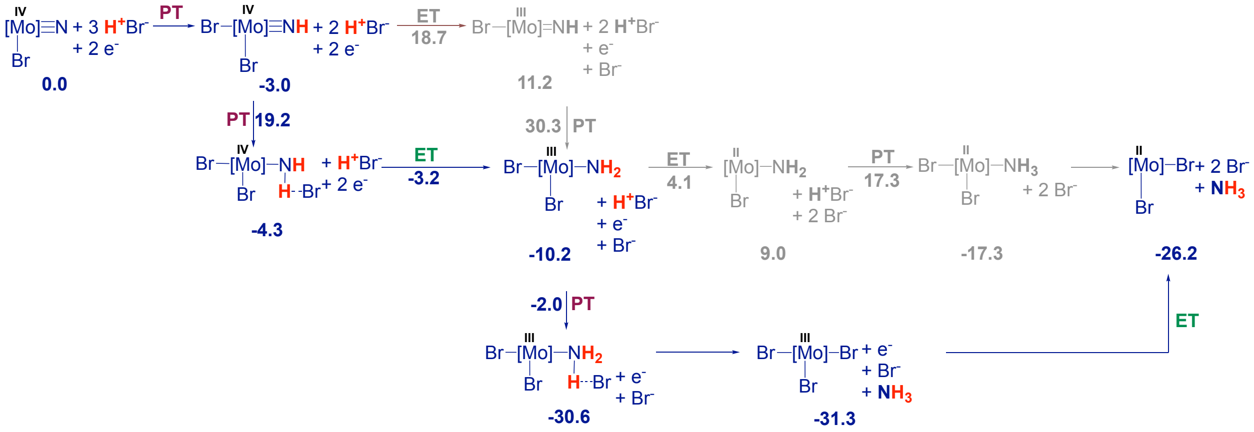

Scheme S7.4. Gibbs free energies for the overall reduction of (PNP)Mo^{IV}(≡N)Br to (PNP)$Mo^{II}Br_2$ and NH_3 via non-consecutive additions of H^+ and e^- (protons first, in color). The "alternating" mechanism has been shown here (in gray) for comparison.

Table S7.6. Energies for the "protons first" pathway for conversion of (PNP)Mo(N)Cl to (PNP)MoCl_2 by addition of protons from H^+Br^-(LutH^+Br^-) and electrons from e^- (CoCp*$_2$). Br^- represents [CoCp*$_2$]$^+Br^-$.Energies (kcal/mol) are referenced to T = 298.15 K and P = 1 atm.

Name	**Spin State**	**ΔE**	**ΔG**
(PNP)Mo(N)Br + 3 H^+Br^- + 2 e^-	Singlet	0.0	**0.0**
TS-PT-1 (Proton Transfer)	Singlet	X.X[b]	**X.X[b]**

(PNP)Mo(NH)Br$_2$ + 2 H$^+$Br$^-$ + 2 e$^-$	Singlet	-4.6	**-3.0**
TS-PT-2’ (Proton Transfer) + H$^+$Br$^-$ + 2 e$^-$	Triplet	4.2	**19.2**
[(PNP)Mo(NH$_2$)Br$_2$]$^+$Br$^-$ + H$^+$Br$^-$ + 2 e$^-$	Triplet	-5.7	**-4.3**
TS-ET-1’ (Electron Transfer) + H$^+$Br$^-$ + e$^-$	Quartet	-	**-3.2**
[(PNP)Mo(NH$_2$)Br$_3$]$^-$[CoCp*$_2$]$^+$ + H$^+$Br$^-$ + e$^-$	Quartet	-29.8	**-9.4**
(PNP)Mo(NH$_2$)Br$_2$ + H$^+$Br$^-$ + e$^-$ + Br$^-$	Quartet	-14.0	**-10.2**
TS-PT-3’ (Proton Transfer) + e$^-$+ Br$^-$	Quartet	-19.8	**-2.0**
[(PNP)Mo(NH$_3$)Br$_2$]$^+$Br$^-$ + e$^-$+ Br$^-$	Quartet	-35.6	**-30.6**
(PNP)MoBr$_3$ + Br$^-$ + **NH$_3$**	Quartet	-24.2	**-31.3**
(PNP)MoBr$_2$ + 2 Br$^-$ + **NH$_3$**	Quintet	-18.4	**-26.2**

[b] TS could not be located even after multiple attempts

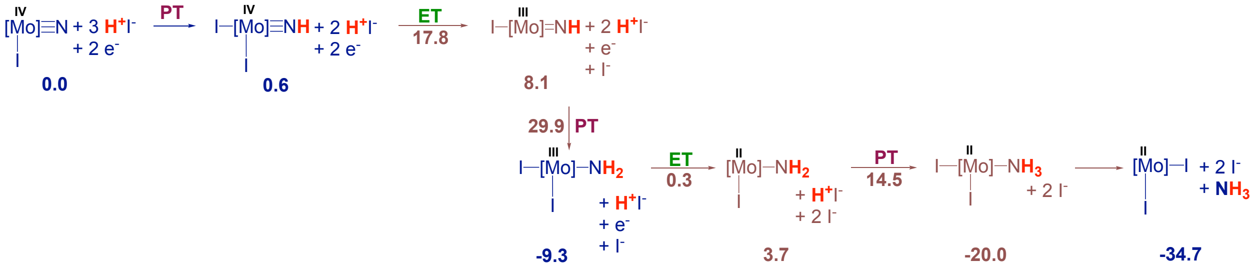

Scheme S7.5. Gibbs free energies for the overall reduction of (PNP)Mo^{IV}(≡N)I to (PNP)Mo^{II}I$_2$ and NH$_3$ via consecutive additions of H$^+$ and e$^-$ (alternating).

Table S7.7 Energies for the “alternating” pathway for conversion of (PNP)Mo(N)I to (PNP)MoI$_2$ by addition of protons from H$^+$I$^-$(LutH$^+$I$^-$) and electrons from e$^-$ (CoCp*$_2$). I$^-$ represents [CoCp*$_2$]$^+$I$^-$. Energies (kcal/mol) are referenced to T = 298.15 K and P = 1 atm.

Name	**Spin State**	**ΔE**	**ΔG**
(PNP)Mo(N)I + 3 H$^+$I$^-$ + 2 e$^-$	Singlet	0.0	**0.0**
TS-PT-1 (Proton Transfer) + 2 H$^+$I$^-$ + 2 e$^-$	Singlet	X.X[c]	**X.X[c]**
(PNP)Mo(NH)I$_2$ + 2 H$^+$I$^-$ + 2 e$^-$	Singlet	-0.2	**0.6**
TS-ET-1 (Electron Transfer) + 2 H$^+$I$^-$ + e$^-$	Doublet	-	**17.8**
[(PNP)Mo(NH)I$_2$]$^-$[CoCp*$_2$]$^+$ + 2 H$^+$I$^-$ + e$^-$	Doublet	-1.5	**17.8**
(PNP)Mo(NH)I + 2 H$^+$I$^-$ + e$^-$ + I$^-$	Doublet	9.0	**8.1**
TS-PT-2 (Proton Transfer) + H$^+$I$^-$ + e$^-$ + I$^-$	Doublet	15.0	**29.9**
(PNP)Mo(NH$_2$)I$_2$ + H$^+$I$^-$ + e$^-$ + I$^-$	Quartet	-11.7	**-9.3**
TS-ET-2 (Electron Transfer) + H$^+$I$^-$+ 2 I$^-$	Triplet	-	**0.3**
[(PNP)Mo(NH$_2$)I$_2$]$^-$[CoCp*$_2$]$^+$ + H$^+$I$^-$+ 2 I$^-$	Triplet	-20.7	**0.2**
(PNP)Mo(NH$_2$)I + H$^+$I$^-$+ 2 I$^-$	Triplet	1.7	**3.7**

TS-PT-3 (Proton Transfer) + 2 I⁻	Triplet	-4.1	**14.5**
(PNP)Mo(NH₃)I₂ + 2 I⁻	Triplet	-25.4	**-20.0**
(PNP)MoI₂ + 2 I⁻ + **NH₃**	Quintet	-24.6	**-34.7**

[c] TS could not be located even after multiple attempts. Potential Energy Surface Scan calculation show the process to be barrierless

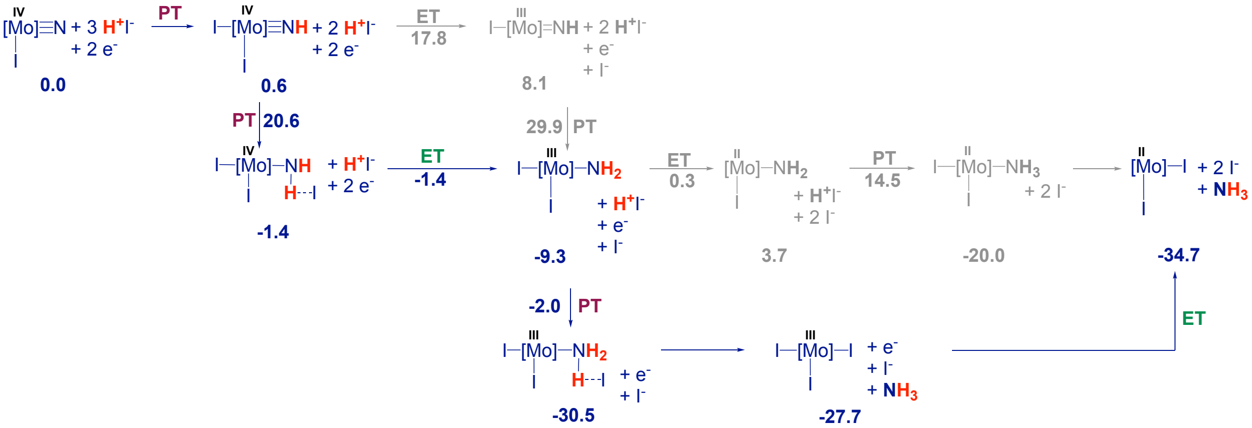

Scheme S7.6. Gibbs free energies for the overall reduction of (PNP)Mo^{IV}(≡N)I to (PNP)Mo^{II}I$_2$ and NH$_3$ via non-consecutive additions of H$^+$ and e$^-$ (protons first, in color). The "alternating" mechanism has been shown here (in gray) for comparison.

Table S7.8. Energies for the "protons first" pathway for conversion of (PNP)Mo(N)I to (PNP)MoI$_2$ by addition of protons from H$^+$I$^-$(LutH$^+$I$^-$) and electrons from e$^-$ (CoCp*$_2$). I$^-$ represents [CoCp*$_2$]$^+$I$^-$. Energies (kcal/mol) are referenced to T = 298.15 K and P = 1 atm.

Name	**Spin State**	**ΔE**	**ΔG**
(PNP)Mo(N)I + 3 H⁺I⁻ + 2 e⁻	Singlet	0.0	**0.0**
TS-PT-1 (Proton Transfer)	Singlet	X.X[c]	**X.X[c]**
(PNP)Mo(NH)I₂ + 2 H⁺I⁻ + 2 e⁻	Singlet	-0.2	**0.6**
TS-PT-2' (Proton Transfer) + H⁺I⁻ + 2 e⁻	Triplet	8.2	**20.6**
[(PNP)Mo(NH₂)I₂]⁺I⁻ + H⁺I⁻ + 2 e⁻	Triplet	-1.0	**-1.4**
TS-ET-1' (Electron Transfer) + H⁺I⁻ + e⁻	Quartet	-	**-1.4**
[(PNP)Mo(NH₂)I₃]⁻[CoCp*₂]⁺ + H⁺I⁻ + e⁻	Quartet	-30.6	**-11.5**
(PNP)Mo(NH₂)I₂ + H⁺I⁻ + e⁻ + I⁻	Quartet	-11.7	**-9.3**
TS-PT-3' (Proton Transfer) + e⁻+ I⁻	Quartet	-17.6	**-2.0**
[(PNP)Mo(NH₃)I₂]⁺I⁻ + e⁻+ I⁻	Quartet	-33.7	**-30.5**
(PNP)MoI₃ + I⁻ + **NH₃**	Quartet	-18.7	**-27.7**
(PNP)MoI₂ + 2 I⁻ + **NH₃**	Quintet	-24.6	**-34.7**

[c] TS could not be located even after multiple attempts

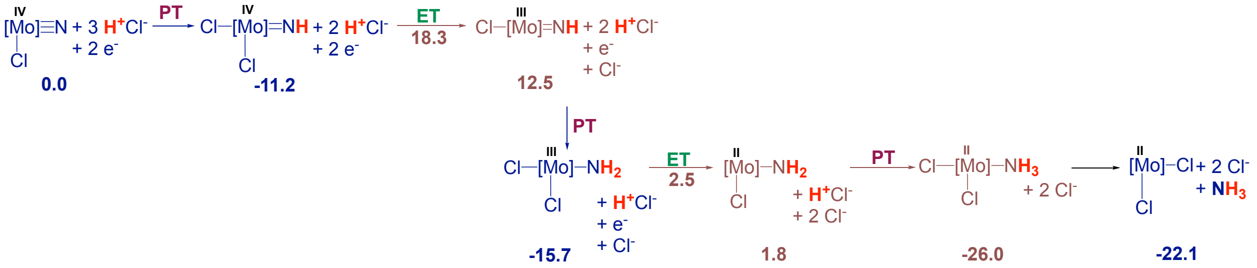

Scheme S7.7. Gibbs free energies for the overall reduction of (PSP)Mo^{IV}(≡N)Cl to (PSP)Mo^{II}Cl$_2$ and NH$_3$ via consecutive additions of H$^+$ (LutH$^+$Cl$^-$) and electrons from e$^-$ (CoCp*$_2$) (alternating).

Table S7.9. Energies for the "alternating" pathway for conversion of (PSP)Mo(N)Cl to (PSP)MoCl$_2$ by addition of protons from H$^+$Cl$^-$(LutH$^+$Cl$^-$) and electrons from e$^-$ (CoCp*$_2$). Cl$^-$ represents [CoCp*$_2$]$^+$Cl$^-$. Energies (kcal/mol) are referenced to T = 298.15 K and P = 1 atm.

Name	**Spin State**	**ΔE**	**ΔG**
(PSP)Mo(N)Cl + 3 H$^+$Cl$^-$ + 2 e$^-$	Singlet	0.0	**0.0**
TS-PT-1 (Proton Transfer) + 2 H$^+$Cl$^-$ + 2 e$^-$	Singlet	X.X[d]	**X.X**[d]
(PSP)Mo(NH)Cl$_2$ + 2 H$^+$Cl$^-$ + 2 e$^-$	Singlet	-13.8	**-11.2**
TS-ET-1 (Electron Transfer) + 2 H$^+$Cl$^-$ + e$^-$	Doublet	-	**18.3**
[(PSP)Mo(NH)Cl$_2$]$^-$[CoCp*$_2$]$^+$ + 2 H$^+$Cl$^-$ + e$^-$	Doublet	-2.4	**17.5**
(PSP)Mo(NH)Cl + 2 H$^+$Cl$^-$ + e$^-$ + Cl$^-$	Doublet	8.7	**12.5**
TS-PT-2 (Proton Transfer) + H$^+$Cl$^-$ + e$^-$ + Cl$^-$	Doublet	X.X[d]	**X.X**[d]
(PSP)Mo(NH$_2$)Cl$_2$ + H$^+$Cl$^-$ + e$^-$ + Cl$^-$	Doublet	-23.0	**-15.7**
TS-ET-2 (Electron Transfer) + H$^+$Cl$^-$+ 2 Cl$^-$	Triplet	-	**2.5**
[(PSP)Mo(NH$_2$)Cl$_2$]$^-$[CoCp*$_2$]$^+$ + H$^+$Cl$^-$+ 2 Cl$^-$	Triplet	-23.6	**2.4**
(PSP)Mo(NH$_2$)Cl + H$^+$Cl$^-$+ 2 Cl$^-$	Triplet	-7.0	**1.8**
TS-PT-3 (Proton Transfer) + 2 Cl$^-$	Triplet	X.X[d]	**X.X**[d]
(PSP)Mo(NH$_3$)Cl$_2$ + 2 Cl$^-$	Triplet	-38.8	**-26.0**
(PSP)MoCl$_2$ + 2 Cl$^-$ + **NH$_3$**	Quintet	-22.5	**-22.1**

[d] TS could not be located even after multiple attempts

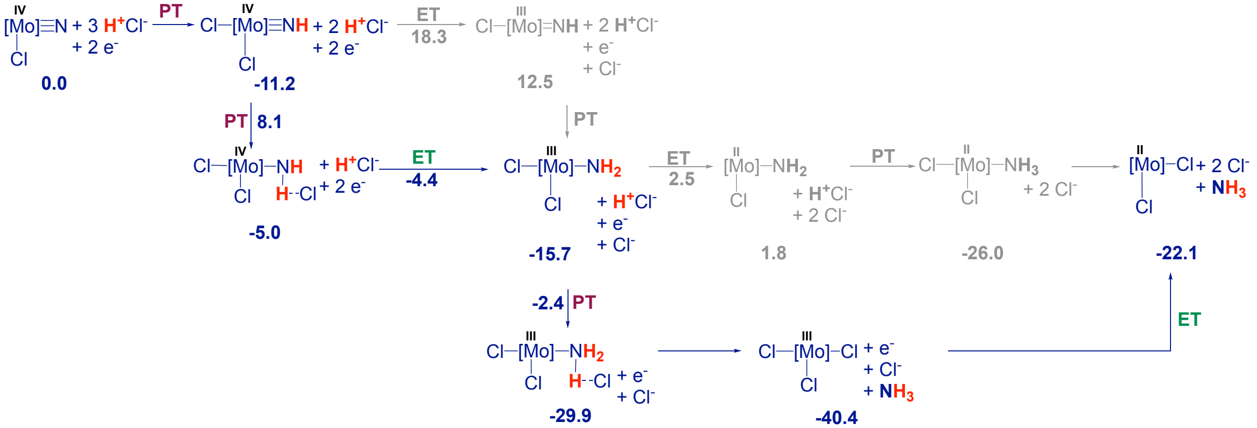

Scheme S7.8. Gibbs free energies for the overall reduction of (PSP)Mo^{IV}(≡N)Cl to (PSP)Mo^{II}Cl$_2$ and NH$_3$ via non-consecutive additions of H$^+$ and e$^-$ (protons first, in color). The "alternating" mechanism has been shown here (in gray). Energies in kcal/mol.

Table S7.10. Energies for the "protons first" pathway for conversion of (PSP)Mo(N)Cl to (PSP)MoCl$_2$ by addition of protons from H$^+$Cl$^-$(LutH$^+$Cl$^-$) and electrons from e$^-$ (CoCp*$_2$). Cl$^-$ represents [CoCp*$_2$]$^+$Cl$^-$. Energies (kcal/mol) are referenced to T = 298.15 K and P = 1 atm.

Name	**Spin State**	**ΔE**	**ΔG**
(PSP)Mo(N)Cl + 3 H$^+$Cl$^-$ + 2 e$^-$	Singlet	0.0	**0.0**
TS-PT-1 (Proton Transfer)	Singlet	X.X[d]	**X.X[d]**
(PSP)Mo(NH)Cl$_2$ + 2 H$^+$Cl$^-$ + 2 e$^-$	Singlet	-13.8	**-11.2**
TS-PT-2' (Proton Transfer) + H$^+$Cl$^-$ + 2 e$^-$	Singlet	-6.5	**8.1**
[(PSP)Mo(NH$_2$)Cl$_2$]$^+$Cl$^-$ + H$^+$Cl$^-$ + 2 e$^-$	Triplet	-8.9	**-5.0**
TS-ET-1' (Electron Transfer) + H$^+$Cl$^-$ + e$^-$	Doublet	-	**-4.4**
[(PSP)Mo(NH$_2$)Cl$_3$]$^-$[CoCp*$_2$]$^+$ + H$^+$Cl$^-$ + e$^-$	Doublet	-36.6	**-14.0**
(PSP)Mo(NH$_2$)Cl$_2$ + H$^+$Cl$^-$ + e$^-$ + Cl$^-$	Doublet	-23.0	**-15.7**
TS-PT-3' (Proton Transfer) + e$^-$+ Cl$^-$	Quartet	-24.6	**-2.4**
[(PSP)Mo(NH$_3$)Cl$_2$]$^+$Cl$^-$ + e$^-$+ Cl$^-$	Quartet	-40.2	**-29.9**
(PSP)MoCl$_3$ + Cl$^-$ + **NH$_3$**	Quartet	-38.5	**-40.4**
(PSP)MoCl$_2$ + 2 Cl$^-$ + **NH$_3$**	Quintet	-22.5	**-22.1**

[d] TS could not be located even after multiple attempts

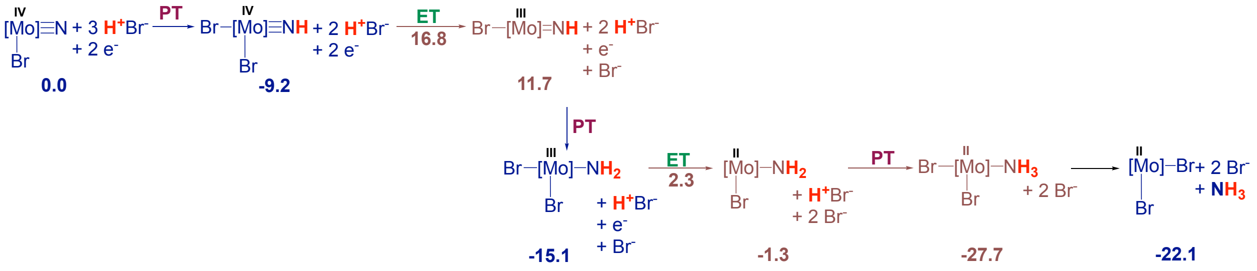

Scheme S7.9. Gibbs free energies for the overall reduction of (PSP)Mo^{IV}(≡N)Br to (PSP)Mo^{II}Br$_2$ and NH$_3$ via consecutive additions of H$^+$ and e$^-$ (alternating).

Table S7.11. Energies for the "alternating" pathway for conversion of (PSP)Mo(N)Br to (PSP)MoBr$_2$ by addition of protons from H$^+$Br$^-$(LutH$^+$Br$^-$) and electrons from e$^-$ (CoCp*$_2$). Br$^-$ represents [CoCp*$_2$]$^+$Br$^-$. Energies (kcal/mol) are referenced to T = 298.15 K and P = 1 atm.

Name	Spin State	ΔE	ΔG
(PSP)Mo(N)Br + 3 H$^+$Br$^-$ + 2 e$^-$	Singlet	0.0	**0.0**
TS-PT-1 (Proton Transfer) + 2 H$^+$Br$^-$ + 2 e$^-$	Singlet	X.X[e]	**X.X[e]**
(PSP)Mo(NH)Br$_2$ + 2 H$^+$Br$^-$ + 2 e$^-$	Singlet	-10.2	**-9.2**
TS-ET-1 (Electron Transfer) + 2 H$^+$Br$^-$ + e$^-$	Doublet	-	**16.8**
[(PSP)Mo(NH)Br$_2$]$^-$[CoCp*$_2$]$^+$ + 2 H$^+$Br$^-$ + e$^-$	Doublet	-0.4	**16.5**
(PSP)Mo(NH)Br + 2 H$^+$Br$^-$ + e$^-$ + Br$^-$	Doublet	10.6	**11.7**
TS-PT-2 (Proton Transfer) + H$^+$Br$^-$ + e$^-$ + Br$^-$	Doublet	X.X[e]	**X.X[e]**
(PSP)Mo(NH$_2$)Br$_2$ + H$^+$Br$^-$ + e$^-$ + Br$^-$	Doublet	-18.5	**-15.1**
TS-ET-2 (Electron Transfer) + H$^+$Br$^-$+ 2 Br$^-$	Triplet	-	**2.3**
[(PSP)Mo(NH$_2$)Br$_2$]$^-$[CoCp*$_2$]$^+$ + H$^+$Br$^-$+ 2 Br$^-$	Triplet	-20.2	**2.2**
(PSP)Mo(NH$_2$)Br + H$^+$Br$^-$+ 2 Br$^-$	Triplet	-4.9	**-1.3**
TS-PT-3 (Proton Transfer) + 2 Br$^-$	Triplet	X.X[e]	**X.X[e]**
(PSP)Mo(NH$_3$)Br$_2$ + 2 Br$^-$	Triplet	-34.1	**-27.7**
(PSP)MoBr$_2$ + 2 Br$^-$ + **NH$_3$**	Quintet	-15.3	**-22.1**

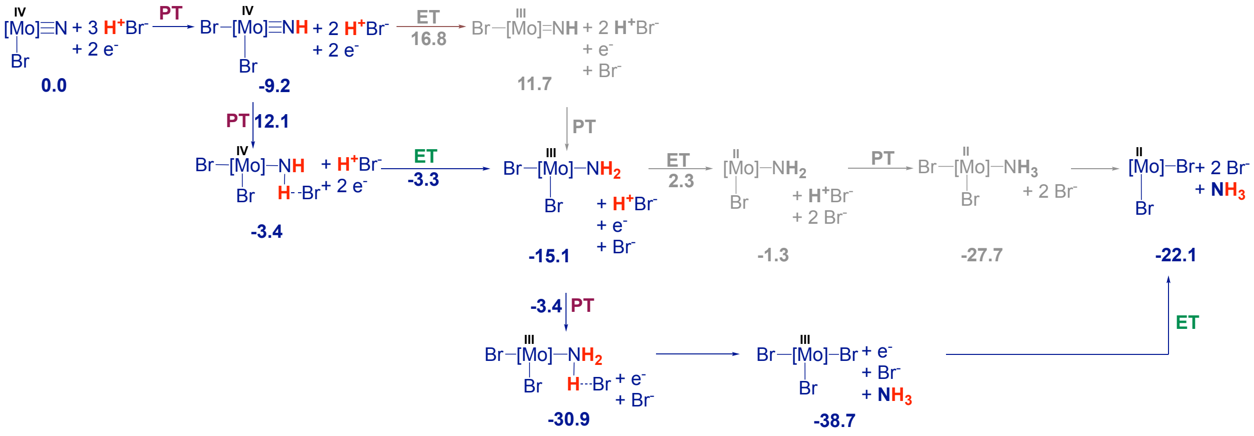

Scheme S7.10. Gibbs free energies for the overall reduction of $(PSP)Mo^{IV}(\equiv N)Br$ to $(PSP)Mo^{II}Br_2$ and NH_3 via non-consecutive additions of H^+ and e^- (protons first, in color). The “alternating” mechanism has been shown here (in gray) for comparison.

Table S7.12. Energies for the “protons first” pathway for conversion of (PSP)Mo(N)Br to $(PSP)MoBr_2$ by addition of protons from $H^+Br^-(LutH^+Br^-)$ and electrons from e^- $(CoCp^*_2)$. Br^- represents $[CoCp^*_2]^+Br^-$.Energies (kcal/mol) are referenced to T = 298.15 K and P = 1 atm.

Name	**Spin State**	**ΔE**	**ΔG**
(PSP)Mo(N)Br + 3 H^+Br^- + 2 e^-	Singlet	0.0	**0.0**
TS-PT-1 (Proton Transfer)	Singlet	X.X[e]	**X.X[e]**
$(PSP)Mo(NH)Br_2$ + 2 H^+Br^- + 2 e^-	Singlet	-10.2	**-9.2**
TS-PT-2’ (Proton Transfer) + H^+Br^- + 2 e^-	Triplet	-0.7	**12.1**
$[(PSP)Mo(NH_2)Br_2]^+Br^-$ + H^+Br^- + 2 e^-	Triplet	-3.3	**-3.4**
TS-ET-1’ (Electron Transfer) + H^+Br^- + e^-	Doublet	-	**-3.3**
$[(PSP)Mo(NH_2)Br_3]^-[CoCp^*_2]^+$ + H^+Br^- + e^-	Doublet	-33.3	**-14.9**
$(PSP)Mo(NH_2)Br_2$ + H^+Br^- + e^- + Br^-	Doublet	-18.5	**-15.1**
TS-PT-3’ (Proton Transfer) + e^-+ Br^-	Quartet	-19.7	**-3.4**
$[(PSP)Mo(NH_3)Br_2]^+Br^-$ + e^-+ Br^-	Quartet	-33.9	**-30.9**
$(PSP)MoBr_3$ + Br^- + **NH_3**	Quartet	-30.9	**-38.7**
$(PSP)MoBr_2$ + 2 Br^- + **NH_3**	Quintet	-15.3	**-22.1**

[e] TS could not be located even after multiple attempts

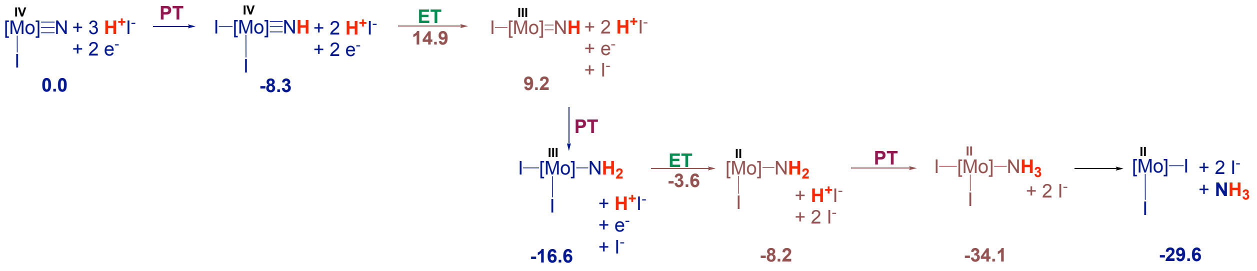

Scheme S7.11. Gibbs free energies for the overall reduction of (PSP)Mo^{IV}(≡N)I to (PSP)Mo^{II}I_2 and NH_3 via consecutive additions of H^+ and e^- (alternating).

Table S7.13. Energies for the “alternating” pathway for conversion of (PSP)Mo(N)I to (PSP)MoI_2 by addition of protons from H^+I^-(LutH^+I^-) and electrons from e^- (CoCp$^*_2$). I^- represents $[CoCp^*_2]^+I^-$. Energies (kcal/mol) are referenced to T = 298.15 K and P = 1 atm.

Name	**Spin State**	ΔE	ΔG
(PSP)Mo(N)I + 3 H^+I^- + 2 e^-	Singlet	0.0	**0.0**
TS-PT-1 (Proton Transfer) + 2 H^+I^- + 2 e^-	Singlet	X.X[f]	**X.X[f]**
(PSP)Mo(NH)I_2 + 2 H^+I^- + 2 e^-	Singlet	-8.5	**-8.3**
TS-ET-1 (Electron Transfer) + 2 H^+I^- + e^-	Doublet	-	**14.9**
[(PSP)Mo(NH)I_2]$^-$[CoCp$^*_2$]$^+$ + 2 H^+I^- + e^-	Doublet	-2.1	**14.8**
(PSP)Mo(NH)I + 2 H^+I^- + e^- + I^-	Doublet	9.0	**9.2**
TS-PT-2 (Proton Transfer) + H^+I^- + e^- + I^-	Doublet	X.X[f]	**X.X[f]**
(PSP)Mo(NH_2)I_2 + H^+I^- + e^- + I^-	Doublet	-18.7	**-16.6**
TS-ET-2 (Electron Transfer) + H^+I^-+ 2 I^-	Triplet	-	**-3.6**
[(PSP)Mo(NH_2)I_2]$^-$[CoCp$^*_2$]$^+$ + H^+I^-+ 2 I^-	Triplet	-23.5	**-3.7**
(PSP)Mo(NH_2)I + H^+I^-+ 2 I^-	Triplet	-9.7	**-8.2**
TS-PT-3 (Proton Transfer) + 2 I^-	Triplet	X.X[f]	**X.X[f]**
(PSP)Mo(NH_3)I_2 + 2 I^-	Triplet	-38.2	**-34.1**
(PSP)MoI_2 + 2 I^- + **NH_3**	Quintet	-20.6	**-29.6**

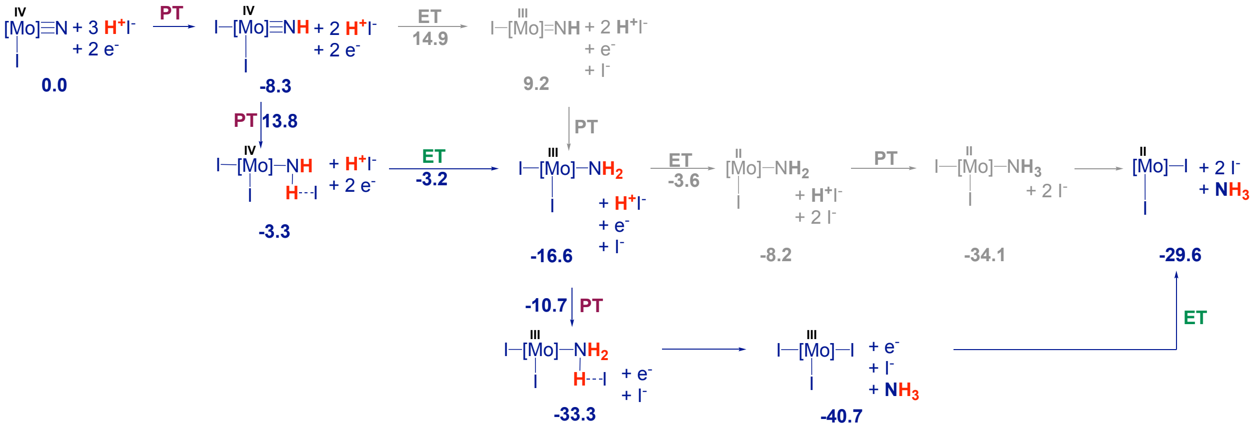

Scheme S7.12. Gibbs free energies for the overall reduction of (PSP)Mo^{IV}(≡N)I to (PSP)Mo^{II}I$_2$ and NH$_3$ via non-consecutive additions of H$^+$ and e$^-$ (protons first, in color). The "alternating" mechanism has been shown here (in gray) for comparison.

Table S7.14. Energies for the "protons first" pathway for conversion of (PSP)Mo(N)I to (PSP)MoI$_2$ by addition of protons from H$^+$I$^-$(LutH$^+$I$^-$) and electrons from e$^-$ (CoCp*$_2$). I$^-$ represents [CoCp*$_2$]$^+$I$^-$. Energies (kcal/mol) are referenced to T = 298.15 K and P = 1 atm.

Name	Spin State	ΔE	ΔG
(PSP)Mo(N)I + 3 H$^+$I$^-$ + 2 e$^-$	Singlet	0.0	**0.0**
TS-PT-1 (Proton Transfer)	Singlet	X.X[f]	**X.X[f]**
(PSP)Mo(NH)I$_2$ + 2 H$^+$I$^-$ + 2 e$^-$	Singlet	-8.5	**-8.3**
TS-PT-2' (Proton Transfer) + H$^+$I$^-$ + 2 e$^-$	Triplet	1.1	**13.8**
[(PSP)Mo(NH$_2$)I$_2$]$^+$I$^-$ + H$^+$I$^-$ + 2 e$^-$	Triplet	-1.5	**-3.3**
TS-ET-1' (Electron Transfer) + H$^+$I$^-$ + e$^-$	Doublet	-	**-3.2**
[(PSP)Mo(NH$_2$)I$_3$]$^-$[CoCp*$_2$]$^+$ + H$^+$I$^-$ + e$^-$	Doublet	-36.0	**-18.4**
(PSP)Mo(NH$_2$)I$_2$ + H$^+$I$^-$ + e$^-$ + I$^-$	Doublet	-18.7	**-16.6**
TS-PT-3' (Proton Transfer) + e$^-$+ I$^-$	Quartet	-24.0	**-10.7**
[(PSP)Mo(NH$_3$)I$_2$]$^+$I$^-$ + e$^-$+ I$^-$	Quartet	-35.1	**-33.3**
(PSP)MoI$_3$ + I$^-$ + **NH$_3$**	Quartet	-30.9	**-40.7**
(PSP)MoI$_2$ + 2 I$^-$ + **NH$_3$**	Quintet	-20.6	**-29.6**

[f] TS could not be located even after multiple attempts

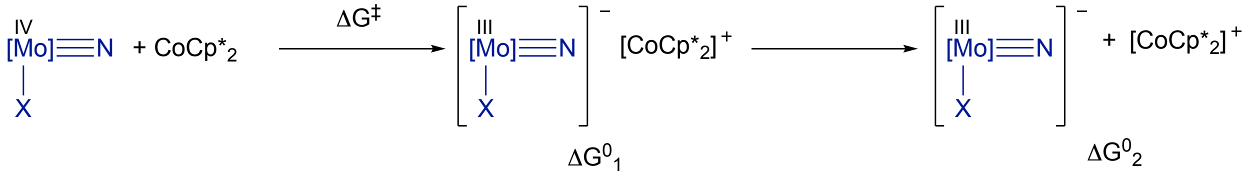

Scheme S7.13 Reduction of (PYP)MoNX complex with $CoCp^*_2$

Table S7.15 Energies (in kcal/mol) for the formation of the contact ion pair and corresponding separated redox complex pair that also highlight the electrostatic energy stabilization of electron transfer processes.

Ligand	X	ΔE_1 (kcal/mol)	ΔG^0_1 (kcal/mol)	$\Delta G^‡$ (kcal/mol)	ΔE_2 (kcal/mol)	ΔG^0_2 (kcal/mol)
^{tBu}PNP	Cl	17.2	33.8	44.6	43.4	47.4
	Br	17.4	34.2	45.6	43.4	46.9
	I	16.6	32.7	42.6	42.6	45.9
tBu-^{Me}PSP	Cl	19.5	35.5	53.3	50.2	52.5
	Br	20.2	36.7	56.5	50.3	52.8
	I	19.4	35.5	54.2	49.7	52.2

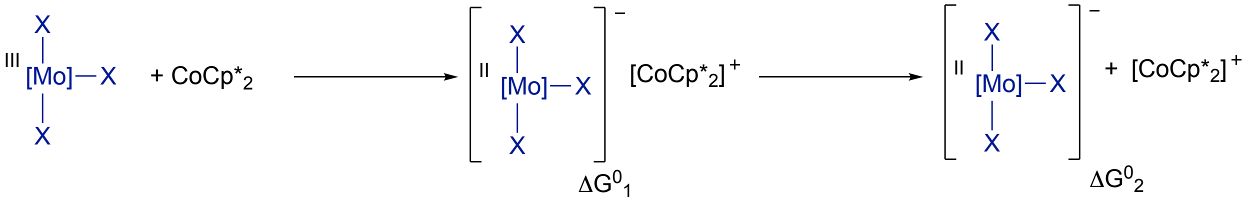

Scheme S7.14 Reduction of $(PYP)MoX_3$ complex with $CoCp^*_2$

Table S7.16 Energies (in kcal/mol) for the formation of the contact ion pair and corresponding separated redox complex pair that also highlight the electrostatic energy stabilization of electron transfer processes.

Ligand	X	ΔE_1 (kcal/mol)	ΔG^0_1 (kcal/mol)	ΔE_2 (kcal/mol)	ΔG^0_2 (kcal/mol)
^{tBu}PNP	Cl	-6.8	13.2	34.1	39.3
	Br	-7.2	12.3	27.6	32.7
	I	-11.1	8.6	24.3	29.7
tBu-^{Me}PSP	Cl	-9.4	10.0	21.8	27.5
	Br	-14.7	4.2	20.9	26.4
	I	-17.1	1.4	17.3	23.3

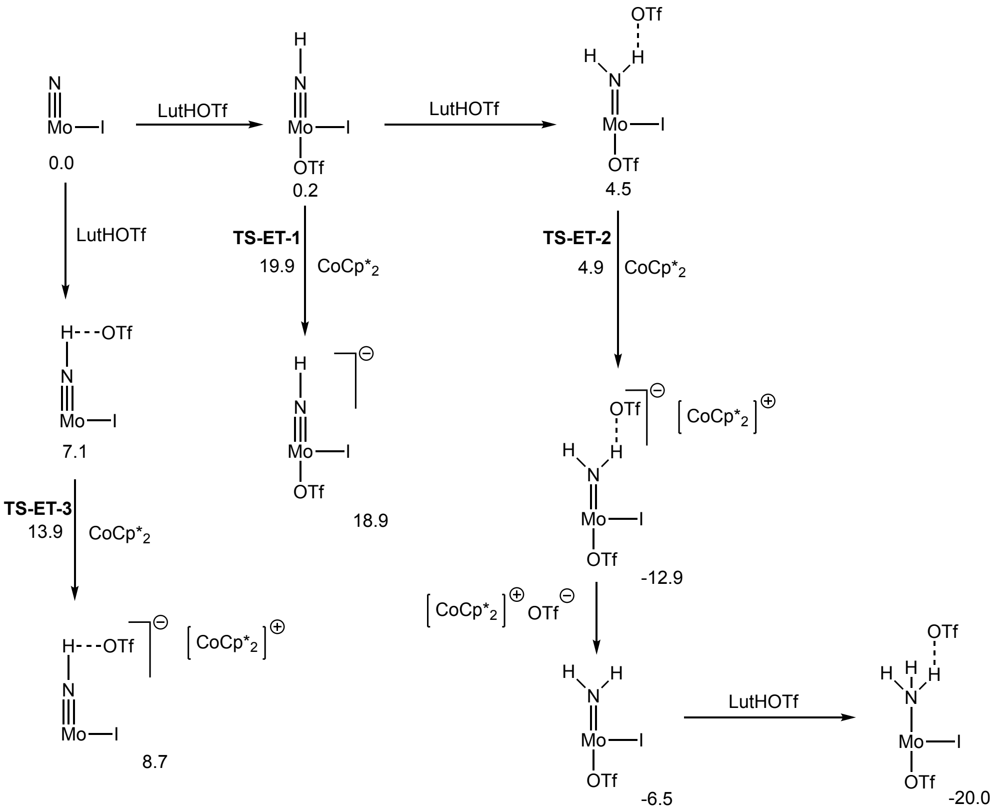

Scheme S7.15. Reduction of (^{iPr}PSP)MoNOTf complex with LutHOTf and CoCp*$_2$

Table S7.17. Energies (in kcal/mol) for the formation of the corresponding complexes.

Name	**Spin State**	ΔE	ΔG
(^{iPr}PSP)Mo(N)(I) + 3 LutH$^+$OTf$^–$ + CoCp*$_2$	Singlet	0.0	**0.0**
Coordinated OTf$^-$			
(^{iPr}PSP)Mo(NH)(I)(OTf) + 2 LutH$^+$OTf$^–$ + Lut + CoCp*$_2$	Singlet	-3.1	**0.2**
TS-ET-1	Doublet	-	**19.9**
[(^{iPr}PSP)Mo(NH)(I)(OTf)]$^-$[CoCp*$_2$]$^+$ + 2 LutH$^+$OTf$^–$ + Lut	Doublet	-1.2	**18.9**
[(^{iPr}PSP)Mo(NH$_2$)(I)(OTf)]$^+$[OTf]$^–$ + 2 Lut + CoCp*$_2$ + LutH$^+$OTf$^–$	Triplet	1.8	**4.5**
TS-ET-2	Doublet	-	**4.9**
[(^{iPr}PSP)Mo(NH$_2$)(I)(OTf)$_2$]$^-$[CoCp*$_2$]$^+$ + 2 Lut + LutH$^+$OTf$^–$	Doublet	-33.9	**-12.9**
(^{iPr}PSP)Mo(NH$_2$)(I)(OTf) + 2 Lut + LutH$^+$OTf$^–$ + [CoCp*$_2$]$^+$OTf$^–$	Doublet	-15.9	**-6.5**
[(^{iPr}PSP)Mo(NH$_2$)(I)(OTf)]$^+$[OTf]$^–$ + 3 Lut + [CoCp*$_2$]$^+$OTf$^–$	Quartet	-28.5	**-20.0**
Un-coordinated OTf$^-$			
[(^{iPr}PSP)Mo(NH)(I)]$^+$[OTf]$^–$ + LutH$^+$OTf$^–$ + Lut + CoCp*$_2$	Singlet	8.9	**7.1**
TS-ET-3	Doublet	-	**13.9**
[(^{iPr}PSP)Mo(NH)(I)(OTf)]$^-$[CoCp*$_2$]$^+$ + LutH$^+$OTf$^–$ + Lut	Doublet	-10.1	**8.7**

S7.2: Relevant geometric parameters (bond distances and bond angles) of the computed (PSP)Mo(N-H$_m$)X$_n$ (m = 0-3, n = 1-2) and (PNP)Mo(N-H$_m$)X$_n$ (m = 0-3, n = 1-2) systems used in this study

Table S7.18. Relevant geometric parameters (bond distances and bond angles) of the computed (PSP)Mo(N-H$_m$)Cl$_n$ (m = 0-3, n = 1-2)

X = Cl	[Mo]XN	[Mo]X(N-H)	[Mo]X(NH–H)	[Mo]X(NH$_2$–H)	[Mo]X(NH$^+$–H)	[Mo](X)NH$_2^+$–H	[Mo]X$_2$(NH–H)	[Mo]X$_2$(NH$_2$–H)
Mo-N (Å)	1.645	1.761	1.981	2.757	1.961	2.307	1.949	2.293
N-H (Å)	n/a	1.019	1.016	1.016	1.017	1.02	1.019	1.019
N-H (Å)	n/a	n/a	1.017	1.018	1.018	1.018	1.018	1.018
N-H (Å)	n/a	n/a	n/a	1.02	n/a	1.02	n/a	1.019
PMoP (°)	152.58	151.32	113.31	110.43	110.26	117.96	150.19	154.36
MoNH (°)	n/a	171.24	121.15	119.63	122.61	108.68	119.59	106.23
MoNH (°)	n/a	n/a	127.88	103.7	127.14	107.94	128.98	108.49
MoNH (°)	n/a	n/a	n/a	109.55	n/a	118.53	n/a	118.6
SMoN (°)	105.86	121.21	100.23	96.98	95.55	96.99	93.38	91.05
NMoP (°)	103.08	104.64	123.4	91.46	119.93	90.08	96.78	92.41
NMoP (°)	100.4	102.69	122.7	156.79	127.6	150.07	106.44	104.68
SMoX (°)	136.59	89.44	173.12	168.99	173.98	167.82	173.44	168.49
SMoX (°)	n/a	n/a	n/a	n/a	n/a	n/a	88.14	91.59

Table S7.19. Relevant geometric parameters (bond distances and bond angles) of the computed (PSP)Mo(N-H$_m$)I$_n$ (m = 0-3, n = 1-2)

X = I	[Mo]XN	[Mo]X(N-H)	[Mo]X(NH–H)	[Mo]X(NH$_2$–H)	[Mo]X(NH$^+$–H)	[Mo](X)NH$_2^+$–H	[Mo]X$_2$(NH–H)	[Mo]X$_2$(NH$_2$–H)
Mo-N (Å)	1.642	1.758	1.963	2.335	1.961	2.314	1.946	2.294
N-H (Å)	n/a	1.02	1.018	1.019	1.018	1.02	1.019	1.019
N-H (Å)	n/a	n/a	1.017	1.018	1.018	1.02	1.019	1.019
N-H (Å)	n/a	n/a	n/a	1.019	n/a	1.02	n/a	1.02
PMoP (°)	152.64	152.69	118.62	108.22	109.74	115.74	152.29	156.11
MoNH (°)	n/a	169.01	114.13	106.08	124.33	107.05	121.34	117.78
MoNH (°)	n/a	n/a	134.41	110.96	125.78	114.6	127.64	106.54
MoNH (°)	n/a	n/a	n/a	117.06	n/a	114.4	n/a	109.75
SMoN (°)	104.78	121.8	81.81	88.75	93.3	92.08	92.92	91.26
NMoP (°)	102.48	103.43	117.71	140.07	127.22	101.59	94.08	89.06
NMoP (°)	99.37	101.05	114.45	107.21	120.01	139.16	104.52	103.34
SMoX (°)	141.81	91.83	178.25	166.24	174.97	168.22	173.52	169.9
SMoX (°)	n/a	n/a	n/a	n/a	n/a	n/a	88.87	92.01

Table S7.20. Relevant geometric parameters (bond distances and bond angles) of the computed (PNP)Mo(N-H$_m$)Cl$_n$ (m = 0-3, n = 1-2)

X = Cl	[Mo]XN	[Mo]X(N-H)	[Mo]X(NH–H)	[Mo]X(NH$_2$–H)	[Mo]X(NH$^+$–H)	[Mo](X)NH$_2^+$–H	[Mo]X$_2$(NH–H)	[Mo]X$_2$(NH$_2$–H)
Mo-N (Å)	1.648	1.749	1.961	2.254	2.002	2.233	2.077	2.327
N-H (Å)	n/a	1.023	1.02	1.017	1.018	1.02	1.015	1.017
N-H (Å)	n/a	n/a	1.018	1.017	1.017	1.019	1.018	1.015
N-H (Å)	n/a	n/a	n/a	1.025	n/a	1.02	n/a	1.026
PMoP (°)	153.35	149.31	130.12	158.67	154.43	153.97	155.84	153.58
MoNH (°)	n/a	154.87	116.16	117.8	115.3	107.78	122.58	123.71
MoNH (°)	n/a	n/a	133.11	99.1	123.32	113.87	114.67	114
MoNH (°)	n/a	n/a	n/a	116.26	n/a	114.3	n/a	94.88
*pyNMoN (°)	102.6	106.05	81.98	101.11	87.45	86.96	87.84	105.94
NMoP (°)	94.05	101.11	105.86	97.58	95.87	97.98	93.22	95.39
NMoP (°)	103.75	105.01	109.58	95.28	96.14	94.01	85.97	86.84
*pyNMoX (°)	144.3	138.61	172.7	176.83	168.95	176.9	177.8	176.56
*pyNMoX (°)	n/a	n/a	n/a	n/a	n/a	n/a	86.47	87.02

**** pyN refers to the N atom of the pyridine ring of the ligand.***

Table S7.21. Relevant geometric parameters (bond distances and bond angles) of the computed (PNP)Mo(N-H$_m$)I$_n$ (m = 0-3, n = 1-2)

X = I	[Mo]XN	[Mo]X(N-H)	[Mo]X(NH–H)	[Mo]X(NH$_2$–H)	[Mo]X(NH$^+$–H)	[Mo](X)NH$_2^+$–H	[Mo]X$_2$(NH–H)	[Mo]X$_2$(NH$_2$–H)
Mo-N (Å)	1.645	1.756	1.949	2.265	2.002	2.235	2.069	2.33
N-H (Å)	n/a	1.028	1.019	1.018	1.018	1.02	1.015	1.016
N-H (Å)	n/a	n/a	1.022	1.017	1.017	1.02	1.017	1.017
N-H (Å)	n/a	n/a	n/a	1.024	n/a	1.02	n/a	1.024
PMoP (°)	152.63	143.4	132.59	158.7	154.64	155.67	155.2	152.07
MoNH (°)	n/a	146.43	116.97	117.89	122.18	112.13	115.44	99.52
MoNH (°)	n/a	n/a	132.05	101.45	115.8	110.71	122.24	123.39
MoNH (°)	n/a	n/a	n/a	115	n/a	113.7	n/a	111.45
*pyNMoN (°)	101.43	94.1	81.99	98.62	87.65	89.46	87.63	105.08
NMoP (°)	104.04	101.53	104.12	96.72	95.73	94.45	91.8	93.97
NMoP (°)	94.33	108.38	109.05	95.37	96.01	96.92	83.36	84.4
*pyNMoX (°)	150.43	156.56	175.8	177.25	171.06	178.52	176.59	175.77
*pyNMoX (°)	n/a	n/a	n/a	n/a	n/a	n/a	88.38	88.11

**** pyN refers to the N atom of the pyridine ring of the ligand.***

S7.3: Comparison of the molecular orbitals of (PSP)MoCl$_3$ and (PNP)MoCl$_3$

The (PYP)MoCl$_3$ complexes have a pseudo-octahedral geometry with three unpaired electrons highly localized in the set of d_{xy}, d_{xz} d_{yz} metal orbitals. In the (PSP)MoCl$_3$ complex, one of the ligand σ*-C-S-C MOs is relatively low energy and is directed toward the metal. Reduction of (PSP)MoCl$_3$ leads to a filled orbital that is still largely Mo d_{xy} (perpendicular to the trans Cl-Mo-Cl (z) axis) but is delocalized into the σ*-C-S-C MO. Reduction of (PNP)MoCl$_3$ shows negligible delocalization into the analogous σ*-C-N-C MO. In addition, in both complexes this filled d_{xy} MO shows delocalization into the σ*-C-P MOs. However, in the case of PSP these are P-C(sp^2) σ* MO's and are expected to be lower in energy and oriented more toward the Mo center than the P-C(sp^3) σ* MO's of (PNP)MoCl$_3$. Accordingly there is more delocalization into the σ*-C-P MOs in the case of the PSP complex. These factors should contribute toward favoring the reduction of (PSP)MoCl$_3$.

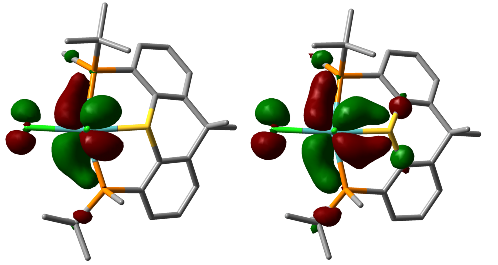	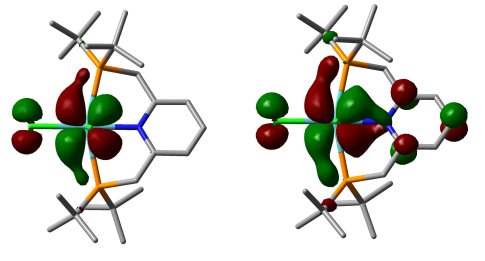
d_{xy} in (PSP)MoCl$_3$ and [(PSP)MoCl$_3$]$^-$ significant back-bonding to σ*-CSC	d_{xy} in (PNP)MoCl$_3$ and [(PNP)MoCl$_3$]$^-$ minima back-bonding to π*-pyridine

Figure S44: Illustration of change in d_{xy} orbitals in (PYP)MoCl$_3$ (Y = S (left side), N (right side) when an electron is added.

Consistently, upon reduction of (PSP)MoCl$_3$, the Mo-S bond contracts from 2.543 to 2.353A, this corresponds to 7.5 % contraction. In comparison, the Mo-N bond in (PNP)MoCl$_3$ is contracted from 2.25 to 2.148 A, corresponding to 4.5% contraction.

In the nitride complexes (PYP)Mo(N)Cl, there are no low-lying metal orbitals. Reduction in this case involves adding an electron to the pyridine ring of PNP or to the aromatic rings of PSP as shown in the given SOMOs of the anions. The reduction is highly unfavorable and energetically similar in both systems.

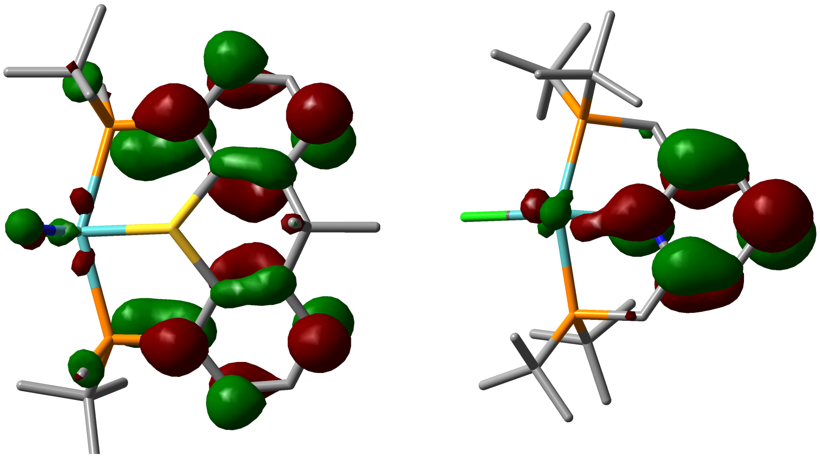

Figure S45: Illustration of SOMO of [(PYP)Mo(N)Cl]$^-$ (Y = S (left side), N (right side) when an electron is added to (PYP)Mo(N)Cl

VIII. References

(S1) Zhou, X. G.; Malakar, S.; Zhou, T.; Murugesan, S.; Huang, C.; Emge, T. J.; Krogh-Jespersen, K.; Goldman, A. S. Catalytic Alkane Transfer Dehydrogenation by PSP-Pincer-Ligated Ruthenium. Deactivation of an Extremely Reactive Fragment by Formation of Allyl Hydride Complexes. *ACS Catal.* **2019**, *9* (5), 4072-4083. DOI: 10.1021/acscatal.8b05172.
(S2) Curley, J. J.; Bergman, R. G.; Tilley, T. D. Preparation and physical properties of early-late heterobimetallic compounds featuring Ir-M bonds (M = Ti, Zr, Hf). *Dalton Trans.* **2012**, *41* (1), 192-200. DOI: 10.1039/c1dt11753j.
(S3) Brookhart, M.; Grant, B.; Volpe, A. F. [(3,5-(CF3)2C6H3)4B]-[H(OEt2)2]+: a convenient reagent for generation and stabilization of cationic, highly electrophilic organometallic complexes. *Organometallics* **2002**, *11* (11), 3920-3922. DOI: 10.1021/om00059a071.
(S4) Giffin, N. A.; Makramalla, M.; Hendsbee, A. D.; Robertson, K. N.; Sherren, C.; Pye, C. C.; Masuda, J. D.; Clyburne, J. A. Anhydrous TEMPO-H: reactions of a good hydrogen atom donor with low-valent carbon centres. *Org. Biomol. Chem.* **2011**, *9* (10), 3672-3680. DOI: 10.1039/c0ob00999g From NLM PubMed-not-MEDLINE.
(S5) Frisch, M. J.; Trucks, G. W.; Schlegel, H. B.; Scuseria, G. E.; Robb, M. A.; Cheeseman, J. R.; Scalmani, G.; Barone, V.; Petersson, G. A.; Nakatsuji, H.; Li, X.; Caricato, M.; Marenich, A. V.; Bloino, J.; Janesko, B. G.; Gomperts, R.; Mennucci, B.; Hratchian, H. P.; Ortiz, J. V.; Izmaylov, A. F.; Sonnenberg, J. L.; Williams; Ding, F.; Lipparini, F.; Egidi, F.; Goings, J.; Peng, B.; Petrone, A.; Henderson, T.; Ranasinghe, D.; Zakrzewski, V. G.; Gao, J.; Rega, N.; Zheng, G.; Liang, W.; Hada, M.; Ehara, M.; Toyota, K.; Fukuda, R.; Hasegawa, J.; Ishida, M.; Nakajima, T.; Honda, Y.; Kitao, O.; Nakai, H.; Vreven, T.; Throssell, K.; Montgomery Jr., J. A.; Peralta, J. E.; Ogliaro, F.; Bearpark, M. J.; Heyd, J. J.; Brothers, E. N.; Kudin, K. N.; Staroverov, V. N.; Keith, T. A.; Kobayashi, R.; Normand, J.; Raghavachari, K.; Rendell, A. P.; Burant, J. C.; Iyengar, S. S.; Tomasi, J.; Cossi, M.; Millam, J. M.; Klene, M.; Adamo, C.; Cammi, R.; Ochterski, J. W.; Martin, R. L.; Morokuma, K.; Farkas, O.; Foresman, J. B.; Fox, D. J. *Gaussian 16 Rev. A.03*, Wallingford, CT, 2016.
(S6) Yu, H. S.; He, X.; Li, S. L.; Truhlar, D. G. MN15: A Kohn-Sham global-hybrid exchange-correlation density functional with broad accuracy for multi-reference and single-reference systems and noncovalent interactions. *Chem. Sci.* **2016**, *7* (8), 5032-5051. DOI: 10.1039/c6sc00705h.
(S7) (a) Francl, M. M.; Pietro, W. J.; Hehre, W. J.; Binkley, J. S.; Gordon, M. S.; DeFrees, D. J.; Pople, J. A. Self-consistent molecular orbital methods. XXIII. A polarization-type basis set for second-row elements. *J. Chem. Phys.* **1982**, *77* (7), 3654-3665. DOI: 10.1063/1.444267. (b) Gordon, M. S.; Binkley, J. S.; Pople, J. A.; Pietro, W. J.; Hehre, W. J. Self-consistent molecular-orbital methods. 22. Small split-valence basis sets for second-row elements. *J. Am. Chem. Soc.* **2002**, *104* (10), 2797-2803. DOI: 10.1021/ja00374a017. (c) Hariharan, P. C.; Pople, J. A. The influence of polarization functions on molecular orbital hydrogenation energies. *Theor. Chim. Acta* **1973**, *28* (3), 213-222. DOI: 10.1007/bf00533485. (d) Hehre, W. J.; Ditchfield, R.; Pople, J. A. Self—Consistent Molecular Orbital Methods. XII. Further Extensions of Gaussian—Type Basis Sets for Use in Molecular Orbital Studies of Organic Molecules. *J. Chem. Phys.* **1972**, *56* (5), 2257-2261. DOI: 10.1063/1.1677527.
(S8) Andrae, D.; Huermann, U.; Dolg, M.; Stoll, H.; Preu, H. Energy-adjustedab initio pseudopotentials for the second and third row transition elements. *Theor. Chim. Acta* **1990**, *77* (2), 123-141. DOI: 10.1007/bf01114537.
(S9) Bezier, D.; Guan, C.; Krogh-Jespersen, K.; Goldman, A. S.; Brookhart, M. Experimental and computational study of alkane dehydrogenation catalyzed by a carbazolide-based rhodium PNP pincer complex. *Chem. Sci.* **2016**, *7* (4), 2579-2586. DOI: 10.1039/c5sc04794c.
(S10) McQuarrie, D. A. Statistical Thermodynamics, Harper and Row, New York, **1973**.
(S11) (a) Marcus, R. A. On the Theory of Oxidation-Reduction Reactions Involving Electron Transfer. I. *J. Chem. Phys.* **1956**, *24* (5), 966-978. DOI: 10.1063/1.1742723. (b) Marcus, R. A. On the Theory of

Oxidation-Reduction Reactions Involving Electron Transfer. II. Applications to Data on the Rates of Isotopic Exchange Reactions. *J. Chem. Phys.* **1957**, *26* (4), 867-871. DOI: 10.1063/1.1743423. (c) Marcus, R. A. On the Theory of Oxidation-Reduction Reactions Involving Electron Transfer. III. Applications to Data on the Rates of Organic Redox Reactions. *J. Chem. Phys.* **1957**, *26* (4), 872-877. DOI: 10.1063/1.1743424. (d) Marcus, R. A. Exchange reactions and electron transfer reactions including isotopic exchange. Theory of oxidation-reduction reactions involving electron transfer. Part 4.—A statistical-mechanical basis for treating contributions from solvent, ligands, and inert salt. *Discuss. Faraday Soc.* **1960**, *29* (0), 21-31. DOI: 10.1039/df9602900021. (e) Marcus, R. A. Chemical and Electrochemical Electron-Transfer Theory. *Ann. Rev. Phys. Chem.* **1964**, *15* (1), 155-196. DOI: 10.1146/annurev.pc.15.100164.001103. (f) Marcus, R. A. On the Theory of Electron-Transfer Reactions. VI. Unified Treatment for Homogeneous and Electrode Reactions. *J. Chem. Phys.* **1965**, *43* (2), 679-701. DOI: 10.1063/1.1696792. (g) Marcus, R. A. On the Theory of Oxidation—Reduction Reactions Involving Electron Transfer. V. Comparison and Properties of Electrochemical and Chemical Rate Constants1. *J. Chem. Phys.* **2002**, *67* (4), 853-857. DOI: 10.1021/j100798a033.
(S12) Lu, T.; Chen, F. Multiwfn: a multifunctional wavefunction analyzer. *J. Comput. Chem.* **2012**, *33* (5), 580-592. DOI: 10.1002/jcc.22885.
(S13) Auer, B.; Fernandez, L. E.; Hammes-Schiffer, S. Theoretical analysis of proton relays in electrochemical proton-coupled electron transfer. *J. Am. Chem. Soc.* **2011**, *133* (21), 8282-8292. DOI: 10.1021/ja201560v.
(S14) Lopez-Estrada, O.; Laguna, H. G.; Barrueta-Flores, C.; Amador-Bedolla, C. Reassessment of the Four-Point Approach to the Electron-Transfer Marcus-Hush Theory. *ACS Omega* **2018**, *3* (2), 2130-2140. DOI: 10.1021/acsomega.7b01425.
(S15) (a) Jones, G. O.; Liu, P.; Houk, K. N.; Buchwald, S. L. Computational explorations of mechanisms and ligand-directed selectivities of copper-catalyzed Ullmann-type reactions. *J. Am. Chem. Soc.* **2010**, *132* (17), 6205-6213. DOI: 10.1021/ja100739h. (b) Davari, N.; Daub, C. D.; Astrand, P. O.; Unge, M. Local Field Factors and Dielectric Properties of Liquid Benzene. *J. Phys. Chem. B* **2015**, *119* (35), 11839-11845. DOI: 10.1021/acs.jpcb.5b07043.
(S16) (a) Peterson, K. A.; Figgen, D.; Goll, E.; Stoll, H.; Dolg, M. Systematically convergent basis sets with relativistic pseudopotentials. II. Small-core pseudopotentials and correlation consistent basis sets for the post-d group 16–18 elements. *J. Chem. Phys.* **2003**, *119* (21), 11113-11123. DOI: 10.1063/1.1622924. (b) Rappoport, D.; Furche, F. Property-optimized gaussian basis sets for molecular response calculations. *J Chem Phys* **2010**, *133* (13), 134105. DOI: 10.1063/1.3484283. (c) Weigend, F.; Ahlrichs, R. Balanced basis sets of split valence, triple zeta valence and quadruple zeta valence quality for H to Rn: Design and assessment of accuracy. *Phys. Chem. Chem. Phys.* **2005**, *7* (18), 3297-3305. DOI: 10.1039/b508541a (d) Weigend, F.; Furche, F.; Ahlrichs, R. Gaussian basis sets of quadruple zeta valence quality for atoms H–Kr. *J. Chem. Phys.* **2003**, *119* (24), 12753-12762. DOI: 10.1063/1.1627293.
(S17) Marenich, A. V.; Cramer, C. J.; Truhlar, D. G. Universal solvation model based on solute electron density and on a continuum model of the solvent defined by the bulk dielectric constant and atomic surface tensions. *J. Phys. Chem. B* **2009**, *113* (18), 6378-6396. DOI: 10.1021/jp810292n